UNVEILING THE EXCITED STATES OF INDIGO, MAYA BLUE, BRAZILWOOD AND DRAGON'S BLOOD

RAQUEL JULIANA BATISTA LOURENÇO RONDÃO

Dissertação submetida à Faculdade de Ciências e Tecnologia da Universidade de Coimbra para apreciação nas provas de Doutoramento em Química, especialidade de Fotoquímica

COIMBRA | 2012

Ao meu pai
que me ensinou que
com arte e um sorriso
se tiram pedras do caminho.
À minha mãe
que todos os dias me ensina
um novo significado da palavra "força".

AGRADECIMENTOS

Porque as caminhadas são mais agradáveis e os obstáculos parecem menores quando os fazemos acompanhados, no fim desta etapa, há que reconhecer aqueles que, de várias formas, me foram acompanhando.

Ao Prof. Sérgio Seixas de Melo agradeço por me ter dado a conhecer o maravilhoso mundo dos corantes e toda a sua riqueza, o apoio, supervisão, disponibilidade, pelos desafios nas mais variadas áreas, amizade e incentivo que sempre demonstrou.

Ao Prof. Jorge Parola por tão bem me ter recebido na Univ. Nova de Lisboa, por todo o apoio, simpatia e incentivo, numa altura em que tudo era novo para mim.

Ao João Pina, um agradecimento muito especial, pois desde o primeiro dia como estagiária de licenciatura foi um exemplo a seguir. Quem me ensinou a dar os "primeiros passos" na fotoquímica, a não ter medo de lidar com os equipamentos e precalços, quem esteve sempre pacientemente disponível em todas as emergências (e foram muitas).

Ao grupo de Fotoquímica e Espectroscopia Molecular do Departamento de Química da Universidade de Coimbra por ter facultado o acesso à instrumentação científica essencial para a realização deste trabalho.

Aos amigos do grupo de fotoquímica, Ana Borba, Ana Marques, Fábio, Telma, Pina, que juntamente com os companheiros de almoço, Andreia (eterna companheira de casa e de sorrisos), Artur, Carlos, Mário, Vanessa, tornaram os dias no departamento de química mais agradáveis, por todos os bons momentos e gargalhadas. E às colegas de laboratório, Catarina, Catherine, Daniela, Ana, Susana, Helena, Solange.

Ao Rui Nunes, por todo o incentivo, ajuda, bons momentos, e presença constante - mesmo quando está do outro lado do oceano.

A todos da Univ. Nova de Lisboa. Prof. Maria J. Melo, Prof. F. Pina, Micaela Sousa por toda a ajuda e disponibilidade, Ana Marta, Raquel Gavarra, e Yoann por me terem feito "sentir em casa" no seu laboratório, e por todos os bons momentos, algumas vezes passados em torno de uma coluna (quase maior que eu) toda vermelha.

A todos os restantes amigos, que apesar de não terem sido nomeados não deixam de ser importantes.

Aos meus pais, que sempre foram um farol. Farol que a certa altura, perdeu algum brilho, mas nem por um instante que fosse perdeu a sua força e razão de ser, sempre resistindo a todas as intempéries.

À minha irmã, sempre disponível para me "melgar".

À família por todo o apoio e confiança.

À Fundação para a Ciência e Tecnologia (F.C.T.) pelo financiamento (SFRH/ BD/ 38882/ 2007).

A todos um enorme **BEM HAJA**!!!

TABLE OF CONTENTS

ABSTRACT xiii

RESUMO xv

ABBREVIATIONS xvii

GENERAL INTRODUCTION

1 INDIGO 5

1.1 BRIEF HISTORY OF INDIGO

1.1.1 THE MILLENARY HISTORY OF INDIGO 7

1.1.2 INDIGO: FROM ANTIQUITY TO MODERN TIMES 9

1.1.3 INDIGO IN THE ANTIQUITY: THE BLUE OF THE EGYPTIANS AND THE PURPLE OF THE PHOENICIANS 12

1.1.4 THE MYTHIC BLUE OF THE HEBREWS: THE *TEKHELET* AND ITS LOST SECRET 15

1.1.5 BIOSYNTHESIS OF INDIGO 17

1.1.6 INDIRUBIN: ISOMER OF INDIGO 20

1.2 THE CHEMISTRY OF INDIGO 21

1.2.1 THE SYNTHETIC VIA: BAYER AND HEUMANN 21

1.2.2 THE COLOUR OF INDIGO AND DERIVATIVES: THE H-CHROMOPHORE AND MODERN THEORIES 23

1.2.3 THE INDIGO'S COUSINS: TYRIAN PURPLE, INDIRUBIN, THIOINDIGO 26

1.2.4 THE STABILITY AND PHOTOPHYSICS OF INDIGO 27

1.2.5 THE INDIGO REDUCED FORM USED FOR DYEING: ANCIENT AND MODERN PATHWAYS 30

1.2.6 THE PHOTOPHYSICS OF LEUCO INDIGO 32

1.2.7 THE BLUE OF THE MAYA CIVILIZATION: MAYA BLUE 33

1.2.8 ZEMBRA PURPLE: IS THERE A POTENTIAL CONNECTION WITH MAYA BLUE? 37

2	**SUBSTITUTED INDIGO DERIVATIVES**		**39**
2.1	SUBSTITUDED INDIGO DERIVATIVES		41
2.2	SPECTROSCOPIC CHARACTERIZATION		43
	2.2.1	SINGLET-STATE	43
	2.2.2	LEUCO TRIPLET STATE	49
2.3	PHOTOISOMERIZATION OF LEUCO INDIGO		52
2.4	CONCLUSIONS		54
3	**EXCITED STATE ISOMERIZATION OF LEUCO INDIGO**		**55**
3.1	INDIGO		57
3.2	MODEL COMPOUND: MPRECIBA		61
3.3	4,4'-DIBUTOXY-7,7'-DIMETHOXY-5,5'-DINITROINDIGO (DBMNI)		62
	3.3.1	THERMAL ISOMERISATION OF DBMNI	66
3.4	PHOTOCHEMISTRY (TRANS-CIS CONVERSION) QUANTUM YIELD		68
3.5	DBMNI, TIME-RESOLVED DEPENDENCE OF THE TRANS-CIS CONVERSION		69
3.6	CONCLUSIONS		72
4	**DEHYDROINDIGO**		**73**
4.1	SPECTRAL DATA		76
4.2	TRIPLET STATE AND SINGLET OXYGEN SENSITIZATION		83
4.3	PHOSPHORESCENCE IN METHANOL		85
4.4	TIME-RESOLVED FLUORESCENCE CHARACTERIZATION		86
4.5	COMPARISON BETWEEN DHI AND INDIGO		91
4.6	THEORETICAL CALCULATIONS ON THE ELECTRONIC STRUCTURES OF THE S_0, S_1 AND T_1 STATES OF DHI		93
4.7	CONCLUSIONS		97

5	**AN INDIGO POLYMER**		**99**
	5.1	SPECTRAL AND PHOTOPHYSICAL PROPERTIES	102
	5.2	PHOTOACOUSTIC EXPERIMENTS	108
	5.3	STABILITY TOWARDS LIGHT	111
	5.4	CONCLUSIONS	112
6	**THIOINDIGO**		**113**
	6.1	SPECTRAL AND PHOTOPHYSICAL DATA	117
	6.2	LOW TEMPERATURE AGGREGATE FORMATION	123
	6.3	COMPARISON OF THIOINDIGO/CBP WITH INDIGO	125
7	**MAYA BLUE & MAYA PINK**		**127**
	7.1	INDIGO/ATTAPULGITE AND INDIGO/SEPIOLITE	131
	7.2	THE CONNECTION OF DHI WITH MAYA BLUE	133
	7.3	THIOINDIGO: A FLUORESCENCE PROBE TO MAYA BLUE	136
	7.4	CIBA BRILLIANT PINK AND ITS INTERACTION WITH THE CLAYS	142
	7.5	TIME RESOLVED DATA	145
	7.6	SOME NOTES	150
	7.7	MOLECULAR DESIGN	152
	7.8	CONCLUSIONS	153
8	**DRAGON'S BLOOD**		**155**
	8.1	DRACORHODIN	161
		8.1.1 ACIDIC MEDIA	162
		8.1.2 BASIC MEDIA	164
		8.1.3 PH JUMP EXPERIMENTS	165
		8.1.4 NETWORK OF CHEMICAL REACTIONS	167
		8.1.5 EXCITED STATE CHARACTERIZATION	169
		8.1.6 CONCLUSIONS	171
	8.2	7,4'-DIHYDROXY-5-METHOXYFLAVYLIUM – DRACOFLAVYLIUM	172
		8.2.1 SPECTRAL DATA	173

8.2.2 EXCITED STATE CHARACTERIZATION 176
8.3 CONCLUSIONS 177

9 BRAZILWOOD 179

9.1 BRAZILIN 183
9.1.1 PURIFICATION OF BRAZILIN 183
9.1.2 pH BEHAVIOUR 185
9.1.3 SPECTRAL DATA 188
9.1.4 EXCITED STATE CHARACTERIZATION 190
9.1.5 INFLUENCE OF LIGHT AND OXYGEN IN THE OXIDATION OF BRAZILIN 192
9.2 BRAZILEIN 194
9.2.1 SPECTRAL DATA 195
9.2.2 EXCITED STATE CHARACTERIZATION 197
9.2.3 BRAZILEIN EXCITED STATE INTRAMOLECULAR PROTON TRANSFER 199
9.3 CONCLUSIONS 201

10 FINAL REMARKS AND FUTURE PERSPECTIVES 203

11 REFERENCES 205

12 EXPERIMENTAL SECTION 219

12.1 MATERIALS AND METHODS 221
12.2 CONVERTION TO LEUCO FORM 221
12.3 MAYA BLUE -TYPE COMPOUNDS SYNTHESIS 222
12.4 ABSORPTION 222
12.5 STEADY-STATE FLUORESCENCE 223
12.5.1 FLUORESCENCE QUANTUM YIELDS AT ROOM TEMPERATURE 223

12.5.2 SOLID-STATE FLUORESCENCE QUANTUM YIELDS 224
12.6 REACTION QUANTUM YIELD 225
12.6.1 REACTION QUANTUM YIELD OF LEUCO FORM PHOTOISOMERISATION 226
12.6.2 REACTION QUANTUM YIELD FOR INDIGO AND POLYMERIC INDIGO 228
12.7 TIME-RESOLVED FLUORESCENCE 229
12.7.1 FLUORESCENCE DECAYS WITH NANOSECOND TIME-RESOLUTION 229
12.7.2 FLUORESCENCE DECAYS WITH PICOSECOND TIME-RESOLUTION 230
12.8 PHOSPHORESCENCE 231
12.9 ROOM TEMPERATURE SINGLET-OXYGEN PHOSPHORESCENCE 231
12.9.1 SINGLET-OXYGEN FORMATION QUANTUM YIELDS 232
12.10 TRIPLET-TRIPLET TRANSIENT ABSORPTION SPECTRA 233
12.10.1 TRIPLET MOLAR ABSORPTION COEFFICIENTS MEASUREMENT 233
12.10.1.1 SINGLET DEPLETION METHOD 233
12.10.1.2 ENERGY TRANSFER METHOD 234
12.10.1.3 PARTIAL SATURATION METHOD 235
12.10.2 INTERSYSTEM CROSSING QUANTUM YIELDS DETERMINATIONS 236
12.11 TIME-RESOLVED PHOTOACOUSTIC CALORIMETRY 237
12.12 REFERENCES 239

ABSTRACT

A comprehensive characterization of the excited state of some of the ancient dyes – indigo, dragon's blood and brazilwood – used to "dye the world" has been the aim of the work presented in this thesis.

The study involves a detailed photophysical and spectroscopic characterization which includes, absorption, fluorescence, phosphorescence (when present) and triplet-triplet absorption spectra together with measurements of quantum yields (fluorescence, phosphorescence, intersystem crossing, internal convertion and singlet oxygen formation) and excited state lifetimes have been obtained.

With indigo (and its substituted derivatives), in its reduced (leuco) form, the occurrence of isomerisation was found to be present in the first excited singlet state with photoreaction quantum yield of 0.09. The excited states of the oxidized and third form of indigo, Dehydroindigo (DHI), was, for the first time fully characterized including with ab initio calculations. It was forund that this spieces displays triplet state yields of 70-80% and negligible fluorescence in contrast with the keto (neutral) form of indigo where the main excited state deactivation pathway occurs via the radiationless $S_1 \sim\sim\rightarrow S_0$ internal conversion channel, mirrored in a very low fluorescence quantum yield $\sim 10^{-3}$ and a fluorescence lifetime of ~140ps.

Thioindigo (TI), and ciba brilliant pink (CBP) (the two are sulphur derivatives of indigo), were studied in solution at 293 and 77K; due to its high fluorescence quantum yield (~0.7) they were used as fluorescent probes for the investigation of the level of interaction (including encapsulation) with attapulgite and sepiolite clays, aiming to get a deeper understanding of Maya Blue (a pigment resulting from the mixing of indigo with attapulgite).

Incorporation of these sulphur derivatives in the clay pores, brought new colors to our laboratory, the original reddish, highly fluorescent (in solution) thioindigo turned into blue in attapulgite and violet in sepiolite, whereas the chlorinated CBP (reddish) turned into pink in both clays. When interacting with attapulgite and sepiolite clays CBP and TI the $S_1 \sim\sim\sim\rightarrow S_0$ was found the major deactivation pathway, in contrast with the behaviour found in solution, where fluorescence dominates with ~60% (solvent dependent) of the quanta loss.

Dracorhodin and Dracoflavylium, two dyes extracted from the resin of dragon's blood tree, have also been characterized, and showed the typical flavylium network of reactions. The kinetics of these reactions was studied in aqueous solutions, and a pK_a of 3.5 for dracorhodin was determined. Dracoflavylium was also investigated in dimethylformamide and in acidified and basified solutions of this solvent and fully spectral and photophysically characterized; similarly to indigo and other investigated dyes, the internal conversion from the singlet excited to the ground state was found the dominant deactivation pathway.

The dyes from Brazilwood, the tree in the origin of the Brazil country name, were extracted and investigated. Brazilwood has uncolored brazilin as major component which when exposed to air and light oxidizes leading to the red brazilein. The photophysical characterization of both brazilin and brazilein was also undertaken, which was found pH dependent.

RESUMO

O principal objectivo do trabalho constante desta tese foi o de obter uma completa caracterização do estado excitado de alguns dos mais antigos corantes – índigo, sangue de dragão e pau do brasil- utilizados desde tempos imemoriais para dar cor ao mundo.

O estudo compreende uma completa caracterização fotofísica e espectral, incluindo, absorção, fluorescência, fosforescência (quando possível) e também absorção tripleto-tripleto juntamente com medidas de rendimentos quânticos (fluorescência, fosforescência, cruzamento intersistemas, conversão interna e formação de oxigénio singuleto) e tempos de vida do(s) estado(s) excitado(s).

Para o índigo, e alguns dos seus derivados substituídos, na forma reduzida (leuco) a ocorrência de isomerização foi investigada no primeiro excitado singuleto com um rendimento quântico de reação para este processo de 0.09. Os estados excitados da forma oxidada do indigo, o dehidroindigo (DHI), foram pela primeira vez completamente caraterizados, nestes se incluindo cálculos *ab initio*. Mostrou-se que esta espécie apresenta rendimentos quânticos de estado tripleto variando entre 70-80% com rendimentos de fluorescência muito baixos; tal verificou-se estar em oposição ao comportamento apresentado pela forma ceto (neutra) do índigo na qual a principal via de desactivação do estado excitado ocorre através do canal de desativação não radiativo de conversão interna $S_1 \sim\sim\rightarrow S_0$, traduzido num rendimento quântico de fluorescência muito baixo $\sim 10^{-3}$ e um tempo de vida de ~140ps.

O tioindigo (TI) e o "ciba brilliant pink" (CBP) -onde em ambos o grupo N-H do índigo foi substituido por enxofre- foram estudados em solução a 293 e 77K; devido ao seu elevado rendimento quântico de fluorescência (~0.7), foram utilizados como sondas fluorescentes do nível de interacção (incluindo

encapsulamento) em argilas, atapulgite e sepiolite, visando uma melhor compreensão do pigmento Azul Maia (pigmento resultante da mistura de índigo com attapulgite).

A incorporação destes tio-derivados nos poros (ou canais?) das argilas, permitiu adicionar novas cores à palete disponível; desde o vermelho original do tioindigo ao azul e violeta resultantes respectivamente da mistura com attapulgite e sepiolite. Quanto ao CBP (igualmente de cor vermelha) este produziu um magnífico e estável rosa em ambas as argilas. Ao serem incorporados nas argilas a conversão interna $S_1 \sim\sim \rightarrow S_0$ mostrou ser o principal processo de desactivação do TI e do CBP, contrastando com o que acontece em solução onde a fluorescência domina correspondendo a 60% (dependendo do solvente) do processo de desativação do estado excitado.

A Dracorodina e o Dracoflavílio, dois compostos extraídos da resina de Sangue de Dragão, foram igualmente estudados nesta tese. Ambos os compostos apresentam a rede de reações caraterística dos flavílios. A cinética destas reações foi seguida em meio aquoso para a Dracorodina e obtido um pK_a de 3.5. O Dracoflavílio foi também caracterizado espectroscopica e fotofisicamente em dimetilformamida e soluções ácidas e básicas deste solvente; tal como se observou com o índigo, e outros corantes investigados, a conversão interna constitui a via dominante de desactivação do estado excitado.

Os corantes do Pau do Brasil, a árvore na origem do nome do país, foram extraídos e estudados. O Pau do Brasil tem como principal componente a brasilina, que quando exposta ao ar e à luz oxida formando a brasileína (de cor vermelha). A caracterização fotofísica de ambas (brasilina e brasileína) foi também efetuada, verificando-se ser dependente do pH.

ABBREVIATIONS

CBP	Ciba Brilliant Pink
DRF	Dracoflavylium
DHI	Dehydroindigo
DMF	N,N-Dimethylformamide
DPT	Double Proton Transfer
DBMNI	4,4'-dibutoxy-7,7'-dimethoxy-5,5'-dinitroindigo
DFT	Density Functional Theory
DMSO	Dimethyl Sulfoxide
Δ_{SS}	Stokes shift
ε_{SS}	Singlet extinction coefficient
E_T	Triplet energy
ESPT	Excited State Proton Transfer
ESIPT	Excited State Intramolecular Proton Transfer
ε_{TT}	Triplet extinction coefficient
ϕ_{Δ}	Singlet oxygen formation quantum yield
ϕ_F	Fluorescence quantum yield
ϕ_{IC}	Internal conversion quantum yield
ϕ_{Ph}	Phosphorescence quantum yield
ϕ_T	Triplet formation quantum yield
FTIR	Fourier Transform Infrared Spectroscopy
FWHM	Full-Width Half-Maximum
HOMO	Highest occupied molecular orbital
HPLC	High-Performance Liquid Chromatography
k_F	Fluorescence rate constant
k_{IC}	Internal conversion rate constant
k_{ISC}	Intersystem crossing rate constant
k_{NR}	Non-radiative rate constant
λ_{max}^{Abs}	Absorption wavelength maximum
λ_{max}^{Fluo}	Fluorescence wavelength maximum
λ_{max}^{Phosp}	Phosphorescence wavelength maximum
$\lambda_{max}^{T_1 \rightarrow T_n}$	Triplet-triplet absorption wavelength maximum
LUMO	Lowest unoccupied molecular orbital
MB	Maya Blue
MpreCiba	Methylated preCiba

VMD	Visual Molecular Dinamics
NMR	Nuclear Magnetic Resonance
PAC	Photoacoustic Calorimetry
S_0	Ground state
S_1	Lowest singlet excited state
S_2	Second singlet excited state
S_Δ	Singlet oxygen sensitization efficiency
SPT	Single Proton Transfer
T_1	Lowest triplet excited state
TI	Thioindigo
TEM	Transmission Electron Microscopy
TDDFT	Time-Dependent Density Functional Theory
τ_F	Fluorescence lifetime
τ_{Ph}	Phosphorescence lifetime
τ_T	Triplet lifetime
XRPD	X-Ray Powder Driffraction

In the world of colour, the creation of the eyes, about 543 millions of years ago, was a crucial step, but at that time the colour also determined who ate dinner and who ended up on the plate. The extinction of dinosaurs was probably the most important volte-face, since then mammals could stop living hidden in the darkness and could come out to daylight, and for that their retina, which was only used in the shadows and was concentrated in rods and colour-blind (achromatic) structures, then evolved to colour shades and forms. This evolution was a significant nutritional advantage, once it turned possible the distinction between plants, animals, seeds, fruits, poison, non-poison.[2,3]

Exceeded the survival motives, the colour has always seduced mankind. Since man started to wear clothes he tried to reproduce nature colours for his garments, artefacts and jewellery.

In antiquity, sight is the primary sense and the first to be mentioned. According to the Judeo-Christian religious tradition, God did not say "Let there be sound", or "Let there be odours", but "Let there be light". And so it was. The theme reappears in the bow of colours across the sky signifying a pact between God and humankind.[4]

Dyestuffs and dyeing are as old as textiles themselves. Especially in the past, for dyeing and painting, almost the same colouring organic material was used.[5] Early dye sources included, plant, animal and mineral extracts. Madder, indigo and saffron were the three ancient dyes used in India *ca* 2500 years B.C..[6]

The earliest book devoted exclusively to professional dyeing was published in Venice, in 1548. This was Gioanventura Rosetti's *Plictho de larte de tentori che insegn tenger pan(n)i banbasi et sede si Per larthe magiore com per Ie comvne*, which included details of dye recipes and techniques employed in Venice, Genova, Florence, and elsewhere in Italy. In particular, it provided the most complete record of the dyers craft at the time when the first South American dyewood was becoming available

in Europe. Until then three primary colours were employed by dyers. Blue was obtained from indigo, either from woad or the indigo plant. Reds were available from the Kermes insect, from the root of the madder plant, and from so-called brazilwood imported from the Far East. Yellows were extracted from weld, Persian berries, saffron and dyers broom. These colours were combined to afford greens, browns, violets and other compound shades; they could be varied with the aid of a mordant. The use of a mordant expand the list of colours that could be obtained from most of these dyes.[7]

Picture of a cupboard with dyes used in XV century, taken at *Albrecht Dürer's house, in Nuremberg. (Personal copy)*

The studies on colour soon started. Aristotle (384-322 B.C.) did some of the early studies and theories about light and colour, using philosophy and painting. He defended that colour is an inherent property of the objects and discovered that mixing two colours a third is produced. In 1666, Isaac Newton performed his *Experimentum Crucis*, and announced that colour is an illusion arising from the response of human visual apparatus to emissions of light. *Experimentun Crucis* consisted in focusing sunlight (or white light) in a glass prism, and a mixture of rays appear in the opposite site, what proved that light is a not a uniform, pure substance. Newton adopted the term "spectrum" to characterize his rainbow image of seven colours.[3]

Actually, according to a consensus of psycho-physiological and philosophical theories, colour sensations are generated in a cerebral "space" fed from photon-photoreceptor interaction in the retina of the eye. The resulting "space" has three dimensions: hue (or chroma), saturation (or "purity"), and brightness (lightness, value or intensity).[2]

The discovery of mauveine, in 1856 by W. H. Perkin, was the turning point in the history of colouration; indeed, mauveine was the first successful synthetic dye, instead of being extracted from natural sources by tedious procedures. This represented the beginning of a "new world", with a wide range of colours available, with good fastness properties and with low to moderate costs. For all reasons the world of the synthetic dyes, and dye manufacture has become a significant part of the chemical industry.[8]

Nowadays, a revivalism in the natural dyes has reborn, moved by several motives, like the reconstruction of ancient and traditional dyeing technology, conservation and restoration of old textiles and museum textiles, and environmental reasons.[6]

1. INDIGO

1.1.1 – THE MILLENARY HISTORY OF INDIGO

The history of indigo as a source of blue colour for textiles, paintings, illumination, etc., has more than four millennia. It is reported to have been used in the XVIII dynasty of Egypt (~ 1600 B.C.). Its longevity as a colouring material has given it a mythical status turning indigo the molecule that made a link between the Western and Muslim civilizations. A large amount of information is available on natural indigo (valid for both the chemical compound and the plant from where it is obtained), but the origin (place and date) of the dye's discovery is still unknown in our days. It seems however certain that wherever indigo-bearing plants grew, earliest man was able to use the extracted pigment. It could hardly have escaped the attention of primitive man that certain plants, not particularly coloured in their own right, when crushed or applied to the skin or clothing, subsequently developed a blue colour which almost outlasted the substrate.[9]

Drawing of a specimen of *Isatis tinctoria*; taken from ref[1]

Indigo belongs to the class of the so-called vat dyes: these are dyes that can be reduced to a compound which is soluble in aqueous alkaline media and is used in this form for dyeing purposes.[9]

KETO

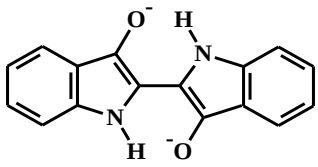

LEUCO

Scheme 1- Structures of indigo's neutral (keto) form (insoluble in water), and reduced (leuco) form (soluble in water).[10]

The yellowish reduced form of indigo is almost colourless – hence its name *leuco*-indigo (from the Greek word for white) – and, of crucial importance in the dyeing process, it is highly soluble in water (Scheme 1). Indigo-bearing plants are endogenous and grow in many parts of the world since antiquity: for example *Isatis tinctoria* in Northern Europe and *Indigofera* species in Asia. The two plants are quite distinct – for example one grows in temperate climates and belongs to the mustard family whereas the other prefers warmer climates and belongs to the pea family – but both yield, in different amounts, the indigo dye.[9]

Indigo has also an animal origin, the mollusc *Murex trunculus* from where Tyrian Purple (6,6'-dibromoindigo) was extracted. This particular origin of indigo is very important to the Jewish religious ritual who calls for the use of indigo-containing biblical *Tekhelet* derived from *Murex trunculus*, but its use seems to have ceased between 570 and 760 A.D..[9]

1.1.2-INDIGO: FROM ANTIQUITY TO MODERN TIMES

Indigo: synthetic, extracted and fabric dyed with indigo.

The art of applying colour to textile fabrics goes far back into antiquity. The finding of coloured fabrics in the course of excavations in Egypt, Asia, and the Americas has proved beyond question that textile colouration was developed independently and practiced by almost all primitive peoples.[11]

Some several primitive groups discovered, by their own, locally different sources of colouring matter. However, as tribes migrated and contact with other groups was established, men learned on dyestuffs which were faster or more brilliant than any to be found on their own vicinity, and trade in dyestuffs began.[11]

As India was the key player of early trade both eastwards and westwards, with a population highly accomplished in textile arts, much technical know-how would have filtered along the trading routes, and subsequently India's trade textiles where to had an enormous impact globally.[12]

As in other areas whose indigo production was subsequently exploited by European colonialists on a vast commercial scale, in Central and South America the dyestuff had long been widely used.[12]

In Central America sixteenth-century Spanish historians noted the local importance of fine textiles as gifts at festivals and weddings and to signify status. Here, as in ancient Egypt, blue was generally a revered colour. [12] The Aztecs also used indigo as medicine, and are responsible for the common name in the region

for the 'blue herb', *iquilite*. The Mayans mixed indigo with an exceptional clay (attapulgite) mineral to produce the 'Maya Blue' pigment, widely used for painting on murals, sculptures and ceramics, as well as textiles.[12]

In Europe from the late eight century the impact of the Viking invasion from Scandinavia was widespread. The Vikings traded in exotic textiles from the Near East to feed Europe's developing taste, as well as introducing their own high quality textiles.[12]

Until the later sixteenth century imported indigo pigment remained an expensive luxury in the northern Europe, largely reserved for paints and inks. All the obstacles and expenses attendant on the long, hazardous journeys by caravan, or sea, made it an exotic commodity like pepper, other dyestuffs and mordants, medicines and perfumes, which all formed part of the overall spice trade. [12] Across much of Asia, where textile manufacture was the main industry, indigo was a mainstay. Prices for indigo dyestuff fluctuated greatly, but often doubled those of other luxury goods. The main dyes apart from indigo were: madder, kermes, brazilwood and, later, lac for reds; saffron, curcuma (turmeric) and safflower (producing also orange and red) for yellows. Combinations of these dyes created an infinite variety of colours, indigo featuring especially in greens, blacks and purples. [12]

Textiles dyed blue with indigo from woad appear in the early Iron Age (c.700 B.C.). While indigo was the centre stage in the textile industry of the Orient, woad was still firmly in Europe's spotlight. Woad was Europe's truly universal dye, used for all blues but also as a 'top' or 'bottom' dye for most other colours. Regions most renowned for woad production were found in France, Germany, Italy and, later, in England. Spain's central regions grew woad, but a good deal more had to be imported. France was Europe's greatest producer of woad, called

there *pastel*. Such was the importance of woad that even in times of war unarmed ships were permitted to enter port to load it.[12]

Despite the wide-scale availability of imported oriental indigo from the seventeenth century, woad was still grown and used in Europe, and all those with a vested interest fought hard for its survival. As well as being a lucrative crop for the producers, its labour-intensive processing provided valuable work for the unemployed. The circumnavigation of the Cape of Good Hope by Portuguese ships in 1498, was responsible for indigo's meteoric rise, setting woad's relegation to the bottom division of the dyeing league and marked a crucial point in indigo's fortunes, as did the Spanish conquest of America in the following century. The Portuguese achievement made possible direct importation by Europe of goods by sea from India, the Spice Islands, China and Japan, and thus avoidance of the heavy duties levied by successive rulers on Asian goods whether in transit overland to the West or by the old sea routes around the Arabian Peninsula. In this way the Portuguese broke the Middle Eastern and Italian commercial control over trade in spices, which included dyestuffs, and in luxury textiles. Indigo was often the most valuable of all the 'spices', and progressively mined the whole European woad industry.[12]

In recent years the art of textile decorating has improved markedly, owing to the introduction of a host of nearly developed dyes and pigment colours, and auxiliary chemicals to facilitate their application. All the natural dyes except a mere handful, including logwood, fustic, and cutch, have been replaced. Modern colours are relatively inexpensive, brilliant in shade, and of a wide range of hues. [11]

The structural determination and synthesis of indigo[13] were triumphs of the growing German chemical industry of that time. Adolf von Baeyer was awarded the Nobel Prize of 1905 in recognition for his contributions to chemical synthesis, citing his synthesis of indigo specifically.[14]

1.1.3 – INDIGO IN THE ANTIQUITY: THE BLUE OF THE EGYPTIANS AND THE PURPLE OF THE PHOENICIANS

In ancient Egypt, where blue colours were revered, many archaeological textile fragments have been preserved thanks to the dry climate, sterile sand and local burial customs. The country's woven textiles were widely esteemed, and weavers began to insert rare blue stripes into the borders of plain linen mummy clothes from the Fifth Dynasty (c.2400 B.C.), probably because only indigo dye is well absorbed by flax fibbers. Indigo-dyed linen and occasionally wool (a much easier fibber to dye) are more commonly found, sometimes as part of multi-coloured patterns, in textiles dating from the Middle Kingdom (from c.2040 B.C.) and particularly the New Kingdom (from c.1560 B.C.). The celebrated funerary wardrobe of Tutankhamun, for example, includes a state robe that is predominantly blue, and also other garments and embroidery threads with some blue.[12]

Hieroglyphic inscriptions, such as those at the largely Ptolemaic temple of Dendera, which show the Egyptians' appreciation of several different shades of blue, mention plants producing a blue colour resembling lapis lazuli. It is botanically possible that local *Indigofera* species could have been used as a blue dye by the ancient Egyptians, but it is most likely that they made use of the woad plant, *Isatis tinctoria*, indigenous in parts of north Africa as well as in Europe and western Asia, even though it is much less efficient as a source of indigo dye than the tropical and subtropical indigo plants.[12]

Another source of blue was the so called Egyptian Blue, the first synthetic pigment. Egyptian Blue is a chemical compound with the formula $CaCuSi_4O_{10}$, and it can be obtained relatively easy if the minerals lime ($CaCO_3$), sand (SiO_2) and a copper mineral (e.g. malachite ($Cu_2(CO_3)(OH)_2$) or azurite ($Cu_3(CO_3)_2(OH)_2$)) or metallic copper are exposed to oxygen (O_2) and, together with a few percent of a

flux such as potassium carbonate (K_2CO_3), sodium (NaCl) or sodium sulfate (Na_2SO_4), are heated to temperatures between 800 and 900ºC.[15]

The blue pigments were invented from necessity. Humans did not have unlimited access to blue as pigment, as blue is not an earth colour, or colour provided by the surface soil. The Egyptians, along with the knowledge about the production of the "Egyptian Blue", transmitted it to many cultures in the Mediterranean area and beyond.[15]

Photograph of Murex snails, and a piece of cotton dyed with Tyrian purple drawn in Albrecht Dürer's house, Nuremberg.(Personal copy)

Shellfish purple is indigo closely related shell-fish dye which was extracted from species belonging to *Muricidae* and *Thaididae* families. This was famously used by aristocratic Phoenicians, Romans and Byzantines, hence the common epithet 'Royal', 'Imperial' or 'Tyrian' (for Tyre, the city, who produced the best quality product). Purple dye became the trademark of the Phoenicians. It reached its apogee as a status symbol during the Roman and Byzantine empires before its relegation to the sidelines of dye history following the Turkish conquest of Constantinople in 1453. Thereafter knowledge of its production methods vanished.[12]

Shellfish purple residues have been found in potsherds of ancient Israel thought to have formed clay dye vessels. Dyed textiles had great significance in Jewish religious ritual. Hebrew law, for example, prescribed the wearing of *tekhelet* fringes and tassels, which are presumed to have been dyed with shellfish purple.[12]

Tyrian purple possessed great brilliance and fastness in comparison with other known dyes.[11]

In Greco-Roman times, the importance of Murex to the city of Tyre was mirrored in the city's coins, many of which bear an image of the snail, 16 others show a dog and a snail. According to the legend, the purple dye was first discovered by Hercules's dog, who was frolicking in the waves, foraging for food; when he emerged from the ocean and returned to his master, with the lips coloured with bright purple from the snails he had consumed.[16]

Is generally accepted that in the Mediterranean the main reddish species were *Murex brandaris* and *Purpura haemastoma*, while the hermaphrodite *Murex trunculus,* produced the bluer hues. Indeed, in addition to purple this mollusc apparently contained pure indigo. It has been argued that this may be related to the gender, the bluer colours being produced during the masculine phase. However, the outcome is certainly also affected by the dyeing methods, climatic conditions and seasons, particularly to sun exposition.[12]

Huge quantities of shellfish had to be killed in order to extract, from the tiny hypobranchial glands, enough of the photo-sensitive whitish secretion containing the precursor to purple: about 10,000 mollusks to obtain 1g of dye.[15]Beaches in Tyre and Sidon as well as in Crete are still piled with heaps of left-over shell deposits. Shellfish purple dyers, like those for indigo, needed dedicated knowledge.[12]

Indeed, the general method for extracting the colour from purple shellfish was to crush the molluscs, shell and all, or open them and remove the gland, then salt the mass for three days, and, finally, boil the whole in water for about ten days. The result was a clear concentrated solution of the dye. Flesh fragments and the insoluble foreign bodies were removed by skimming. The fabric was exposed to

sunlight after steeping in the solution in order to develop the true brilliant colour of Tyrian purple.[11]

The chemical formula of Tyrian purple is related to the formula for indigo. It is the indigo molecule brominated at the 6,6' positions.[11]

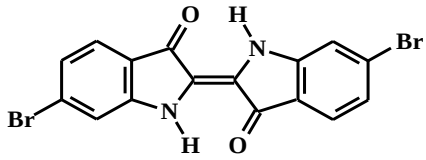

Scheme 2- Structure of Tyrian purple (6,6'-dibromoindigo)[10]

1.1.4 – THE MYTHIC BLUE OF THE HEBREWS: THE *TEKHELET* AND ITS LOST SECRET

In the ancient world, colours and dyes held great social and economic importance. Dyes like *tekhelet*, extracted from rare sources, could only be used by the wealthiest and most powerful people.[16]

In the Bible of the Hebrews, "blue (*tekhelet),* purple (*argaman*) and scarlet (*tola'at-shani*)" yarns are listed along with gold, silver and copper as gifts suitable for God (Exodus 25:4). The desert Tabernacle was made of ten strips of "fine twisted linen, of blue, purple and scarlet yarns, with a design of cherubim worked into them" (Exodus 26:1). In the Torah, God instructs his people to "make for themselves fringes on the corners of their garments (and) attach a cord of blue (*tekhelet*) to the fringe at each corner" (Numbers 15:37) as a reminder to keep his other commandments.[16,17]

The source for this biblical blue dye is not mentioned in the Bible, and although it is discussed in the Talmud and other ancient sources, the process for obtaining the dye was lost by the Jews. By the turn of the first millennium A.D., *tekhelet* was no longer available. It is not totally clear why *tekhelet* disappeared: perhaps it was because of its high cost or because Jews had lost access to materials needed for its production.[16,17]

At some point, a cheaper alternative was made available although, this too, felt out of use along with *tekhelet*. A blue dye made from the *kala ilan* plant (popularly known as indigo or woad) came to be used by unscrupulous merchants, despite many rabbis' objections. The dye from *kala ilan* looked just like *tekhelet*; the Talmud says that only God could distinguish between the two.[16]

There are some aspects that still need some attention, the gender of the *Murex* snail (male or female) originate indigo and 6,6'-dibromoindigo, respectively, so the dye obtained is not pure. 6-bromoindigo (MBI) can also be formed, if the hypobranquial gland contents of male and female are mixed before all precursors present have formed 6,6`-dibromoindigo and indigo. If sufficient MBI is thus produced, the dyeing will not be violet but purple. This explains why banded dyed with *Murex* may vary in hue from reddish to bluish purple. [17,18]

The *Murex* gland, when first removed from the snail, is yellowish, but when exposed to the air (for five to ten minutes), it becomes purple.[16,17] The molecule is capable of forming a chemical bond with wool, which is what makes it a permanent colour that will not wash out. To create a permanent bond, several chemical reactions must take place. First, limestone or another base must be added to water to create a basic solution. In the following step, the solution must be reduced— meaning that the oxygen must be removed, using a chemical such as ammonia (Pliny in his *Natural History* recommended using old urine, which contains ammonia). This causes the dye to dissolve and the solution to turn into a

darkish yellow-brown colour. At this point, the dye is ready for dyeing purposes. Wool dipped in the solution will remain white until it is pulled out and re-oxygenated through contact with air. Sunlight causes the bond between the bromine atoms and the indigo molecule to break down, leaving only indigo—blue dye—active in the solution.[16]

In order to recover the recipe and therefore the identity of an ancient Jewish ritual an Israeli association has been created **'P'til Tekhelet'**, established for the Promotion and Distribution of Tekhelet. (http://www.tekhelet.com/).

1.1.5- BIOSYNTHESIS OF INDIGO

The indigo dye is obtained from the leaves of *Indigofera tinctoria* by a fermentation process which has probably not changed for over 3000 years.[9,12] Bundles of tied pieces of *Indigofera* are packed into fermenting vats, and covered with water, in order to promote fermentation, which ceases in about 10-15 hours. The yellowish liquor formed, is beaten, by men or machinery, and changes its colour, from green, to blue, and finally the indigo precipitates to the bottom of the vats. This pulpy mass of indigo, after drawn off the supernatant, is boiled with water (to remove impurities), filtered and pressed to remove as much of the moisture as possible, cut into cubes and left to air dryness.[9]

Since *Indigofera tinctoria* and *Isatis tinctoria* are different kind of plants, one is a bush and the other is a flower, they have different approaches in order to obtain the dye product.

Going from *Isatis tinctoria* the process pass also by fermentation. The seeds are sown in a deep rich well drained loam. When the plants grow they are weeded twice, taking out the leaves and subsequently washed. Using a wool mill, the leaves

are crushed, and after that, using the hands, the pulp is drained and kneads into ball ("woad balls"). One to four weeks is the time needed to dry those balls. When dried, the balls are broken up and pilled into layers 2-3 feet deep, and sprinkled with water. Fermentation, initially vigorous, takes place over about 9 weeks and generates a disgusting odour. When complete, the dark clay-like material is dried, sifted and packed into barrels for sale to dyers or woad merchants. The quality of woad was said to improve with time, being twice as efficient after four years' storage.[9]

The chemical transformations that occur in the processing of the leaves from the woad plant are outlined in Scheme 3. [9,19]

Photograph of Indigo balls, drawn in Albrecht Dürer's house in Nuremberg. (Personal copy)

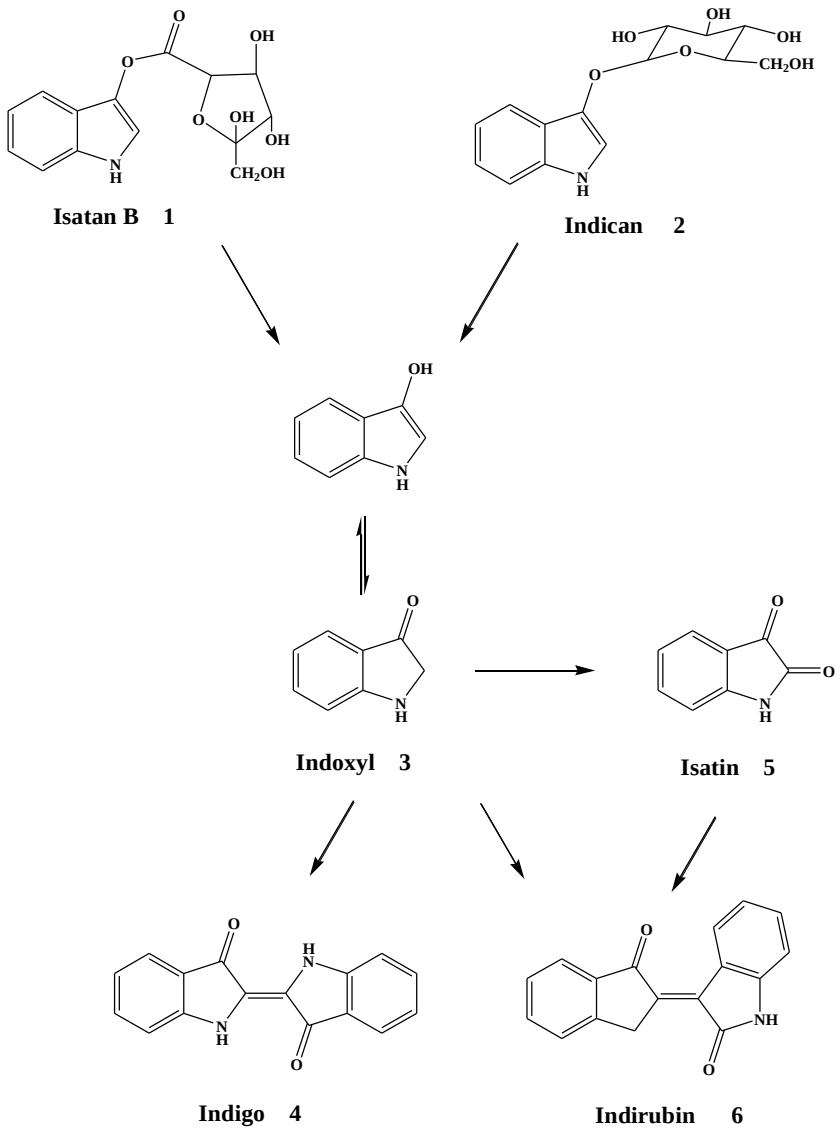

Scheme 3 – Formation of indigo from indoxyl derivatives present in woad leaves. Free indoxyl is released by hydrolysis from isatan B and indican and, subsequently, dimerizes to indigo. Isatin is generated from indoxyl in an oxygen-rich environment (with action of oxigenase enzyme) as a side reaction; the condensation of indoxyl and isatin gives rise to indirubin.[19,20]

Some studies[19] mention the fact that the woad ball manufacture is the key step in the production of indigo from woad, increasing the indigo yield and reducing the proportion of indirubin, considered of less value than indigo. It is likely that, when the leaves are crushed, the indoxyl is cleaved from isatan B and indican by enzymes of plant and/or bacterial origin to release the free indoxyl (Scheme 3).[19] In the main body of the freshly prepared woad ball, microbial respiration would probably lower the oxygen tension, which would return to atmospheric levels as the ball dried slowly. This limited oxygen supply facilitated indigo formation, and by restricting oxidation of indoxyl to isatin (5), constrained indirubin formation (Scheme 3).[19] The amount of dye that can be obtained from woad (*Isatis tinctoria*) is much less than that from *Indigofera*.[9]

1.1.6- INDIRUBIN: ISOMER OF INDIGO

Indirubin (Scheme 4), is the 3, 2'-bisindole isomer (red-coloured) of indigo, found as active principle in the traditional Chinese curative medicine. This compound is currently known to be pharmacologically active against various diseases, including leukaemia, inflammation, psoriasis and skin rashes. [20,21] It is produced by a natural fermentation process using indican as a substrate, which is abundant in the same plants used to extract indigo. In this process, indican is converted into indoxyl by the activity of β-glucosidase, after which indigo is generated by spontaneous oxidation of indoxyl (Scheme 3). A small amount of indirubin can also be produced as the end product of the oxidation between indoxyl and isatin (a

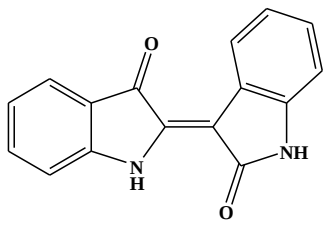

Scheme 4 - Indirubin

derivative generated by an oxygenase) in this process.[20,22,23] The amount of obtained indirubin has more to do with the extraction method then with the origin or species of the natural source.[23]

1.2- THE CHEMISTRY OF INDIGO

1.2.1- THE SYNTHETIC VIA: THE BAYER AND HEUMANN REACTIONS

Indigo was, for many centuries, obtained from natural sources. The chemical structure of indigo was first proposed by von Baeyer in 1869, and eleven years later he reported the first successful synthesis, a multistage route starting from *o*-nitrocinnamic acid.[24] Indeed, later on, in 1880, Adolph von Baeyer developed a method – the Baeyer-Drewson reaction, Scheme 5, an Aldol Condensation reaction - to produce the first synthetic indigo.[13] This reaction works well for small scale reactions but is not adequate for large scale industrial production of indigo; the reaction (Scheme 5) involves the use of o-nitrobenzaldehyde which is dissolved in acetone in aqueous sodium hydroxide, leading to indigo production, within a few seconds, in good yield.[24]

Until Baeyer came up with the correct structural formula for indigo, synthetic via for indigo were few and with no commercial importance. With a target structure to aim for, synthetic routes proliferated, but most were uneconomic owing to the high cost of the starting materials. Thus, the route of indigo persisted for several years after Baeyer's elucidation. However, in the first six months of 1900, manufacturers in Germany exported 930 tons of synthetic indigo and the demand for the natural product fell by 40 per cent.[25]

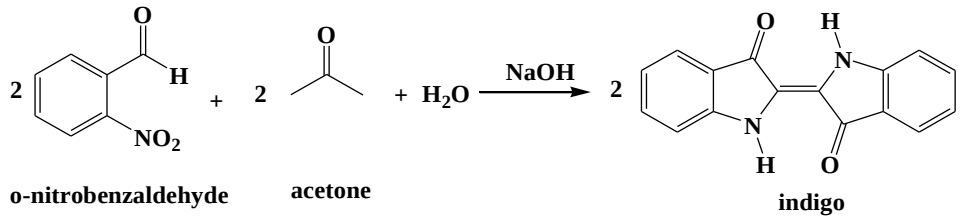

Scheme 5- The Baeyer-Drewson reaction of 2-nitrobenzaldehyde with acetone in basic conditions to produce indigo. [13]

The first successful commercial synthesis of indigo, due to Heumann in 1897, is shown in Scheme 6.

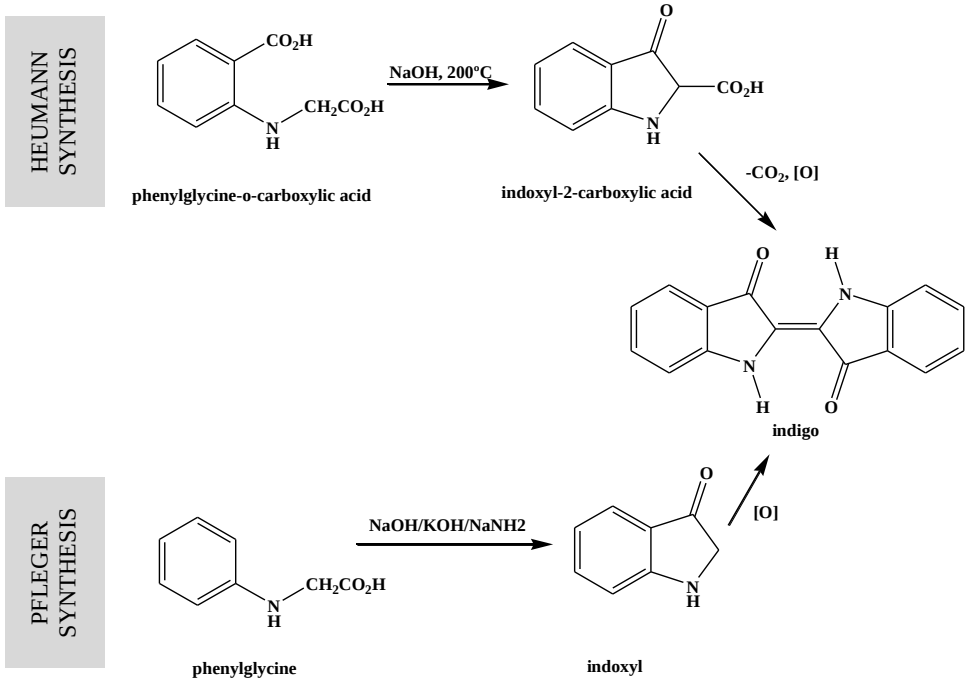

Scheme 6 - Heumann and Pfleger synthesis for indigo. [26]

In this classical synthesis, phenylglycine-*o*-carboxylic acid is converted by fusion with sodium hydroxide at around 200 °C, in the absence of air, into indoxyl-2-carboxylic acid. This material readily decarboxylates and oxidises in air to indigo. A much more efficient synthesis, which forms the basis of the manufacturing method in use today, is due originally to Pfleger (1901). In this route, also illustrated in Scheme 6, the more readily available starting material, phenylglycine is treated in an alkaline melt of sodium and potassium hydroxides containing sodamide. This process leads directly to indoxyl, which undergoes spontaneous oxidative dimerisation in air to indigo.[26]

1.2.2 - THE COLOUR OF INDIGO AND DERIVATIVES: THE H-CHROMOPHORE AND MODERN THEORIES

In 1883 Bayer stated the Z-(cis) configuration for indigo, and only in 1928, Reis and Schneider[27], using X-ray crystal structure measurement, established that the correct structure is of the E – (trans) isomer. [28,29]

A unique and intriguing feature of indigo is that it absorbs at long wavelengths for a relatively small molecule, and the reason is the small energy difference between its ground and excited states.[28]

One way to classify dyes is to divide them into two types of groups: the chromophore, and the auxochrome. The chromophore group is the group of atoms mainly responsible for the colour, and auxochromes, provide "enhancement" of the colour.[30] Dilthey and Wizinger[31] refined that theory and stated that the chromophore is commonly an electron accepting group, and the auxochromes are usually electron donating and these groups are linked to one another through a conjugated system. [28,30] This gave rise to the concept of the

donor/acceptor dye type. Indigo can be considered as a donor-acceptor dye. The heterocyclic nitrogen atoms are electron donor groups while the carbonyl groups (C=O) are acceptors.[28] Semiempirical calculations performed from the 1960s to the 1980s led to the conclusion that the basic chromophore of the indigo dyes is the central C=C bond together with the adjacent C=O and N-H groups, which due to the particular design of indigo, where this groups are in a *trans* and H like geometry lead to the designation of indigo as an H-chromophore .[32-34,35]

Another explanation for the colour in indigo is, for example, based on the valence-bond theory. The assumption is made that the ground state of indigo closely resembles the structure given in Scheme 6, and the first excited state consists of resonance contributions from charge separated structures.[28]

Theoretical and experimental studies showed that neither the benzene rings nor the double bonds in the five-member rings are essential for the characteristic indigo spectrum.[28,29,33] Thus, the basic chromophore of the indigo dyes is the partial structure shown in Scheme 7.[28,32,33,36] This H-chromophore structure is responsible for the lowest transition observed in the visible spectra of indigoid dyes, which is close to 2 eV.[29]

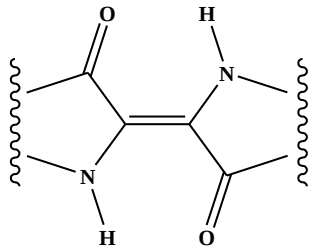

Scheme 7– The H-chromophore unit of indigo[28]

Ab initio methods were also used to support the H-chromophore teory.[29,35,37,38] From those studies arise the transition HOMO→LUMO as the responsible for the blue colour indigo, this corresponds to a $\pi \rightarrow \pi^*$ transition. As can be seen in Figure 1, the HOMO lies in the central C=C bond and the nitrogen atoms and the LUMO in the central C-C bonds and oxygen atoms.[35-37]

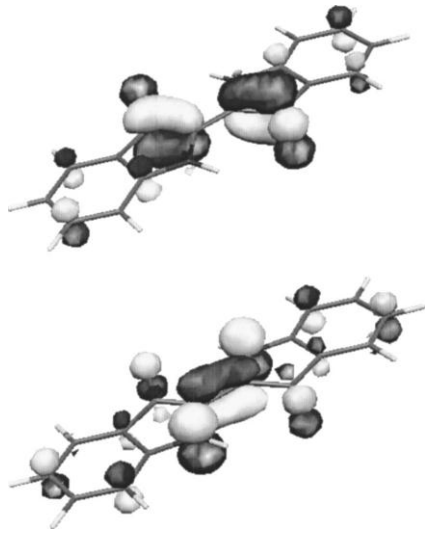

Figure 1 – Schematic representation of the HOMO (bottom) and LUMO (top) on indigo in CCl_4, from Jaquemin D. *et al.*.[37]

The position of the lowest absorption band (and therefore the colour) in indigo depends strongly on the solvent media, ranging from red (540nm) in the gas phase, to violet (588nm) in a nonpolar solvent such as CCl_4, and to blue in polar solvents such as ethanol (606nm) or in the solid state.[32,33,39]

Substituents may affect the energy level of the excited state either by (a) increasing or (b) diminishing electron release from the nitrogen atom or electron

withdrawal by the carbonyl group.[39] Substitutions at the 5,5'-positions lead to bathochromic shifts, and substitutions at 6,6' to hypsochromic shifts.[29,39]

1.2.3 - THE INDIGO'S COUSINS: TYRIAN PURPLE, INDIRUBIN, THIOINDIGO

The first synthesis of the sulphur analogue of indigo blue – thioindigo- was reported by Friedländer in 1906.[40] The synthesis was made from a multiple-step reaction involving anthranilic acid as the starting material.[41] Friedländer was thus able to produce a new, relatively stable red dye by substituting a sulphur atom on the -NH- group (see Scheme 8).[40] Anthranilic acid was a relatively inexpensive reagent, this reaction was commercially feasible and the industrial companies Kalle and Company, quickly followed by Farbwerke vorm. Meister, Lucius & Brunin and Ciba, produced this dye and several others with simple structural modifications.[41]

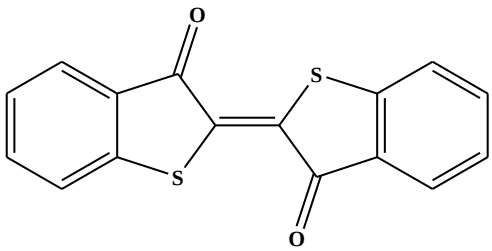

Scheme 8 – Structure of thioindigo

In thioindigo, the substitution of nitrogen with sulphur removes the internal hydrogen bonds of indigo, thus leading to a hypsochromic shift of the

absorption wavelength maxima, and allows a *trans-cis* isomerism. Remarkably, the hypso-shift was already pointed out by Friedländer in 1908, as he measured the first λ_{max} of thioindigo: 547nm in chloroform.[42]

Thioindigos are well-known photochromic dyes[33,35,36,39-45] with a reversible photochemical *cis–trans* isomerization.[27,28] They also typically exhibit a higher quantum yield of conversion from the *cis* to the *trans* form (rather than from the *trans* to the *cis* form) and a concomitant high fluorescence quantum yield of the *trans* form[43,45] . The *cis* form typically has very low, nearly immeasurable, intrinsic fluorescence. [43,45,46]

Indirubin (Scheme 4) and Tyrian Purple (Scheme 2) are, spectral and photophysically, much more closely related to indigo than is thioindigo.[10,38]

1.2.4 - THE STABILITY AND PHOTOPHYSICS OF INDIGO

One characteristic feature of the photochemistry of indigo is the absence of a photoinduced *trans* → *cis* isomerisation, that is, the twisting around the central C=C bond. The same applies to ring-substituted derivatives of indigo, which possess intramolecular hydrogen bonds between the adjacent C=O and the N-H groups. For indigo derivatives in which the intramolecular hydrogen bonds are absent, like thioindigo, the *cis* isomer can be readily generated by photoexcitation. [35,42,45,47]

Indigo has an extremely short lifetime of the lowest singlet excited state, which is related to its photostability. It has been found that the S_1 lifetimes of indigo, as well as of its ring-substituted compounds, such as indigo carmine (5,5'-indigodisulfonic acid disodium salt) or Tyrian purple (6,6'-dibromoindigo), are of the order of several tens or hundreds of picoseconds in the (natural) keto

form.[10,48-50] The excited-state lifetime of indigo is much shorter than the S_1 lifetimes of the leuco (reduced) form of indigo,[10,51] dehydroindigo (the oxidized form of indigo)[52], as well as other derivatives, such as thioindigo,[42,45] which are of the order of nanoseconds. These findings have suggested that a particularly efficient radiationless decay mechanism exist in indigo which is responsible for its exceptional photostability.[35,48,49] This mechanism will be further detailed in this thesis.

One of the possible mechanisms of the efficient deactivation of indigo is the occurrence of an excited state intramolecular proton transfer (ESIPT) along the hydrogen bonds between the adjacent C=O and N–H groups[44,45,47-49] Kobayashi and Rentzepis attributed the fast decay of the transient absorption of indigo to ultrafast internal conversion which is enhanced by excited state proton transfer rather than twisting of the central C=C bond.[53] In Coimbra, Seixas de Melo *et al.* found that the fluorescence of indigo and of its derivatives possessing at least one intramolecular hydrogen bond exhibits biexponential decay.[48,49] They assigned the short-time and long-time components to decays of the reactant (keto) and the product (enol) forms of ESIPT, respectively.

Iwakura *et al.* detected the transient formation of a single OH bond (rather than of two OH bonds) in the excited state of indigo carmine by a pump–probe measurement with sub-5 femtosecond time resolution.[54,55] They concluded that the ESIPT in indigo takes place via a single proton transfer (SPT) process rather than a double proton transfer (DPT) process. In a previous work Elsaesser *et al.*, on the other hand, on the basis of transient infrared spectra, were unable to find any evidence of ESIPT in indigo since a) their time-resolved IR spectra revealed that the NH stretching in the S_1 state was shifted to lower frequency only by 40cm^{-1} compared to the ground state, b) no evidence of a transient OH band

was found around 3200 cm^{-1} in the excited molecule, c) the C=O stretching mode at 1640cm^{-1} remained virtually unchanged upon photo-excitation.[56]

Nagasawa *et al.* found that the S_1 lifetime of indigo carmine, the sulfonated and the water soluble derivative of indigo, in solution strongly depends on solvent polarity.[57] They concluded that intermolecular hydrogen bonds between solute and solvent molecules play a more essential role in the deactivation process of indigo than the intramolecular hydrogen bonds of the solute molecule.

Using *ab initio* methods, Yamazaki *et al.* revealed, in a recent work[35], that the mechanism of the exceptional photostability of indigo is the excited state intramolecular proton transfer (ESIPT) reaction along the hydrogen bonds between the adjacent C=O and N–H groups.[35] The *trans* →*cis* photoisomerization via the twisting of the central C=C bond is strongly suppressed by the rigidity of the five-member rings. They also concluded that the potential energy for the SPT is much lower than the barrier for DPT. This can be explained by structural changes occurred during the ESIPT – the adjacent N-H and C=O groups have to approach each other, and for SPT this implies some rocking from those groups relatively to the central C=C bond. For DPT, the adjacent N-H and C=O groups, on both sides of the molecule, have to approach each other simultaneously – and this is not possible, so the option would be the shortening of the central C=C bond or deformation of C=O group. These deformations would raise considerably the energy of DPT structure, making this hypothesis impracticable. The same study also refers that the mono-enol form of indigo, the product of SPT, is more stabilized by the solvent, than the keto form. This internal conversion, accessible via the SPT process, causes a very fast nonradiative decay from the S_1 to the S_0 state.[35]

1.2.5 - THE INDIGO REDUCED FORM USED FOR DYEING: ANCIENT AND MODERN PATHWAYS

Some natural dyestuffs are "substantive", or "direct", meaning that with heat they will fix directly to a fibre with which they have affinity. However, most natural dyestuffs belong to a large group known as "adjective", which require an intermediate chemical substance, called a mordant, to make them fast.[6] The dye itself bonds with the mordant during the dyeing process. Found in this group are the majority of the natural dyes. Colours produced by mordant dyeing vary greatly depending upon which mordants are used, the basic ones being alum, iron and, in a less degree, chromium, although there were many other organic ones in the past. Indigo needs no mordant to make it fast to light and washing (its blue keto form is insoluble in water), and is deposited on the fibres as microscopic particles without needing to form a thorough chemical bond with them. This makes it exceptionally suitable for dyeing any type of fibre. [6]

The first stage of the dyeing process is to dissolve and reduce the insoluble dyestuff in a warm (about 50ºC) alkaline solution in a "vat" (named after the deep wooden barrels used by medieval woad dyers).[12] That is why indigo belongs to the group of vat dyes, which are almost insoluble in most organic solvents and in water, but can be converted into the water-soluble leuco form which, in most cases, is pale yellow. It is with the subsequent oxidation that the textile turns blue.[10,58]

In the antiquity the dyeing of textiles with indigo demanded fermentation processes that include urine and bacteria (Clostridium spp.),[59] where the bacteria interacts directly with the indigo particles without a redox mediator.[59-61] With the advent of the modern chemical industry and after the introduction of chemical methods, at the end of the 19th century, specifically with the accessibility of the reducing agent sodium dithionite ($Na_2S_2O_4$), the dyeing process also become

achievable on the industrial scale. Although there are several modern methods for reducing indigo to leuco indigo, including electrochemical[62,63] and bacterial[59] methods, the more conventional is still the use of sodium dithionite in alkaline media.[58,64,65]

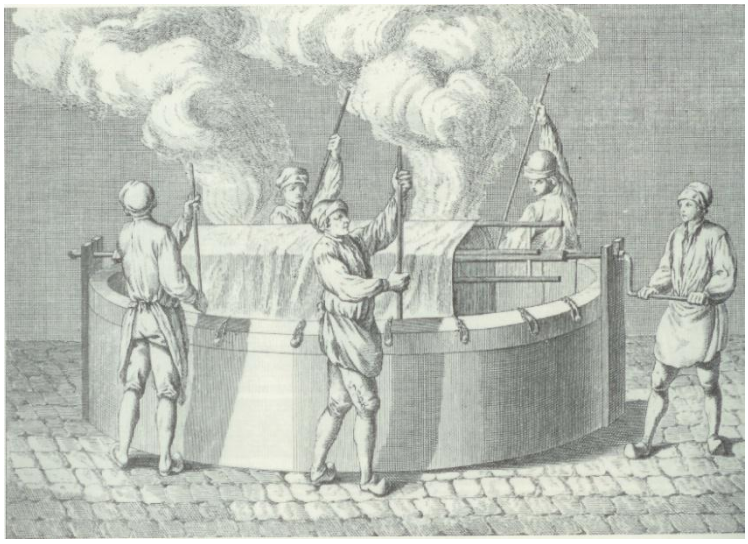

Men dyeing cotton in a vat [66]

Electrochemical reduction was first reported by Grothus in 1807 (quoted in ref[67]). The electrochemical processes are initiated by charge transfer from the electrode into an electrolyte solution; concerning indigo this process can be done using different approaches: direct electrochemical reduction; electrocatalityc hydrogenation; indirect electrochemical reduction (anthraquinoid mediator); indirect electrochemical reduction – using an iron-complex mediator, triethanolamine.[67]

Pre-reduced indigo is a much more convenient and easy-way to use indigo to dye, and it emerged with the advent of synthetic indigo. It consists in leuco

indigo in a stabilized pre-reduced form, so, a separate vatting stage is not needed. The major problem with these compounds is the occurrence of side reactions and impure products.[67]

Due to the environmental regulations, namely in terms of sulphate emissions, there have been several attempts to reduce the effluents. Catalytic hydrogenation has become a successful alternative to the dyeing vat, has been a great commercial and environmental success, and most European and American mills use this dyeing concept today.[67]

Reduction by bacteria (also referred in section 1.1.5) is confined commercially to a small market segment, more related to traditional methods, but due to its sustainable process, the bacterial system is being re-equated.

1.2.6 - THE PHOTOPHYSICS OF LEUCO INDIGO

During the reduction process of the neutral form (keto) to leuco form of indigo the hydrogen bonding between N-H and C=O groups, responsible for having the molecule in a *trans* planar configuration, is destroyed. These hydrogen-bonds are responsible for the fast (via ESPT) and dominant internal conversion deactivation channel that dominates the photophysical behaviour of indigo's keto form.[10,48,49,53]

The structure of the leuco form has been clearly established by NMR spectrometry and deuterium substitution.[65,68] The absorption spectrum is significantly blue-shifted relative to the keto parent. The fluorescence emission becomes now an efficient and competitive process for the deactivation of the excited state. In a general way the radiative (k_F) and radiationless rate (k_{NR})

constants have approximately the same order of magnitude because of a decrease in the k_{NR} and increase in the k_F values relative to keto indigo.[10,48,49]

1.2.7 - THE BLUE OF THE MAYA CIVILIZATION: MAYA BLUE

Maya Blue (MB) is a blue pigment used in Central America, mostly in Mexico, from VIII to XVI century A.D. to decorate pottery, statues, and wall paintings. Its colour shows various hues, ranging from light turquoise to dark greenish blue. [69,70] MB was rediscovered in 1931 by Merwin (quoted in ref [71-73]) while exploring the remains of the Temple of the Warriors in Chichen Itza (Yucatan)- Mexico.

Mayan seacoast Village scene – reproduction of a painting originally executed on one of the inner walls of the Temple of the Warriors, using MB.[69]

Shepard[74] first introduced the idea of MB resulting from embedding a dye into certain clays in Yucatan, whereas Gettens[72] systematised acid attack tests for identifying MB. Van Olphen[75] prepared pigmenting materials with properties close to that of MB using different procedures, establishing that Maya Blue was an organic/inorganic hybrid made of indigo and a clay called "White earth" by the ancient Maya people. Later on, the existence of other clay, sepiolite, was also suggested to be present, together with attapulgite (or palygorskite) or even in replacement of this.[73,76-78]

Despite the many archaeological discoveries exploited since then, its composition remained a mystery in the subsequent 30 years. The exceptional stability is undoubtedly the most stunning characteristic of MB. Even after centuries, the splendid murals of Bonampak and Chichen Itza maintained their vivid aspect.[71] In addition to its magnificent look, Maya Blue is resistant to diluted mineral acids, alkalis, solvents, oxidants, reducing agents, moderate heat, and even biocorrosion.[76,79]

Over the past 50 years, analytical advances have provided the pieces to the puzzle of Maya Blue. X-ray powder diffraction (XRPD) demonstrated the presence of the clay mineral palygorskite.[80] Later, indigo was identified in MB[72,75] and confirmed with infrared spectroscopy[71,81]. Indeed, Maya Blue is a complex structure formed by palygorskite (or sepiolite) and indigo (obtained from the Maya's common plant *Indigofera suffruticosa*). However, a simple mixture of palygorskite and indigo is not resistant to chemical attack. Eventually the recipe was rediscovered: the dye/clay mixture requires heating to, at least, 100 ◦C to produce Maya Blue.[75,81] Although the pieces of the puzzle – indigo and palygorskite clay – have been identified, researchers struggled since then to explain how they fit together to create a material with such remarkable properties. Molecular modelling calculations on Maya Blue were carried out[82-84]

demonstrating that no impediment existed for indigo to be inserted into the interior of the clay channels, which run the whole length of the clay fibres. Transmission electron microscopy (TEM) analysis suggested that nanoscale Fe, Ti and Mn impurities discovered in Maya Blue samples may influence its appearance.[79]

Palygorskite, of ideal composition $(Mg,Al)_4Si_8(O,OH,H_2O)24\cdot nH_2O$, can be described as a continuous set of layers formed by two-dimensional tetrahedral and octahedral sheets.[85-87] Palygorskite exhibits two different polytypes: one monoclinic and one orthorhombic. Both polytypes show a discontinuous 2:1 tetrahedral:octahedral layers structure with one 2:1 unit joined to the next by inversion of the SiO_4 tetrahedra along Si-O-Si bonds.[85-87] The tetrahedral and octahedral mesh gives rise to a series of rectangular tunnels of 6.4×3.7Å dimensions. Such clays are therefore crossed by zeolite-like channels and permeated by weakly bound, non-structural (zeolitic) water. Magnesium and aluminium cations complete their coordination with tightly bound water molecules (structural water).[81,85,87] Sepiolite possess a structure similar to palygorskite (or attapulgite), but with longer channels 10.6×3.7Å, and ideal composition $Mg_8Si_{12}O_{30}(OH,H_2O)_4\cdot nH_2O$. [81,85,87]

Chiari *et al.*[82] refined the crystal structure of palygorskite and Maya Blue using synchrotron radiation XRPD and found that the indigo molecules located in the channels were highly disordered. Neutron diffraction on Maya Blue prepared with deuterated indigo, locate, according to the authors, without ambiguity indigo inside the clay channels.[88,89]

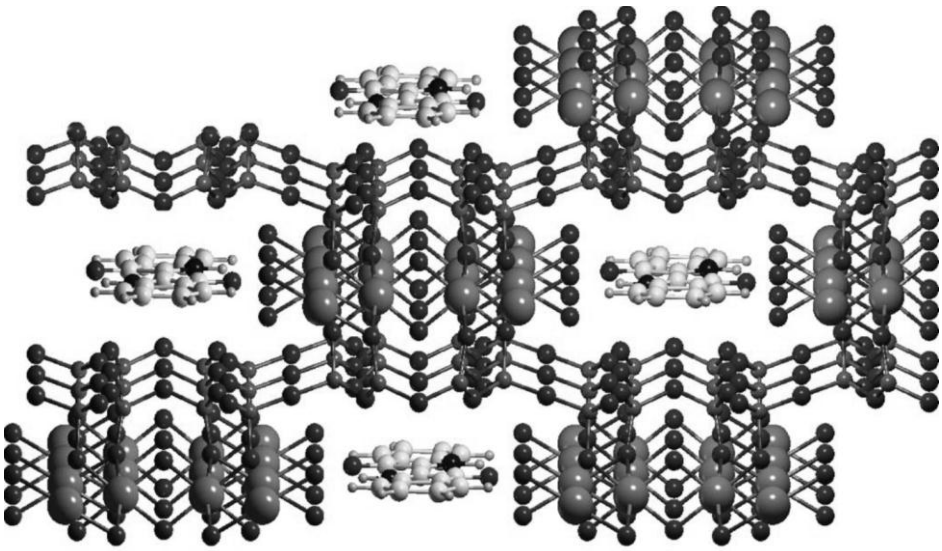

Figure 2 - Structure of Maya Blue, from ref. [81]

Despite all the literature available on Maya Blue there are still mysteries to unveil, one of them is the correct location of the dye in the clay. There are two different approximations/views. Some investigations of properties and from simulations state that indigo molecules can be incorporated.[78,83,90] Incorporation is also supported by molecular models of sepiolite and attapulgite, where the pore size is large enough to accommodate indigo molecules; other points favouring this model are the intrinsic properties of the pigment, like colour, photochemical behaviour and resistance to acid and alkalis.[71,83,90] However, others point out to another direction and mention that interaction between the external silanol groups and the carbonyl and amino groups are more important and, consequently, indigo molecules are located at the surface of the clay tunnels.[91] A model has been recently proposed, and assumes that the faces of the fibbers in the external

channels are covered by indigo molecules, but these are not deep inside the internal channels.[81,89,91-94]

Sanchez del Rio *et al.* mention, comparing the two clays, that when incorporated with attapulgite the pigments are much more resistant to acid attack than when this is made with sepiolite.[73] This is due to the larger size of the channels in sepiolite.

1.2.8 - ZEMBRA PURPLE: IS THERE A POTENTIAL CONNECTION WITH MAYA BLUE?

During excavations done at the island of Zembra, in Tunisia, a sample of purple clay earth in a stratigraphic layer dating back to the third century B.C. was discovered.

Several tests were made in order to identify the colouring matter (test of vat and mordant dyeing, selective solubility test, alteration reaction of dibromoindigotin test, HPLC), and the presence of dibromo-indigotin was, according to the authors, undoubtedly established. X-ray fluorescence, scanning electron microscopy, FTIR and Raman spectroscopy, among another methods proved the presence of a clay.[95]

Zembra Purple was found to be constituted of purple clay earth, conical shells with an elliptical base of the *Patella* genus and granules of wood coal.[95]

2. Substituted Indigo Derivatives

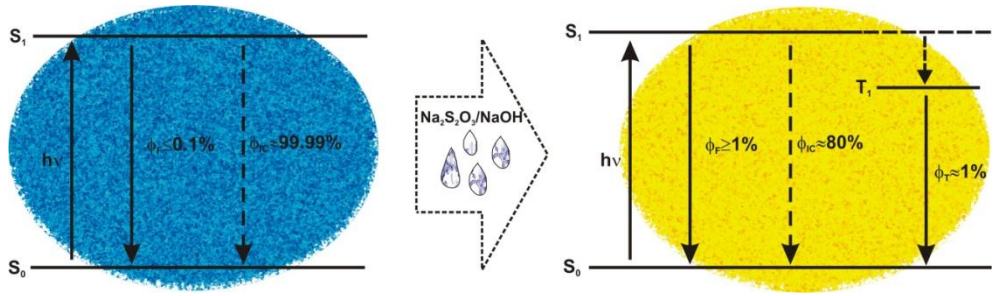

In the past recent years the photophysics of indigo has been deeply investigated by Seixas de Melo *et al.*[10,48-50,52,58,96] They showed that with indigo and some of its common derivatives (including Tyrian Purple, indigocarmine and indirubin), the major deactivation pathway for the keto form, is made through the internal conversion deactivation channel, whereas with the leuco form there is competition between internal conversion, triplet state formation, and fluorescence. Indigo owes its high bathochromicity to the special orientation of the electron donor (NH) and acceptor (C=O) groups, known as the H-chromophore.[10,28,32,33,36] The colour of the blue dye is given by the keto neutral form, whereas the reduced form, leuco indigo, is the water soluble form of indigo from which the dyeing process emanates.

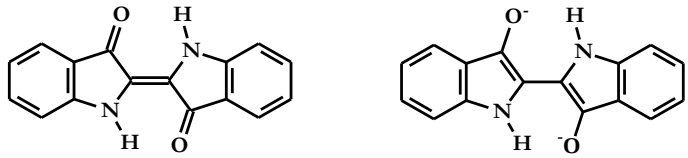

Keto indigo (neutral) **Leuco indigo (reduced)**

Scheme 9 – Structures of indigo in its neutral and reduced forms

2.1 – SUBSTITUTED INDIGO DERIVATIVES

A comprehensive investigation of the electronic spectra and photophysical properties of eleven different indigo derivatives, including indigo and Tyrian Purple in its reduced form has been undertaken, a comparison with the keto (whose data were previously published) form was also established. [96]

The structures and acronyms (including numbering) of the investigated compounds are depicted in Scheme 10. These were divided in three families according to the degree of substitution (di-, tetra-, or hexa-substituted). Numbering of the atoms is given for indigo.

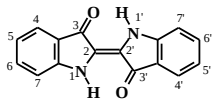

Indigo

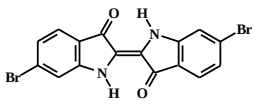

Tyrian Purple

Family 1

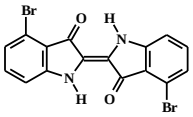

(1) *4,4'*-diBrIndigo

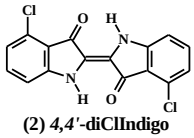

(2) *4,4'*-diClIndigo

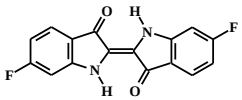

(3) *6,6'*-diFIndigo

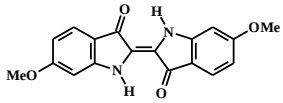

(4) *6,6'*-diMeOIndigo

Family 2

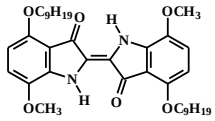

(5) *4,4'*-diOC$_9$H$_{19}$, *7,7'*-diMeOIndigo

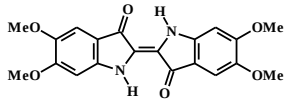

(6) *5,5', 6,6'*-tetraMeOIndigo

Family 3

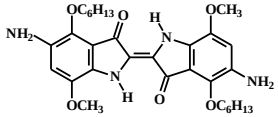

(7) *4,4'*-diOC$_6$H$_{13}$, *5,5'*-diamino, *7,7'*-diMeOIndigo

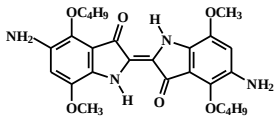

(8) *4,4'*-diOC$_4$H$_9$, *5,5'*-diamino, *7,7'*-diMeOIndigo

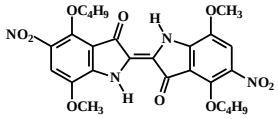

(9) *4,4'*-diOC$_4$H$_9$, *5,5'*-dinitro, *7,7'*-diMeOIndigo

Scheme 10 – Structures and acronyms for the substituted indigo derivatives.

For the keto forms of the compounds in Scheme 10, it was found that the radiationless rate constants, k_{NR}, dominate the deactivation processes of S_1 and that the radiative rate $S_1 \sim\sim\rightarrow S_0$ internal conversion process is the main deactivation channel for the compounds with 99% of the quanta loss made through this channel, see Table 2.[96]

2.2-SPECTROSCOPIC CHARACTERIZATION

2.2.1-SINGLET-STATE

Figure 3 presents the absorption and fluorescence spectra of the reduced (leuco) form, for one selected compound of each family presented in Scheme 10, in dioxane solution at room temperature. For purposes of comparison, the spectra for the keto forms are also presented in Figure 3.[96]

Data for leuco-indigo and leuco-Tyrian purple were previously obtained in dimethylformamide (DMF)[10], and for the correspondent keto forms of the compounds in Scheme 10 in dioxane[49]. Upon addition of the reducing agent, small precipitated particles are observed that induce some light scattering, which is mirrored by a tail in the absorption spectra at longer wavelengths (Figure 3). However, the presence of these aggregates does not change the characteristic pale yellow colour of the solution.

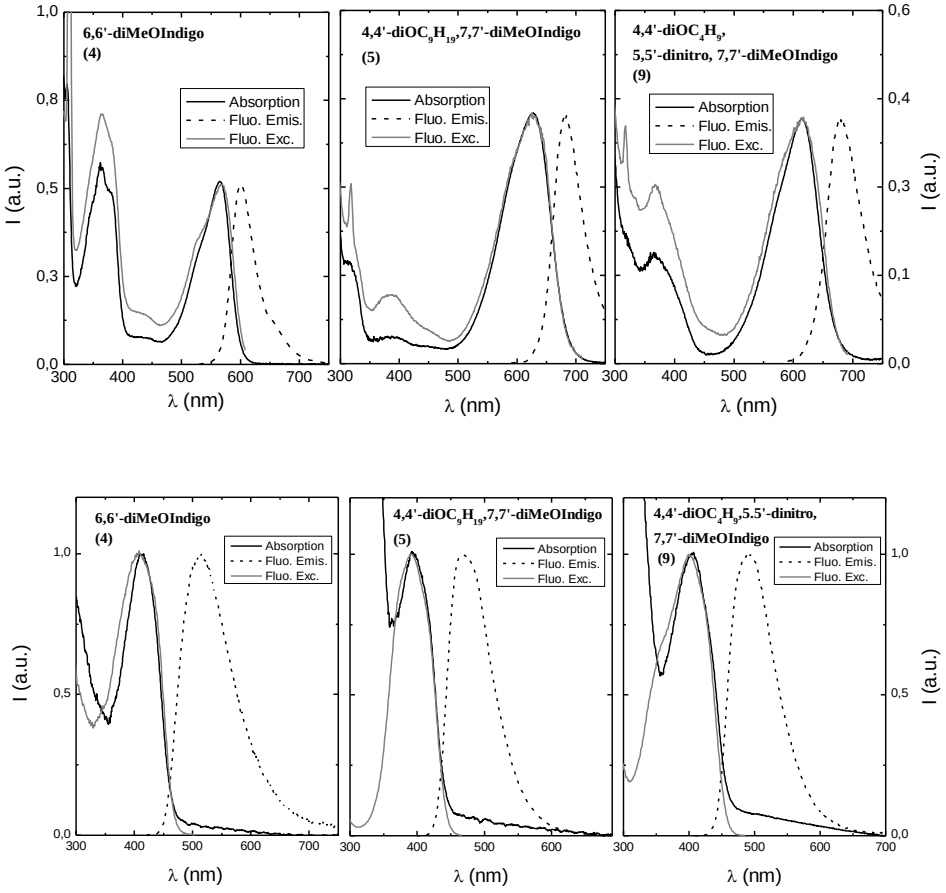

Figure 3- Top panels: Absorption, fluorescence emission and excitation spectra (normalized) for representative **family 1, 2** and **3** compounds (Scheme 10) in dioxane in their keto forms[96]; **Low panels:** Absorption, fluorescence emission and excitation spectra (normalized) for representative **family 1, 2** and **3** compounds in dioxane at T= 293K in their leuco forms.

Comparing the leuco and keto forms, it is worth highlight the significant blue shift of the absorption spectra. Moreover, the Stokes shift (SS in Table 1) display values of ~90nm, which is in contrast with the smaller value found for the keto forms, ~40nm (Table 2).[49] This difference suggests that in the leuco forms

the ground and excited state structures are significantly different, while in the keto form they are more similar, due to the N-H···O=C hydrogen bonds that keep indigo in a *trans* planar configuration and is responsible for the fast (and dominant) internal conversion deactivation channel (through intra or intermolecular proton transfer). For leuco forms (see Scheme 9) this hydrogen bonding no longer exists, opening the door to a possible photoisomerization process, (see Chapter 3 – Excited State Isomerization of Leuco Indigo).

In Table 1 the photophysical parameters for indigo and its derivatives here investigated are summarized.

The blue shift occurred as consequence of indigo's reduction, carries, for all the compounds, the absorption wavelength maxima to ~400-430nm range. This indicates that substitution does not significantly affects the absorption characteristics of the leuco forms, which in contrast to what was found with the corresponding keto forms.[49] The extinction coefficients are also high, which is a characteristic feature of allowed π,π^* transitions.[97]

From observation of Table 1, it can be seen that the ϕ_F values are now *ca* two orders of magnitude higher than those found for keto form (~10^{-3}-10^{-4}). Fluorescence lifetimes have also suffered a significant increase, and are now found in the nanosecond time range. This evidences that internal conversion is no longer the (almost) exclusive main deactivation channel, and fluorescence becomes a competitive deactivation pathway for excited leuco indigo derivatives.

Table 1- Spectroscopic and photophysical data for the **leuco** forms of the compounds in dioxane solution,T=293 K.[58]

Compound	$\lambda_{abs}^{máx}$ (nm)	ε_{SS} ($M^{-1}cm^{-1}$)	$\lambda_{fluo}^{máx}$ (nm)	ϕ_F	τ_F (ns)**	k_F (ns^{-1})	k_{NR} (ns^{-1})	SS (cm^{-1})
Indigo	415	21160	500	0.462	3.33	0.139	0.161	4096
Tyrian Purple (*6,6'*-diBrIndigo)	430	13050 *	505	0.225*	3.77*	0.06*	0.206*	3454
Family 1								
4,4'-diBrIndigo (1)	430	14780	505	0.367	2.89	0.128	0.218	3454
4,4'-diClIndigo (2)	430	18300	503	0.223	3.20	0.0684	0.238	3375
6,6'-diFIndigo(3)	412	11400	518	0.0393	0.55	0.0703	1.719	4967
6,6'-diMeOIndigo (4)	413	17540	515	0.0468	0.55	0.0849	1.730	4796
Family 2								
4,4'-diOC_9H_{19},*7,7'*-diMeOIndigo (5)	397	24170	475	0.221	2.20	0.0995	0.351	4136
5,5', 6,6'-tetraMeOIndigo (6)	410	15430	510	0.0702	0.52	0.134	1.388	4782
Family 3								
4,4'-diOC_6H_{13},*5,5'*-diamino, *7,7'*-diMeOIndigo (7)	408	13470	490	0.160	2.30	0.0678	0.356	4102
4,4'-diOC_4H_9,*5,5'*-diamino, *7,7'*-diMeOIndigo (8)	405	8280	480	0.234	2.50	0.0928	0.304	3858
4,4'-diOC_4H_9,*5,5'*-dinitro, *7,7'*-diMeOIndigo (9)	403	24580	490	0.213	2.28	0.0859	0.317	4406

*data in DMF taken from ref.[10]

** major component of a biexponential decay

Table 2- Spectroscopic and photophysical data for the **keto** forms of the compounds in dioxane solution,T=293K.[96]

Compound	$\lambda_{abs}^{máx}$ (nm)	ϕ_F	τ_F (ns)	$\phi_\Delta \approx \phi_T$	ϕ_{IC}	k_F (ns^{-1})	k_{NR} (ns^{-1})	SS (cm^{-1})
Indigo[a]	610	0.0023	0.14	0.00117	0.996	0.0164	7.12	43
Tyrian Purple (*6,6'*-diBrIndigo) [a]	601	0.0071	0.323	0.000552	0.992	0.022	3.07	39
Indigocarmine[a]	618	0.0015	0.110	0.0008	0.998	0.0136	9.08	43
Family 1								
4,4'-diBrIndigo (1)	602	0.00462	0,150	0.00235	0.992	0.0308	6.64	35
4,4'-diClIndigo (2)	600	0.00406	0,134	0.001	0.994	0.0303	7.43	33
6,6'-diFIndigo(3)	570	0.00169	0,068	0.00113	0.997	0.0248	14,68	35
6,6'-diMeOIndigo (4)	566	0.000337	0,015[b]	0.0005	0.999	0.0225	66.64	44
Family 2								
4,4'-diOC_9H_{19},*7,7'*-diMeOIndigo (5)	629	0.000175	0.190	0.00117	0.999	0.00092	5.26	51
5,5', 6,6'-tetraMeOIndigo (6)	588	ND[c]	-	0.000186	0.999	-	-	-
Family 3								
4,4'-diOC_6H_{13},*5,5'*-diamino, *7,7'*-diMeOIndigo (7)	732	ND[c]	-	0.0012	0.998	-	-	-
4,4'-diOC_4H_9,*5,5'*-diamino, *7,7'*-diMeOIndigo (8)	730	ND[c]	-	0.0003	0.999	-	-	-
4,4'-diOC_4H_9,*5,5'*-dinitro, *7,7'*-diMeOIndigo (9)	615	0.00011	0.032[b]	0.00083	0.968	0.00342	31.25	65

[a]data in DMF taken from ref.[10], with the exception of $\phi_\Delta \approx \phi_T$ values (these work) and thus the split of the radiationless rate constants into k_{IC} and k_{ISC}.

[b] Value determined in benzene

[c] emission could not be detected with our current experimental conditions, i.e, $\phi_F \leq 10^{-5}$

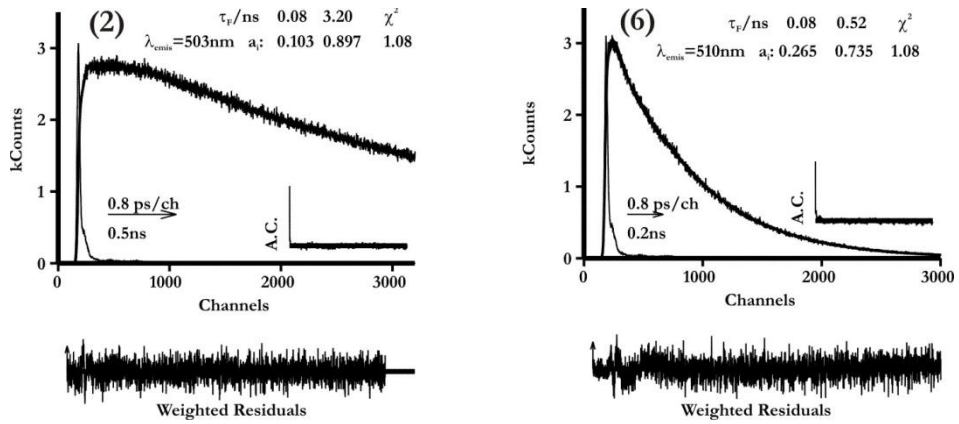

Figure 4- Fluorescence decays and pulse instrumental response obtained for the leuco form of some selected compounds (2) and (6) in dioxane at T=293K. The emission wavelengths and obtained decays times are shown as insets in the figure. Also shown are the weighted residuals, autocorrelation functions (A.C.) and the χ^2 values for a better judgment of the quality of the fits.

The substitution position instead of the degree of substitution, is what seems to affect more the spectral behaviour of these compounds. Indeed, if one observes **family 1** compounds **1** and **2**, which have bromine and chlorine atoms in the 4,4' position, these display similar spectral (absorption and emission wavelength maxima) and the same happens with compounds **3** and **4** which are substituted in the 6,6' positions by different groups. Nevertheless, when substitution is now made in the 6,6' positions a much more significant Stokes shift is seen when compared with the derivatives with substitution in the 4,4´positions. The same is valid for the fluorescence quantum yields which are one order of magnitude lower when substitution is at the 6,6' position and the lifetimes (~5 times lower with 6,6' compounds with regards to 4,4' substitution), see Table 1.

With **family 2** compounds, again substitution in positions 4,4' and 7,7' in (**5**) relative to 5,5' and 6,6' in (**6**) leads to significant differences in the absorption and emission wavelength maxima (and consequently in the Stokes shift, SS, values) and in the ϕ_F and τ_F values. Although with these two compounds the substituents are not identical, the groups basically consist in a O-R (with R= alkyl group) which shows that it is the substitution pattern and not the group that rules out the observed properties of these compounds.

With **family 3** since the position of substitution is the same for the three compounds (**7**, **8** and **9**) the spectral and photophysical parameters are now approximately identical.

By now comparing the values between **families 2** and **3** -for example compounds **4** and **6**- it can be seen that substitution in the 6,6' positions is responsible for the low ϕ_F and τ_F values, thus showing that this substitution lowers the contribution of the radiative decay channel.

2.2.2 – LEUCO TRIPLET STATE

The presence of strong transient triplet-triplet signal is another difference brought up by the reduction of indigo. Figure 5 shows the transient triplet-triplet absorption spectra for one representative compound of each family; additional data (extinction coefficients, wavelength maxima and intersystem crossing yields) can be found in Table 3. Comparison with indigo and its di-substituted derivatives shows that the higher substituted compounds (tetra- and hexa-) present a more pronounced depletion in the singlet absorption region, followed by intense signals in the 450-500nm region. This is further evidenced by the increase

Table 3- Transient triplet-triplet parameters (triplet-triplet extinction coefficients, absorption wavelength maxima, intersystem crossing yield), together with radiationless rate constants (k_{IC} and k_{ISC}) and the $S_1 \sim\sim\rightarrow S_0$ internal conversion yield for the leuco forms of indigo and three representative derivatives of families 1, 2 and 3 in dioxane, T = 293 K.

Compound	$\varepsilon_{TT}\left(M^{-1}cm^{-1}\right)$	$\lambda_{T_1\rightarrow T_n}^{max}$ (nm)	ϕ_T	ϕ_{IC}	$k_{IC}\left(ns^{-1}\right)$	$k_{ISC}\left(ns^{-1}\right)$
Indigo	31030	480	0.0127	0.525	0.857	0.0038
***4,4'*-diBrIndigo (1)**	20500	480	0.0130	0.620	0.869	0.0045
***4,4'*-diOC$_9$H$_{19}$,*7,7'*-diMeOIndigo (5)**	28710	470	0.0278	0.751	0.888	0.0125
***4,4'*-diOC$_4$H$_9$,*5,5'*-diamino, *7,7'*-diMeOIndigo (8)**	20170	470	0.0342	0.732	0.894	0.0136

on the ϕ_T value, Table 3, going from indigo (lower) to *4,4'*-diOC_4H_9,*5,5'*-diamino,*7,7'*-diMeOIndigo (8) (higher). This growth shows that the degree of substitution is determinant for the efficiency of the $S_1 \sim\sim\rightarrow T_1$ intersystem crossing process.

From Table 1 it can be seen that albeit the dominant decay channel is the internal conversion (~80 to 89 % of the *quanta* is lost through this channel) this contribution has decreased relative to keto indigo where 99,99 % (Table 2) of the *quanta* is lost through this channel. From Tables 1 and 2 the rate constants of fluorescence and internal conversion are, for all the compounds, of the same order of magnitude, whereas the intersystem crossing values are one to two orders of magnitude lower (Table 3).

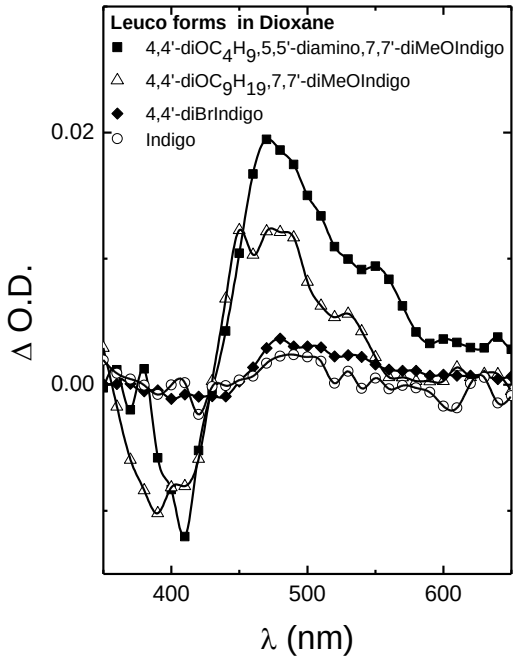

Figure 5- Transient triplet-triplet absorption spectra obtained for indigo and some selected indigo derivatives (leuco form) in dioxane, T=293K.

2.3 –PHOTOISOMERIZATION OF LEUCO INDIGO

The biexponential decays, with different relative proportions, Figure 4, give a signal of the potential coexistence of two species (conformers) in leuco indigo.

Furthermore this biexponential behaviour does not seem compatible with excited state proton transfer (present in keto forms) since the contribution of the two components/species is dependent on the irradiation time (Figure 6).

Exploring the possible presence of two conformers, we conducted a time-resolved experiment with compound 8 in highly viscous glycerol (η= 1.412 Pa s). The decays were obtained with what may be considered as a time zero—that is, the solution is prepared and immediately measured (within 5 min)—and then after 60 minutes of irradiation with a wavelength of 392 nm (laser wavelength of the ps-TCSPC equipment). The fluorescence decays, obtained under these two conditions, depicted in Figure 6, clearly show two components whose pre-exponential factors (concentrations at time zero) change with the time of irradiation. The pre-exponential factor associated to the shorter component ($\tau_F \approx$140–160 ps) increases, after one hour of irradiation, with the concomitant decrease of the longer component ($\tau_F \approx$1.32–1.53 ns). This clearly indicates that a light-induced process (nonexistent in the keto structures) is present, and that it is compatible with a photoisomerization process. This will be detailed in the next chapter.

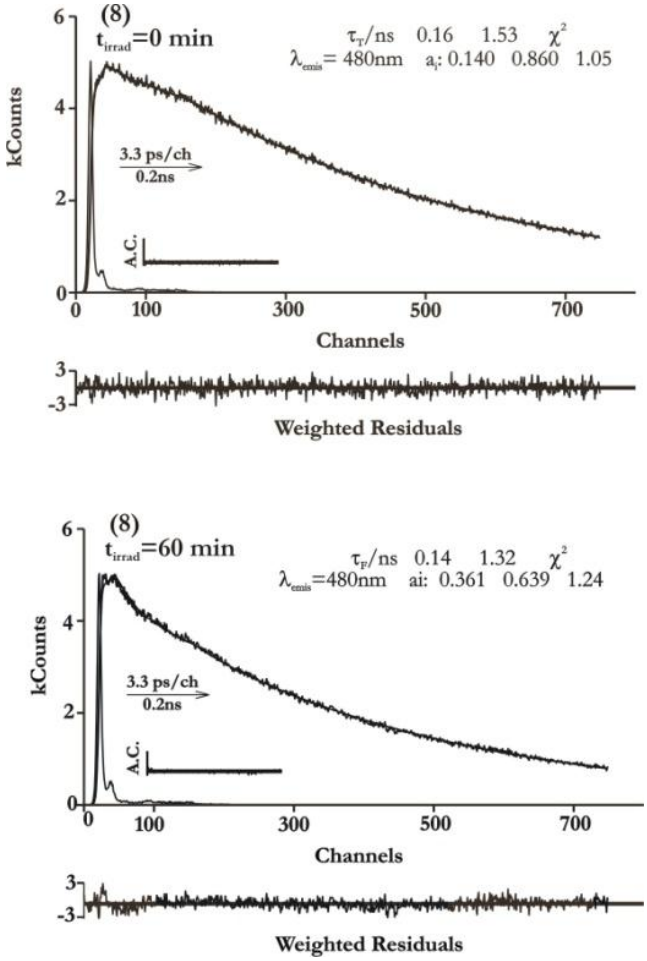

Figure 6. Fluorescence decays and pulse instrumental response obtained for the leuco form of *4,4'*-diOC_4H_9,*5,5'*-diamino,*7,7'*-diMeOIndigo (8) in glycerol at T=293 K, with irradiation time=0 min (upper curve) and after 60 min of irradiation (lower curve). The emission wavelengths and decay times obtained are shown as insets. Also shown are the weighted residuals, autocorrelation functions (A.C.) and the χ^2 values for a better judgment of the quality of the fits. The excitation wavelength is 392 nm and the emission wavelength 480 nm.

2.4-CONCLUSIONS

The electronic spectral and photophysical properties of eleven indigo derivatives, including indigo and Tyrian purple, in their leuco forms, have been investigated. These were found to depend on the location and degree of substitution. With the di-substituted derivatives, substitution in the diagonal 6,6'-positions leads to ϕ_F values that are one order of magnitude lower when compared to the disubstituted in the 4,4'-positions. With the tetra-substituted compounds (family 2) the substitution in the 6,6'-position also leads to a three-fold decrease of the ϕ_F values when compared to other substitution(s). The internal conversion is the dominant deactivation channel for the leuco compounds in dioxane, although fluorescence and intersystem crossing are also important deactivation pathways for the excited state. This is in sharp contrast to what was found for the neutral keto form of indigo and its derivatives where more than 99.99% of the *quanta* is lost through the internal conversion channel, and may explain the loss of stability of the leuco when compared to the keto forms. This possibility has not been generally considered but may be explained by a more populated triplet excited state in the leuco form which would then prime the molecule to be more reactive.

A time-resolved study showed that the decay profiles change with the time length of irradiation, which is compatible with a light-induced process (photoisomerization) and the presence of two conformers.

3. Excited State Isomerization of Leuco Indigo

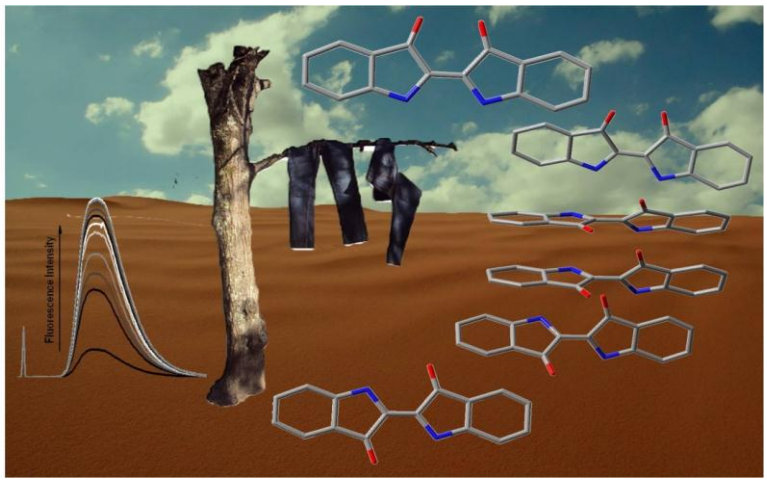

When studying the indigo derivatives in their leuco forms, the hypothesis of a photoisomerization process has emerged. In order to further prove and detail this process, three different compounds were chosen, indigo, 4,4'-dibutoxy-7,7'-dimethoxy-5,5'-dinitroindigo (DBMNI) and the methylated pre-Ciba (MpreCiba) – a model compound where rotation around the central C-C bond is blocked (structures presented later in this chapter).

The results are rationalized in terms of a photoisomerization (conversion) reaction, occurring in the first excited singlet state of *trans* to *cis* forms of leuco-indigo.

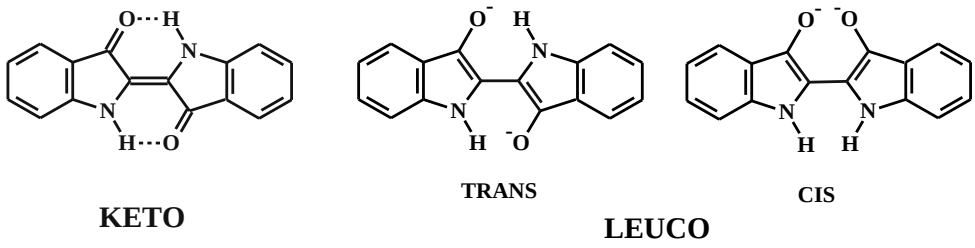

Scheme 11- Structures of indigo's neutral (keto) and reduced (leuco, *trans* and *cis*) forms.

3.1-INDIGO

A solution of leuco-indigo was submitted to UV-irradiation, and an increase in both the emission intensity at the wavelength maximum and fluorescence quantum yield were observed.

The efficiency of the Excited State Intramolecular Proton Tranfer (ESIPT) is, in indigo neutral (keto) form, strongly associated with the planar geometry, which is responsible for (and the consequence of) the intramolecular hydrogen bonds between the N-H and C=O groups.[10,48] To this planar conformation two structural features are fundamental: the close proximity between the N-H and C=O groups and the double-bond nature of the central carbon–carbon bond connecting the two indole-like moieties. In the case of the leuco form, the central carbon–carbon bond has a reduced bond order intermediate between double- and single-bond character, thus allowing different non-planar conformations, both in the ground and excited state.The changes registered were intended to be due to a (*trans-cis*) isomerisation induced by light (photoisomerization).

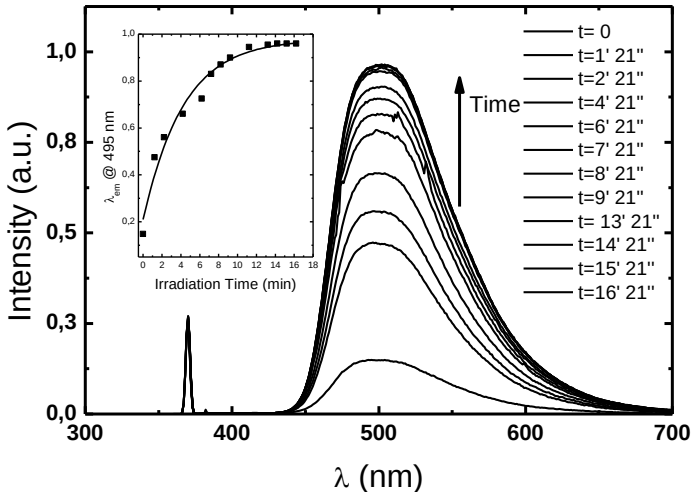

Figure 7- Fluorescence emission spectra of indigo's leuco species in dioxane obtained with different irradiation times at T= 293 K. The Rayleigh scattering peak at the excitation wavelength (λ_{exc}= 370 nm) is presented showing that the variation in the emission intensity is not due to light fluctuations but solely due to

the properties of the molecule under investigation; also shown as inset is the plot of the intensity at 495 nm *vs.* the irradiation time.

As can be seen from Figure 7, the fluorescence quantum yield values are low for t=0 ($\phi_F \approx 10^{-2}$) increasing to $\phi_F \approx 0.2\text{-}0.3$ when a steady-state equilibrium has been accomplished; these later values are in agreement with those previously published[10,58] for the leuco form of indigo (and related molecules) where full conversion was achieved by leaving the sample under daylight exposure for approximately 20 minutes.

We should expect, if this process is a pure *trans-cis* photoisomerization, to see differences, even small, in both the absorption and fluorescence wavelength maxima. Considering that differences in the conjugation (electron delocalization) between *cis* and *trans* leuco forms are not very significant and rotation around the central C-C bond allows the thermodynamically more stable isomer to be formed, the absorption spectra taken at the beginning (before irradiation) and at the end of the experiment do not show appreciable differences (see Figure 8). However, the excitation spectra, obtained under the same conditions, revealed completely different spectral bands both in shape and maxima (see Figure 8). These changes in the excitation spectra cannot be attributed to incomplete keto-leuco interconversion, since inspection of the absorption spectra of the keto form (Fig 8, top panel) shows a valley, therefore with a negligible absorption, precisely in the region where the intense absorption band of the leuco form occurs. As can also be seen from Figure 8B, there is an increase in intensity of the excitation spectra with time; however, and in addition to this increment, it is also possible to observe a small change in the shape of the spectra. This mirrors both the gradual conversion of the keto into the leuco form and the possibility of an initial leuco *trans* to be gradually converted into the (more stable) leuco *cis* conformer.

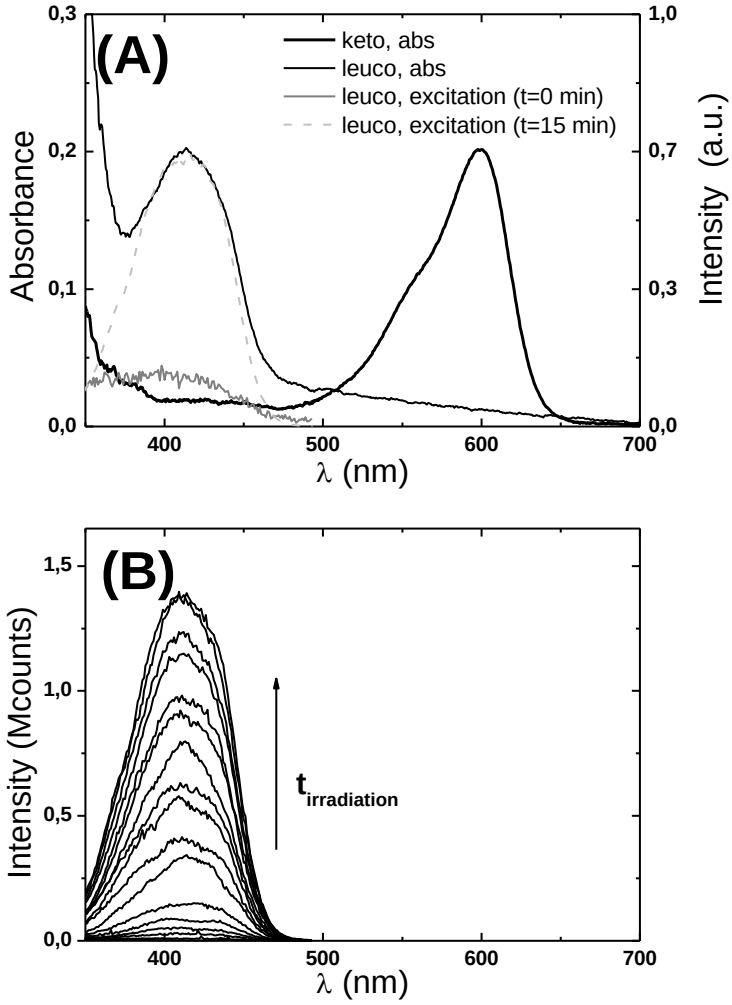

Figure 8 - (A) Leuco's indigo absorption and excitation spectra in dioxane obtained before and after irradiation under the conditions of Figure 7. Also shown is the absorption spectrum of indigo's keto (neutral) form, also in dioxane. **(B)** excitation spectra collected at different times for the leuco form of indigo in dioxane at T=293 K; the total time of irradiation is t= 15 min.

3.2-MODEL COMPOUND: MPRECIBA

In order to elucidate the real occurrence of photoisomerization, we studied the leuco form of an indigo derivative, MpreCiba, whose structure (Scheme 12) precludes the possibility of photoisomerization. The absence of evolution in the fluorescence quantum yield with UV irradiation of the leuco form of this compound is shown in Figure 9.

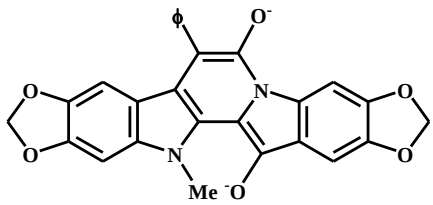

Scheme 12 – Structure of MpreCiba in its leuco form

Note that the geometry of this compound is analogous to the *trans* form of leuco-indigo. Moreover, the emission maximum (500 nm) of this reduced species is different from its keto form where it is found at 680 nm.[48] The fluorescence quantum yield and lifetime of leuco-MpreCiba are respectively ϕ_F=0.0026 and τ_F = 40ps (major component of the decay with λ_{em}=500nm, although a second component with a value of ~1.1-1.6 ns has a non-negligible contribution and whose origin is not yet clear to us).

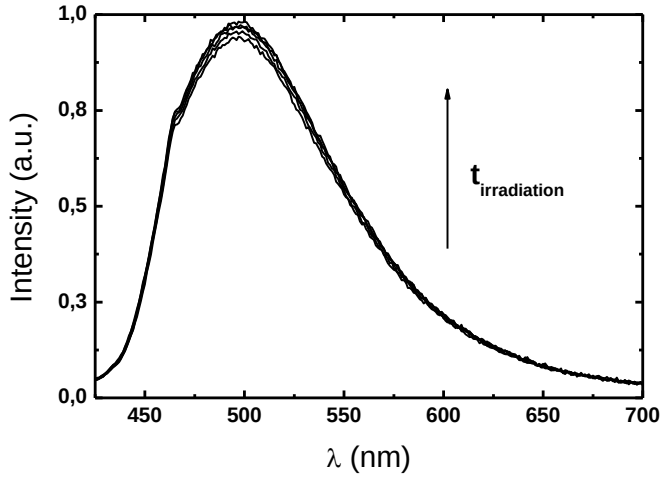

Figure 9- Fluorescence emission spectra of the leuco form of MpreCiba in dioxane obtained with different irradiation times at T= 293 K; the excitation wavelength was set to 408 nm.

The photophysical characteristics of MpreCiba whose *trans* (rigid) structure has ϕ_F and τ_F values (0.0026 and 40ps) close to those found for the leuco form of indigo and DBMNI ($\phi_F \sim 10^{-2}$ and $\tau_F \sim 0.12$ ns) at times before (or early stages of) irradiation, reinforces the hypothesis of an initial *trans* geometry.

3.3-4,4'-DIBUTOXY-7,7'-DIMETHOXY-5,5'-DINITROINDIGO (DBMNI)

For the leuco form of the hexa-substituted indigo derivative, 4,4'-dibutoxy-7,7'-dimethoxy-5,5'-dinitroindigo (DBMNI) (Scheme 13) a similar behaviour to that previously observed for leuco-indigo was found to occur with initial values for ϕ_F of the order of ~0.002 increasing upon photoconversion to 0.2, i.e., two orders of magnitude higher.

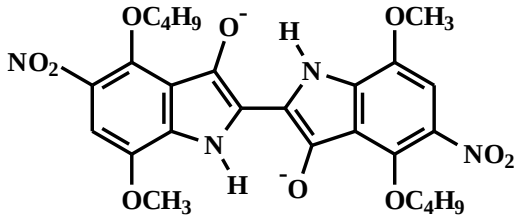

Scheme 13 – Structure of reduced form of 4,4'-dibutoxy-7,7'-dimethoxy-5,5'-dinitroindigo (DBMNI)

From Figure 10 we can see that once more, with UV irradiation, there is an increase in the ϕ_F value.

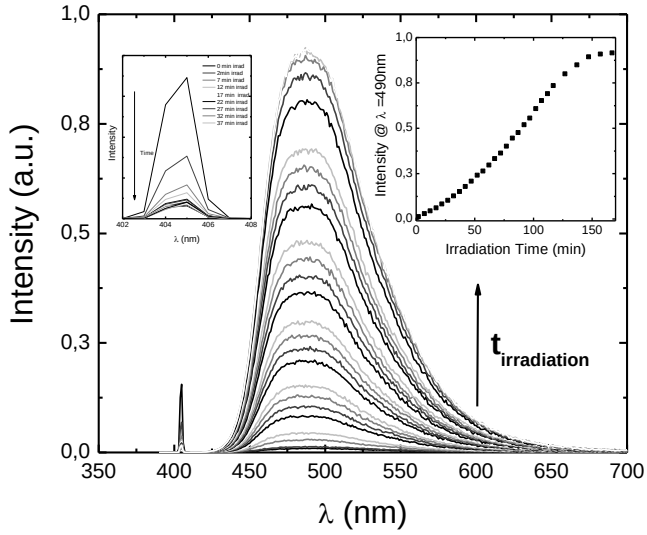

Figure 10- Fluorescence emission spectra of the leuco species 4,4'-dibutoxy-7,7'-dimethoxy-5,5'-dinitroindigo (DBMNI) in dioxane obtained with different irradiation times ($t_{irradiation}$) at T=293 K and λ_{exc}= 405 nm. Shown as insets are the intensity dependence with time obtained at λ_{em}= 490 nm and the magnified region of the Rayleigh peak (402-408 nm).

However, it can also be seen that the intensity of the Rayleigh peak is not constant until ~2 min. It is worth noting that time zero in our experiments is set immediately after preparation of the solution, trying to avoid as much as possible exposure to light. During the first minutes it is likely that part of the sample molecules are still being converted. Indeed, removal of the two first data points in the inset of Figure 10 does not lead to any deviation of the data and therefore to the overall discussion and conclusions made.

The excitation spectra collected at the emission maxima (500 nm) as a function of the irradiation time is shown in Figure 11B. It is once more shown that the form to which the initial leuco is being converted is gradually becoming more emissive. Again the question that is raised is if the observed pattern is truly due to a progressive conversion of the keto (blue) form, less emissive, into the leuco, more emissive (colourless or pale yellow) form of DBMNI. However, from the absorption (and excitation) spectra, no sign of the keto band (~610 nm) could be observed, Fig 11A.

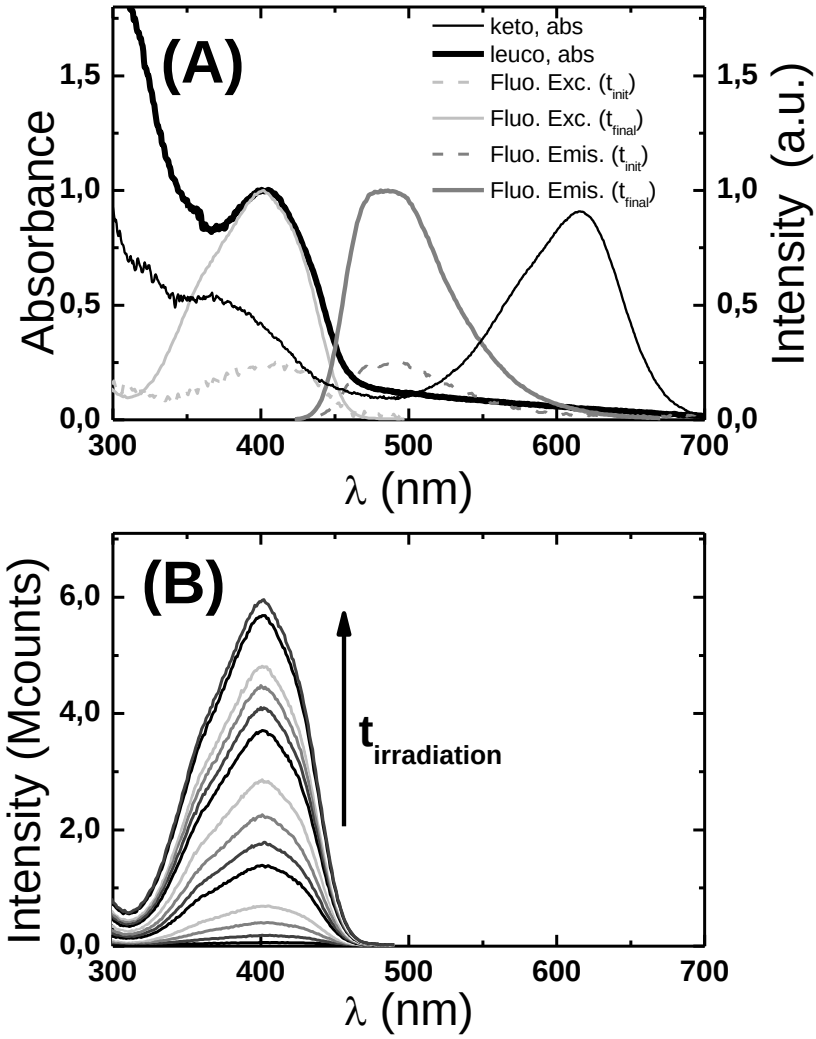

Figure 11- (A) Leuco's absorption and excitation spectra for DBMNI obtained before and after irradiation (under the conditions of Figure 10). In the labelling, t_{init} stands for the initial time (i.e., t≅0) and t_{final} for the final time which is t≅170 min (see figure 10). Also shown is the absorption spectrum of DBMNI keto (neutral) form. **(B)** Fluorescence excitation spectra for DBMNI in dioxane, collected at λ_{em}= 500 nm and at different times (periods of irradiation), with a total time of irradiation ($t_{irradiation}$) of 30 min.

3.3.1 - THERMAL ISOMERISATION OF DBMNI

The occurrence of thermal isomerisation, concomitant with the photochemical isomerisation process, was investigated at 20°C and 14 °C, by measuring the emission from two samples, one under irradiation at 370 nm and the other kept in the dark, Figure 12. Although at dark there is still a significant isomerisation (right panels in Figure 12), it is far less intense (as seen by the total intensity) when compared with that induced by light, i.e., the photoisomerisation process. It is also worth remembering that the light exciting the sample (λ_{exc}= 370 nm), in order to obtain the fluorescence spectra, precludes a complete dark experiment even if narrow slits (0.5 mm) are used.

When the fluorescence emission intensity at 490 nm is plotted *vs* time, see Figure 13, it becomes clear that thermal isomerisation accounts for almost 50% of the observed increase in the fluorescence emission quantum yield.

From Figure 13 it can also be observed that for an identical time value, the rate of thermal formation of the leuco-*cis* isomer is higher at 20ºC than at 14ºC, showing the thermal dependence of the isomerization process. Lowering the temperature could, in principle, decrease the thermal reactivity to a point where the photochemical reactivity would predominate; however, even at 14 °C, the thermal reactivity still accounts for ca. 50% of the total increase in the fluorescence emission.

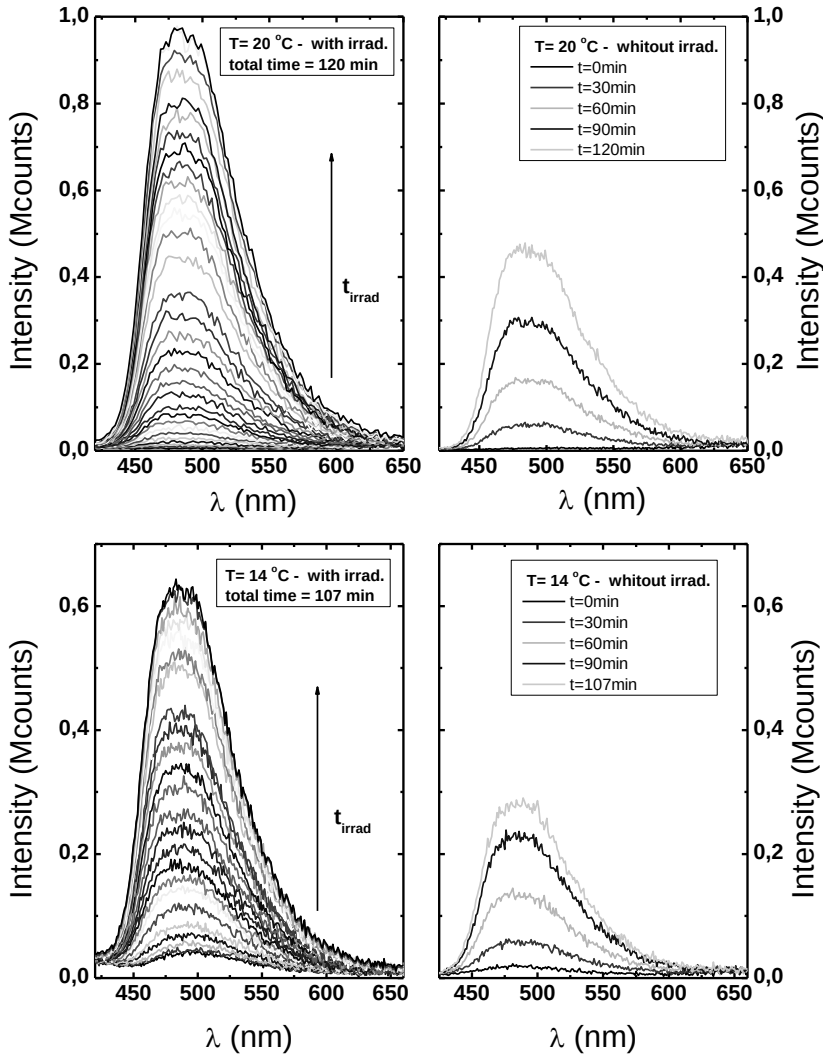

Figure 12- Fluorescence emission spectra for DBMNI in dioxane obtained at two different temperatures (top panels 20º C and bottom panels 14º C) with (left) and without (right) irradiation as a function of time. Excitation is at 370 nm.

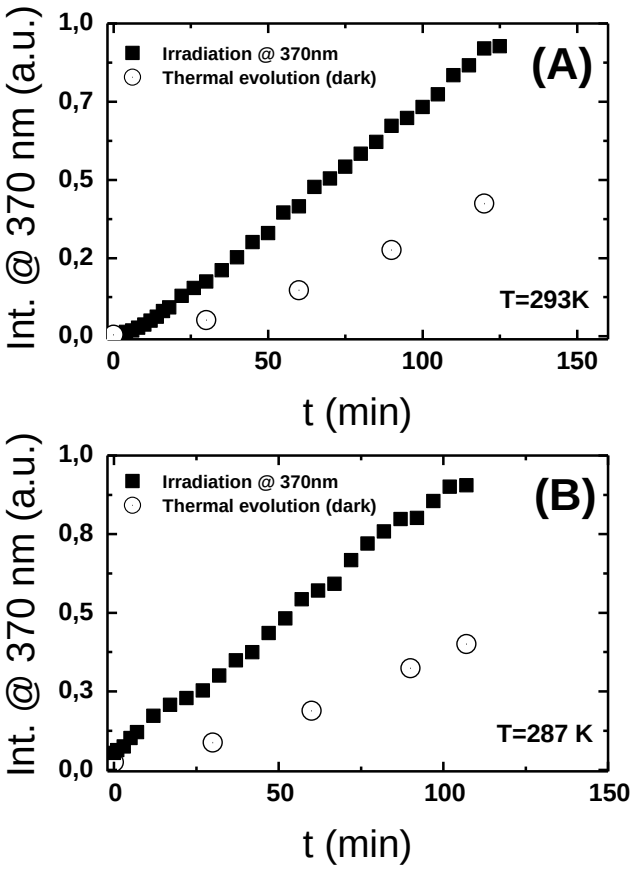

Figure 13- Changes in fluorescence intensity at 490 nm for 4,4'-dibutoxy-7,7'-dimethoxy-5,5'-dinitroindigo (DBMNI) in dioxane at **(A)** 20 °C and **(B)** 14 °C, as a function of time, with and without irradiation at 370 nm.

3.4 - PHOTOCHEMISTRY (*TRANS-CIS* CONVERSION) QUANTUM YIELD

Photochemical quantum yields of reaction were also obtained for indigo (ϕ_R=0.9) and DBMNI (ϕ_R=0.007) in dioxane. From the definition of quantum yield (ϕ = amount of reactant consumed or product formed/ amount of photons

absorbed), so it can be considered that for the same amount of light absorbed, the production of the *cis*-isomer is much more efficient with indigo than it is with DBMNI. This would explain the difference in the irradiation time needed to achieve a total isomerization (≈ 20 min to indigo and ≈ 100 min to DBMNI). Indeed, the huge (two orders of magnitude) difference between the ϕ_R values of indigo and DBMNI may have different reasons. A possible explanation lies in the fact that the number and type of substituents in DBMNI may lead to severe sterical constrains to rotation (*trans-cis* isomerization) leading to an effective deactivation of the excited state through radiationless processes.

3.5 – DBMNI, TIME-RESOLVED DEPENDENCE OF THE TRANS-CIS CONVERSION

Fluorescence decays as a function of the irradiation time were obtained for DBMNI in dioxane at 20 ºC. If the *trans* to *cis* photoisomerization occurs, with coexistence of the two isomers that are both emissive, it is anticipated that these two will present different decay times, which was indeed found to occur in the present study, and in the previous chapter. Indeed the decays collected at the initial stages of irradiation and up to ~300 min, could only be fitted with biexponential decay laws according to Equation 1,

$$I(t) = a_1 e^{-t/\tau_1} + a_2 e^{-t/\tau_2} \qquad (1)$$

From these, two decay times with values of 120 ps and 2.17 ns could be obtained and were found roughly constant with the irradiation time; however, the associated pre-exponential factors were found to vary with the (same) time of irradiation.

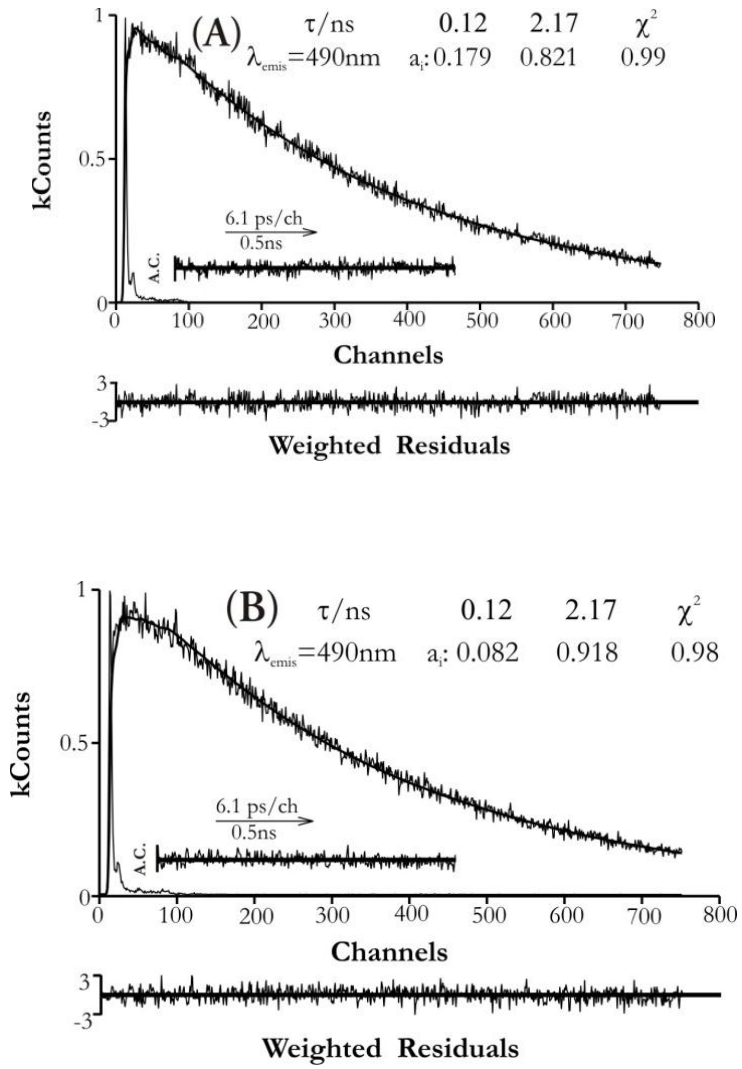

Figure 14- (A) Fluorescence decays and pulse instrumental response for 4,4'-dibutoxy-7,7'-dimethoxy-5,5'-dinitroindigo in dioxane, at T=293K, at t=0min. **(B)** Fluorescence decay after 300min of irradiation. Shown as insets are the decay times and pre-exponential factors. Also shown are the weighted residuals, autocorrelation functions (A.C.) and the χ^2 values for a better judgment of the quality of the fits, λ_{exc}=372 nm.

In Figure 14, the fluorescence decays, collected immediately after the preparation of the solution (Fig. 14A) and after 300 min (14B) of irradiation are shown. The decays show the initial presence of the *cis* and *trans* leuco forms that gradually converge into a single decay time; this is consistent with the steady-state data (Figure 10) and with the above discussion on the (photo)conversion of the initial *trans* into the *cis* leuco form of DBMNI, leading to an almost mono-exponential decay (the contribution of the second decay component represents less than 0.5% of the fluorescence decay, i.e., practically negligible), Figure 14B. Indeed, as can be seen from Figure 10, it is likely that the photostationary state still contains both the *cis* and *trans* conformers, even though being the contribution of the former strongly dominant. Moreover this is further shown in the variation of the pre-exponential factors (a_1 and a_2), mirroring the concentration at time zero of these two forms of leuco-DBMNI, which evolve reciprocally with the time of irradiation, Figure 15.

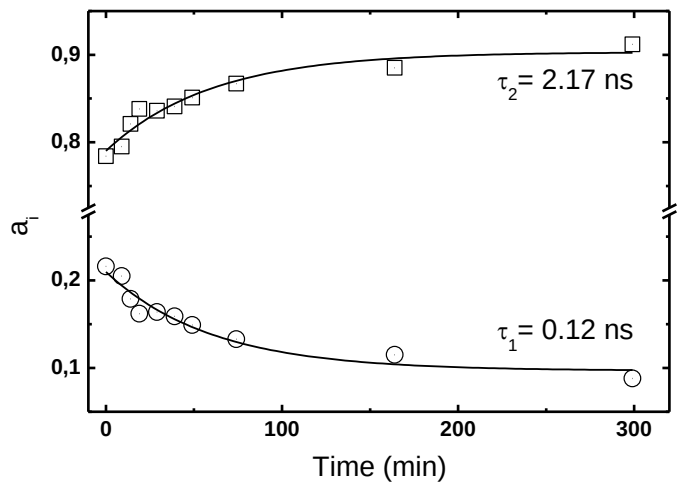

Figure 15- Dependence of the pre-exponential factors (a_i) in Eq. 1 with the irradiation time. The decay times in the end are roughly constant with values of ~120 ps and 2.17 ns as indicated in the figure.

3.6- CONCLUSIONS

With the formation of the leuco form, the hydrogen bonds, that were keeping the indigo in a stable *trans* planar configuration, are no longer available, and the central C-C bond goes from double (keto form) to single (leuco form) thus allowing free rotation along the central C-C bond.[10,58] This rotation gives rise to interconversion *cis* and *trans* isomers, and in this particular case to photoisomerization.

The photoisomerization process was investigated by means of the fluorescence emission dependence of the leuco form of indigo and one of its derivatives (DBMNI), with different irradiation times. MpreCiba was used as model compound - once rotation around the central C-C bond is not allowed. Time-resolved data was additionally used to show the presence of the *trans* to *cis* conversion in indigo.

Photochemical reaction quantum yields were also obtained showing that the photoconversion process has significant different values for indigo and DBMNI, and that for the later the lower value is likely to be due to the high level of substitution reducing the rotation around the C-C central bond in this leuco form.

4.DEHYDROINDIGO

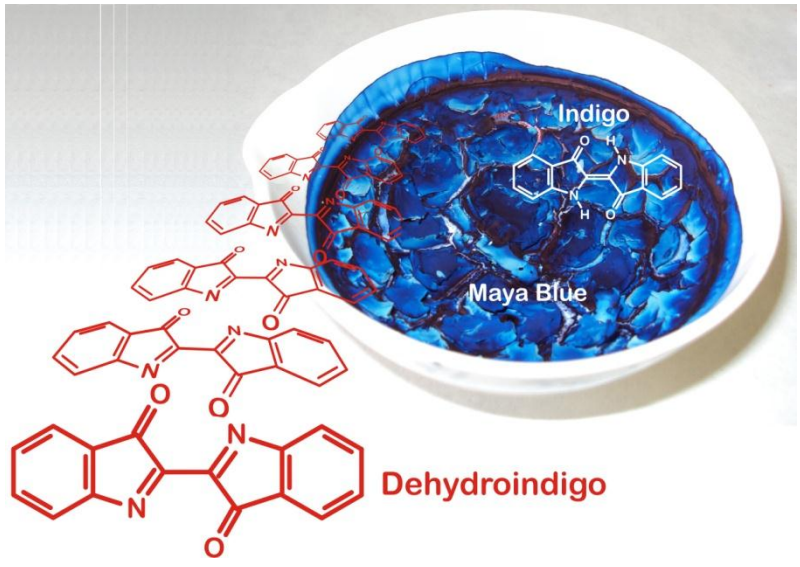

Dehydroindigo (DHI) the oxidized (and third form) of indigo can be considered (due to the lack of studies) the forgotten form of indigo (see Scheme 14). The leuco form, the water-soluble, used to dye, when exposed to oxygen brings to the clothes the wonderful blue colour; perhaps because of that and also by the limited stability of DHI this has not received much attention.

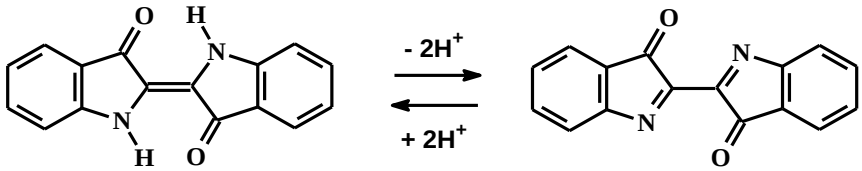

Indigo **Dehydroindigo**

Scheme 14 – Interconversion between the neutral indigo and its oxidized form – dehydroindigo

Nevertheless, although not usually as an isolated species, DHI has gained recent interest since it was identified in the procedure leading to Maya Blue[85,87,90,98], the source of blue of this ancient civilization, considered as the first fabricated organic (indigo)-inorganic (clay) hybrid.[75,99,100] Its chemical structure, although puzzling until recently, seems to involve the incorporation of indigo into palygorskite or sepiolite clays. This incorporation protects the organic dye, leading to an outstanding stability which has made possible the preservation of the colour for centuries in paintings submitted to severe environment conditions, in particular those involving light (photodegradation).

Although indigo takes up hydrogen on conversion into leuco-indigo and more energetic reduction even breaks up the double bond[101], it can also be dehydrogenated by the reaction given in Scheme 14. The oxidation or reduction of

indigo depends on the solvent media. In the case of reduction to the leuco form, the formation of a highly reducing media (usually sodium dithionite in alkaline solution) is needed, whereas oxidation, with formation of dehydroindigo, is made with a strongly oxidizing reagent (bromine was used in our case)[52].

One of the first things noticed with dehydroindigo was the ability of this to dissolve in a larger variety of organic solvents in contrast with indigo. Another point worth of notice was the fastness to hydrogenation back to indigo, by even vestigial amounts of water. Therefore, the characterization the "pure" DHI in solution was a real challenge. Indeed, it was never possible to obtain DHI completely free of indigo. Nevertheless since indigo and DHI absorb (and emit) in different spectral regions it was possible to obtain a detailed spectral and photophysical characterization of DHI in solution.

4.1 – SPECTRAL DATA

DHI absorbs in the visible region, with a wavelength maxima (λ_{max}) at 455 nm (toluene) and 400 nm (methanol), displaying an orange-brown colour in both the solid state and in liquid solution. As will be shown below, this compound is highly sensitive to the polarity and particularly to the water content of the media. Therefore dehydroindigo clearly presents different absorption (and emission) maxima and photophysical parameters depending on the solvent.

The absorption spectrum of DHI in toluene displays two bands in the visible region with λ_{max}= 455 nm and 600 nm, see Figure 16. These were attributed to dehydroindigo and indigo, respectively. The longest wavelength absorption band, associated with indigo, has its origin in the incomplete conversion (from the synthetic procedure) of the later into dehydroindigo or to a

(residual) formation of indigo (from dehydroindigo) by hydrogen abstraction (Scheme 14) of the solvent; this occurs even though the solvent has been dried to exhaustion.

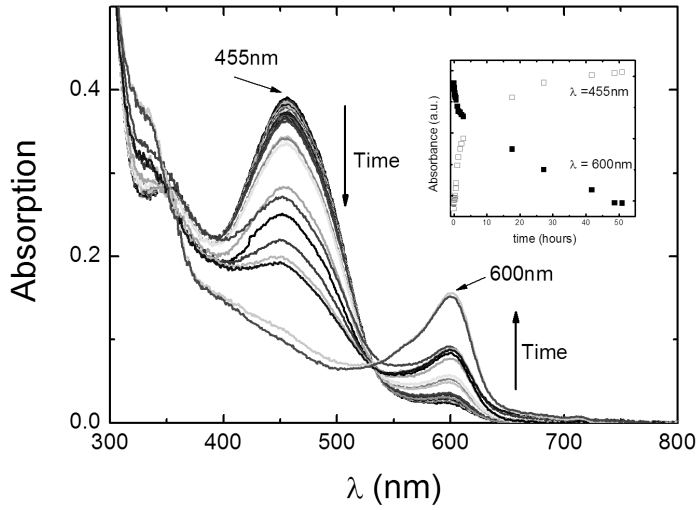

Figure 16 - Dehydroindigo absorption spectra variation with time, in non dried toluene at T=293K. Show as inset plot is the dependence with time of the absorption maxima of DHI and indigo.

The conversion of DHI into indigo is clearly shown in Figure 16, where dehydroindigo was dissolved in non dried toluene, and the absorption spectra were taken at periodic intervals of time for ~40 min. The band at 600nm (indigo) increases at the expenses of the decrease of the 455nm (DHI) band, with a clear isosbestic point at 531nm. After exhaustive drying of toluene the presence of the two bands (DHI and indigo) is still observed, but there is no effective change (evolution) of spectra with time. Also in Figure 16, we can see as inset plot, the

dependence with time of the absorption values at 600 and 455 nm; from there it can be seen that the formation of indigo is concomitant with the decrease of DHI and that after ~40 hours the formation of indigo at the expenses of DHI is (essentially) complete, with the final coexistence of the two forms (neutral and oxidized) in solution.

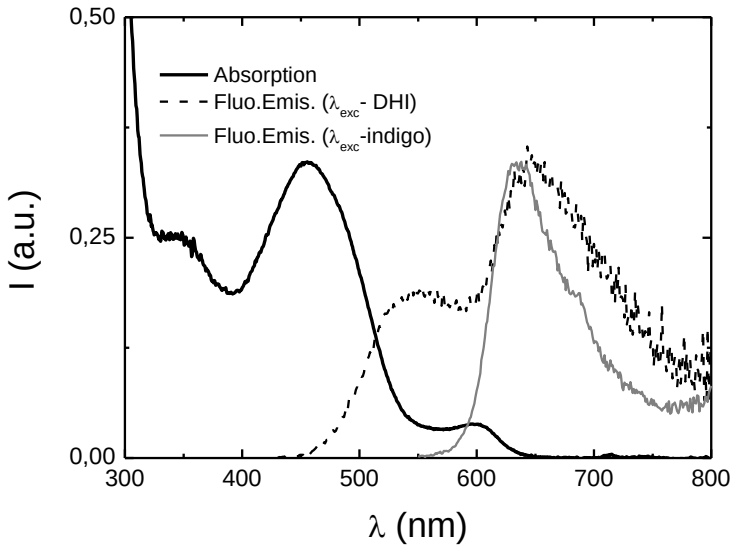

Figure 17 – Fluorescence emission spectra of DHI in toluene, obtained with two different excitation wavelengths, one corresponding to the absorption of DHI (λ_{exc}=455nm) and the other to the absorption of indigo (λ_{exc}=600nm), at 293K.

In Figure 17, it can be seen that in toluene (and the same behaviour is found in benzene as solvent) the emission spectrum of DHI is dependent of the excitation wavelength. When excitation is made at 455nm (dehydroindigo) the emission spectra shows two bands with maxima (λ_{em}) at ~540nm and ~645nm, see Table 4. However, when excitation is at 600nm (indigo absorption band) a single

band is observed with a wavelength emission maxima, at 640 nm[10]. These results support the coexistence of dehydroindigo and indigo in the emission spectra and that when excitation is made in the absorption region of DHI, two emission bands are observed (indigo and DHI), whereas when the excitation is made in the absorption band of indigo - where dehydroindigo does not absorb - the resultant emission is solely from indigo.

In methanol DHI displays a different spectral behaviour from that observed in toluene, Figure 18. In addition to the indigo absorption band (shifted to λ_{max}=607 nm, Table 4), the 455nm band, previously observed in toluene/benzene, is now blue-shifted to 400 nm. Moreover, when excitation is made in this band, the emission of DHI is now only 5 nm blue-shifted, λ_{max} =535nm, relative to toluene. In addition, the fluorescence quantum yield in methanol increases by ca. one order of magnitude when compared with toluene (or benzene), see Table 5.

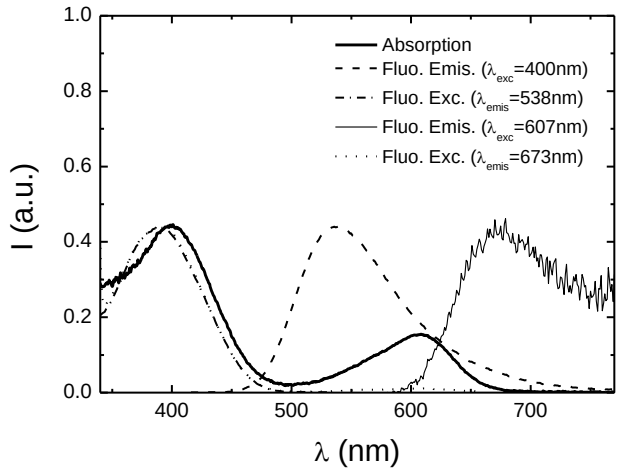

Figure 18- Absorption, fluorescence emission and excitation spectra (normalized) for dehydroindigo in methanol, at T=293K.

Table 4 - Spectral parameters (absorption and emission wavelength maxima and singlet and triplet extinction coefficients) for dehydroindigo in several solvents at T= 293 K.

Solvent	λ_{abs}^{max} (nm)	ε_{ss} $\left(M^{-1}cm^{-1}\right)$	λ_{fluo}^{max} $(nm)^{*}$		ε_{TT} $\left(M^{-1}cm^{-1}\right)$
Toluene	455,600	4870 ±150	544, 645 with λ_{exc}=455nm	636 with λ_{exc} =600nm	10240 (±400)
Benzene	456, 600	5056 ± 90	541, 645 with λ_{exc} =457nm	635 with λ_{exc} =600nm	10947 (±108)
Methanol	400, 607	3005 ±68	535 with λ_{exc} =400nm	672 with λ_{exc} =606nm	8975 (±375)

* the wavelength maxima of the bands were obtained with the excitation wavelength (λ_{exc}) indicated.

Table 5 - Photophysical parameters (fluorescence quantum yield, singlet oxygen quantum yield, phosphorescence quantum yield and triplet formation quantum yield) for dehydroindigo in several solvents at T= 293 K.

Solvent	ϕ_F**		ϕ_Δ	ϕ_{Ph}	ϕ_T
Toluene	0.00032 (±0.00003) with λ_{exc} =455nm	0.0012 (±0.0001) with λ_{exc} =600nm	0.60 (±0.01)	N.D.	0.71 (±0.05)
Benzene	0.000081 (±0.000004) with λ_{exc} =457nm	0.0010 (±0.00005) with λ_{exc} =600nm	0.83 (±0.07)	N.D.	0.83 (±0.08)
Methanol	0.0250 (±0.0003) with λ_{exc} =400nm	0.0011 (±0.0001) with λ_{exc} =607nm	0.15 (±0.01)	0.159 (±0.013)	0.156 (±0.014)

** the fluorescence quantum yields were obtained from the integrated bands which were obtained with the excitation wavelength (λ_{exc}) indicated.

ND- not determined

In Figure 18 it can be seen that the excitation spectra observed at the dehydroindigo and indigo emission bands, reproduce the bands of the absorption spectra of these two species, (although there is a small shift between the absorption and excitation bands of DHI). However, this difference is due to the fact that with the absorption, the spectrum of DHI overlaps that of indigo, leading to the small shift in the band, which is not observed in the excitation spectrum since it reproduces the "absorption" of the "pure" DHI.

In molecules where the lowest lying singlet states are of n,π* and π,π* origin, hydrogen bonding can be established between the nitrogen or oxygen (in the present case in the C=O group) atoms and the solvent molecules, resulting in a stabilization of the n, π* and inversion of the lowest lying neighbouring n, π* and π,π* states.[102] In toluene, the water molecules are available to promote an efficient hydrogen bonding with the lone pair electrons of the oxygen in the carbonyl groups of DHI. This consequently leads to a stabilization of the n, π* state (relative to the π,π*), by decreasing the energy of the non-bonding orbitals which results in a poor fluorescence emission (low ϕ_F in Table 5), which is also a way of identification of an n, π* state.[102] In contrast, when methanol is used as solvent, the hydrogen-bond ability of this solvent is not so efficient (as compared with water) and consequently there is a poor stabilization of the n,π* state, and now the lowest lying state is of π,π* origin. Indeed, in Table 5 the ϕ_F (see below further discussion) is much lower in toluene than it is in methanol. Also the location of the 400 nm band in toluene (which is blue-shifted relative to methanol) implies that this is an S_2 of π,π* origin whereas the n,π* transition is buried underneath this intense band. This is also totally compatible with the molecular orbital contours obtained by TDDFT calculations; see discussion below.

Table 5 reveals that in marked contrast with keto indigo, where the main deactivation channel of the excited state is the radiationless internal conversion[49,103,104], or with leuco indigo where fluorescence, internal conversion and intersystem crossing coexist[103], with DHI (in toluene and benzene), triplet state formation is now the main deactivation route for the first singlet excited state. In methanol, although the ϕ_T value decreases to 0.156, this is still significantly higher than the value of the keto form, the blue indigo (ϕ_T= 0.0068)[50]. We can see that now the intersystem crossing is an important pathway for excited state deactivation in comparison with indigo, thus providing conclusive evidence that the N-H groups (presumably through proton transfer to C=O) have a crucial role in the excited state deactivation (and hence photostability) of indigo.

4.2 – TRIPLET STATE AND SINGLET OXYGEN SENSITIZATION

The transient triplet-singlet difference absorption spectra of dehydroindigo in toluene (which is identical to the spectra in benzene) is depicted in Figure 19A. A strong absorption with maximum at 605 nm and depletion at 450 nm is observed. The decay traces in the depletion and maxima regions are identical, thus showing that the ground-state is recovered at the expenses of the generated transient triplet generated. In methanol (Figure 19B), the transient triplet-triplet spectra shows a depletion band at 400 nm, consistent with the absorption spectra, Figure 18, with a maximum at 450 nm.

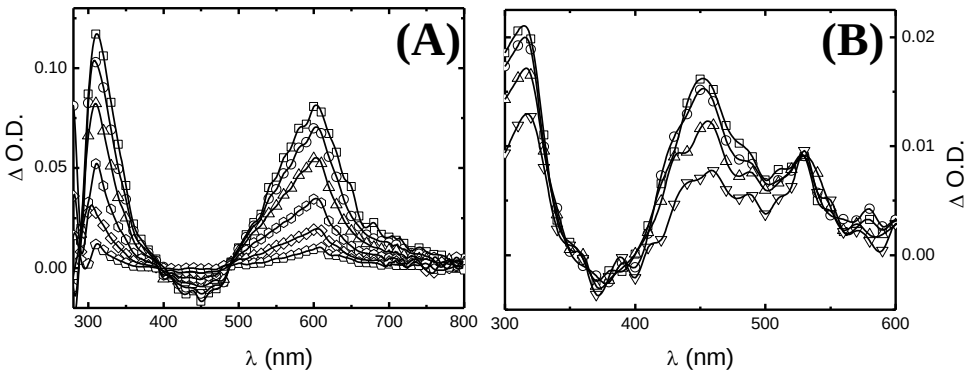

Figure 19 - Transient triplet-triplet absorption spectra obtained for dehydroindigo in toluene **(A)**, and methanol **(B)**, obtained with different delay times after laser flash, T=293K.

In the case of the non-protic solvents benzene and toluene, the intense transient signals are also mirrored in the high intersystem crossing values obtained (see Table 5).

Singlet oxygen was sensitized by DHI and the respective quantum yields were obtained in the three solvents: toluene, benzene and methanol (seeTable 5). In the situations where DHI is dominant (over indigo) the values are high, thus showing that the triplet state efficiently transfers energy to molecular oxygen. In the case of methanol, the ϕ_Δ values are smaller, but still in agreement with the values obtained for ϕ_T, see Table 5. This behaviour is similar to what is seen with other systems with lowest energy π,π^* triplet states[50,105] (which is the case of DHI, see below) where the efficiency of singlet oxygen production from the triplet state is high, S_Δ~1, which is not necessarily always true when the triplet state is of n, π^* origin.[106]

4.3 - PHOSPHORESCENCE IN METHANOL

The phosphorescence emission spectrum of DHI was obtained in a rigid glass of methanol, Figure 20. Despite the fact that neutral keto indigo does not phosphoresce, phosphorescence emission of leuco-indigo was previously observed for indigocarmine in methanol[10,103]. With the phosphorescence of DHI we have observed an emission maxima of 540nm, a quantum yield of 0.159 (see Table 5) and a lifetime ~190ms, which are characteristic parameters of a triplet of π,π^* origin, similarly to what was found for the keto-indigo.[50] The closely relation between the ϕ_T and ϕ_{Ph} values shows that, in methanol, the triplet state mainly deactivates radiatively.

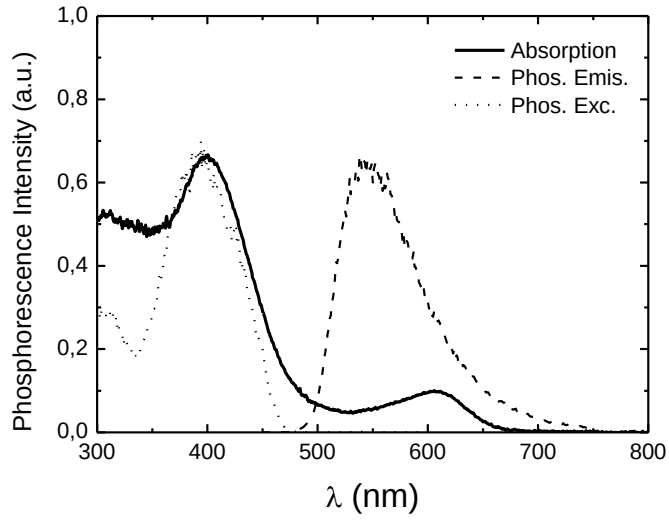

Figure 20 - Absorption, phosphorescence emission and excitation spectra (normalized) for dehydroindigo in methanol, at T=77K.

4.4 - TIME-RESOLVED FLUORESCENCE BEHAVIOUR

The fluorescence decays of DHI were obtained in a non viscous media (methanol - Figure 21), and in a viscous media (glycerol – Figure 22). The decays are clearly dependent on the emission wavelength.

The decays were collected with a time resolution of ≈3 ps[107], and could be fitted with triexponential decay laws according to Equation 2,

$$I_\lambda(t) = \sum_{ij} a_i e^{-t/\tau_j} \qquad (2)$$

where $I_\lambda(t)$ is the fluorescence intensity at the emission wavelength λ, a_i (with i= 1, 2, 3,…) the pre-exponential factors and τ_j (j= 1, 2, 3) the decay times, see Figure 21 and 22.

One would expect that DHI to decay mono-exponentially. However, these were found to be triexponential. A possible explanation for the triexponential nature of the decays involves (rotational) isomerisation, as follows. The instantaneously excited DHI decays with 10-20 ps. This can further convert in the excited-state, into two other structures/conformers of DHI (with different angles between the two isatin-like moieties, Scheme 15); based on this data, the presence of some of these two species/conformers in the ground-state cannot be completely ruled out. With excitation at 425 nm, these two conformers emit with decay times of 680 ps and ~2 ns. This is again illustrated in Scheme 15.

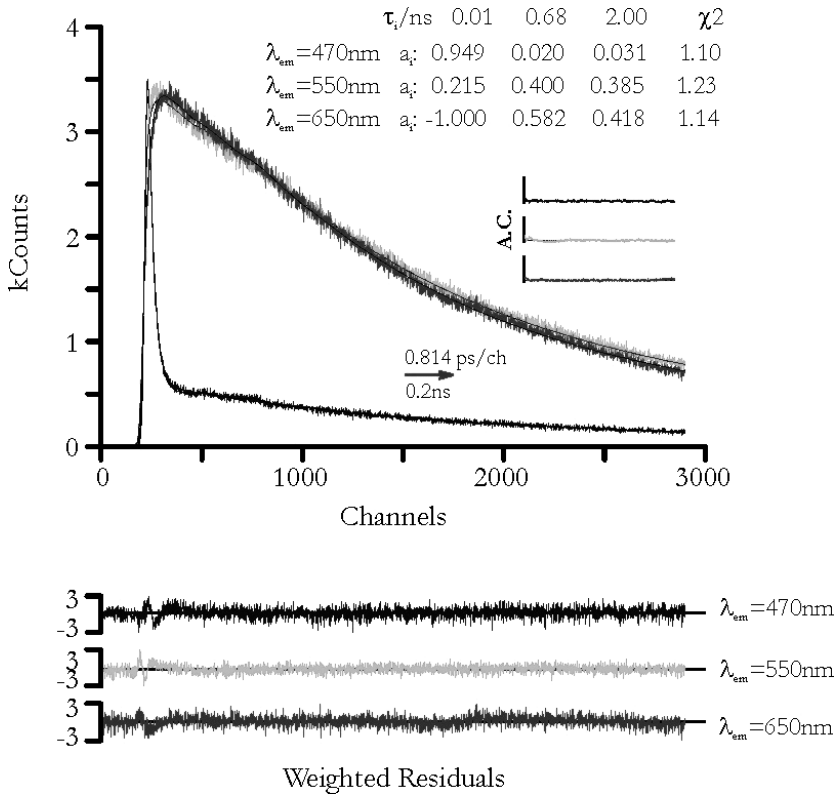

Figure 21 - Fluorescence decays of **dehydroindigo in methanol**, at T=293K, with excitation at 425 nm and collected at 470nm, 550nm and 650nm. Shown as insets are the decay times (τ/ns), pre-exponential factors (a_i), and chi-squared values **(χ^2).** Also shown are the weighted residuals for a better judgment of the quality of the fits.

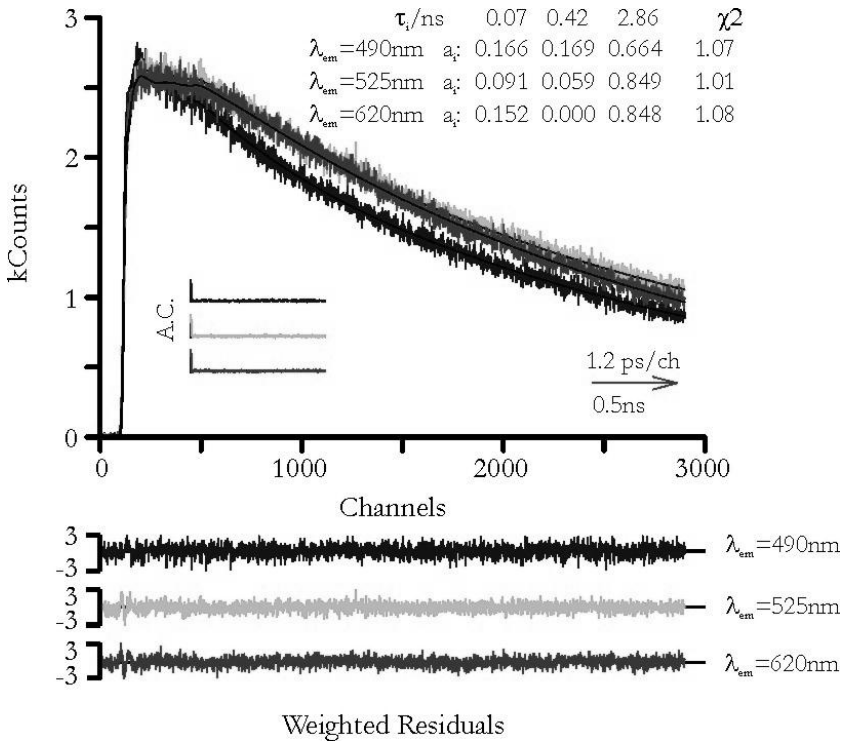

Figure 22 - Fluorescence decays of **dehydroindigo in glycerol**, at T=278K (-20ºC), with excitation at 425 nm and collected at 490nm, 525nm and 620nm. Shown as insets are the decay times (τ/ps), pre-exponential factors (a_i), and chi-squared values (χ^2). Also shown are the weighted residuals for a better judgment of the quality of the fits.

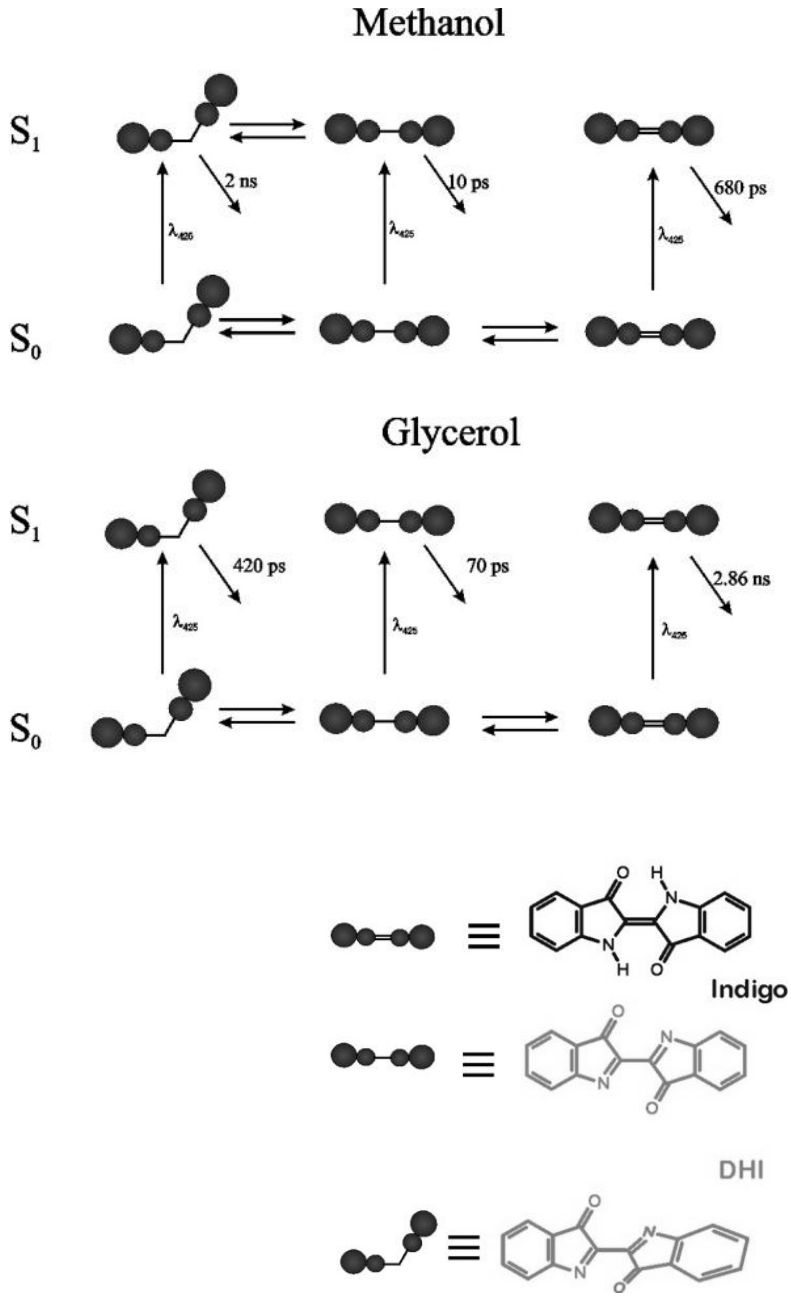

Scheme 15 – Schematic presentation of the kinetics in the ground- and first excited singlet state for DHI in methanol and glycerol.

In methanol, the rising component (negative pre-exponential factor), associated to the shorter component shows that this species gives rise, in the excited-state, to the two other species with longer decay components and that this process most likely involves a rotation around the central C-C bond connecting the two isatin-like moieties. Since the model compound, isatin, is known to be nonfluorescent[108] (which was also verified in this work) this means that none of the conformers involves a total conjugation rupture (decoupling) between the two (isatin-like) moieties.

It is worth remembering, once more, that the excitation spectra collected all over the emission spectra of DHI overlaps with the absorption of this compound. This indicates that the DHI conformers absorb in the same spectral region, with very similar absorption maxima, i.e., they are within the homogeneous broadening of these bands.

A further analysis of the possible involvement of rotational isomerism comes from changing the viscosity of the solvent. Although poorly soluble in several solvents, DHI was found to be soluble in glycerol (a highly viscous solvent, η (20ºC)= 1.412 Pa s). At low temperature, -20 ºC, (Figure 22) the decays are, as with methanol, dependent of the emission wavelength. However, now the decay times have larger values than those found in methanol but, more significantly, the negative pre-exponential factor is absent. This shows that the conversion of one conformer into the other (involving rotational process) is precluded (at least in the excited state) and that the contribution of the different conformers comes from their relative proportions in the ground state.

4.5 – COMPARISON BETWEEN DHI AND INDIGO

Scheme 16 summarizes the overall spectral and photophysical data obtained for DHI, data for indigo are also presented.[10,50,109]

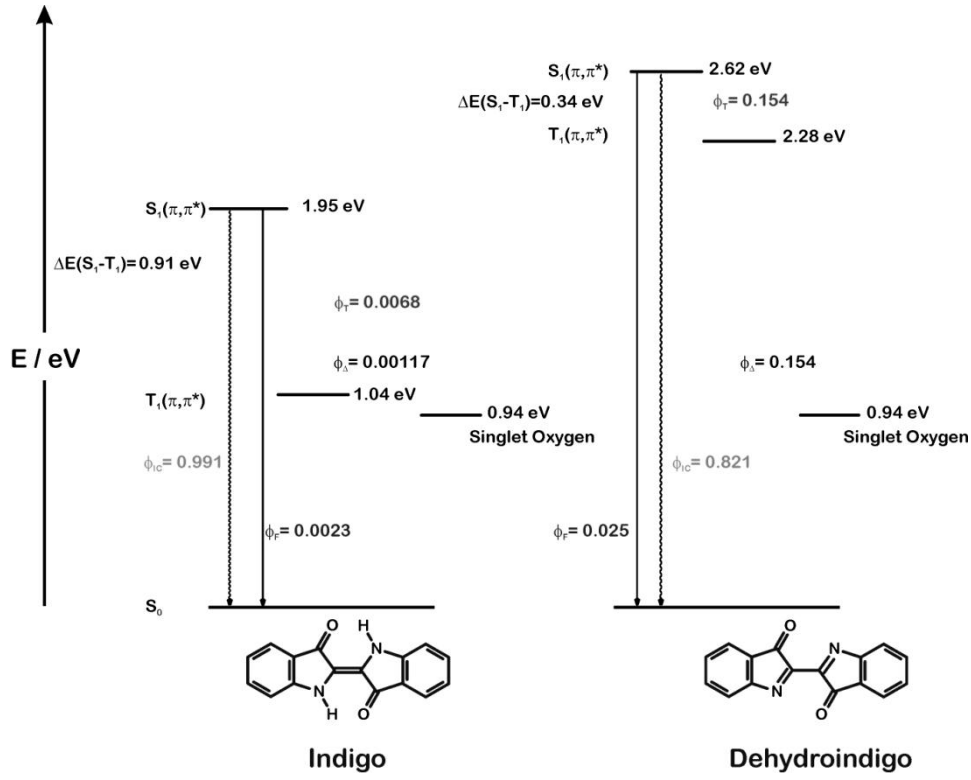

Scheme 16- Jablonsky-like diagram showing for indigo (left) and DHI in methanol (right) the different values for the quantum yields of excited state deactivation and energies (in eV) of the lowest lying singlet and triplet excited states.[52]

The first clear difference lies in the fact that the single bond character between the two isatin-like moieties in DHI breaks up the H-chromophore[110,111] character of indigo leading to a difference of 0.67 eV between the S_1-S_0 energy gap and consequently in the colour displayed by these two forms of indigo. This is also valid for the triplet energy with now an even more pronounced difference of 1.24 eV. It further implies that, in marked contrast with indigo, DHI has a much smaller singlet-triplet energy splitting, leading to a very efficient $S_1 \sim\sim\rightarrow T_1$ intersystem crossing process, and also a high efficiency of singlet oxygen sensitization, $S_\Delta = \phi_\Delta / \phi_T \sim 1$. Further studies (including theoretical calculations) on this oxidized species of indigo particularly on the relevance of rotational isomerism, consequence of the single bond character of the central carbons of the molecule, in the properties of the lowest singlet and triplet excited states can potentially explain the amazing differences displayed by the three forms of this molecule.

The analysis of the deactivation rate constants for DHI is complex because of the multiexponential nature of the decays, indicating that several species decay, thus contributing to the overall deactivation of DHI in S_1. However, since we observe that the species contributing more to the total fluorescence (at longer wavelengths) is the longer component, with a value of 2 ns in methanol and a ϕ_T value of 0.156 (Table 5), we obtain a value for the intersystem crossing rate constant, $k_{ISC} = 7.8 \times 10^7\ s^{-1}$. These together with the 0.34 eV value of the S_1-T_1 energy splitting, are values typically close to those found for aromatic hydrocarbons[112], providing convincing evidence that the triplet state of the oxidized form of indigo is, similarly to its neutral keto indigo[50], of π,π^* origin.

In toluene, S_1 is of n,π^* origin whereas T_1 (or the interacting triplet) is of π,π^* origin. In methanol S_1 is of π,π^* origin and T_1 is still of π,π^* origin. As a consequence of this and in full agreement with El-Sayed rules, the intersystem

crossing process (as seen by the ϕ_T value) is more efficient in toluene (ϕ_T=0.89, Table 5) than it is in methanol (ϕ_T=0.189) since in the first case the coupling involves singlet and triplet states of different origin and in the second case of identical (π,π^*) origin.[97,113,114]

4.6 – THEORETICAL CALCULATIONS ON THE ELECTRONIC STRUCTURES OF THE S_0, S_1 AND T_1 STATES OF DHI

Within the framework of the density functional theory (DFT), the structures of the ground and excited states of DHI could be further accounted. The molecular geometries of DHI were optimized at the B3LYP/6-31G** level without imposing any symmetry constrains. Different structures for the S_0, S_1 and T_1 electronic states, showed in Figure 23 through the bond distances in these three states, were obtained.

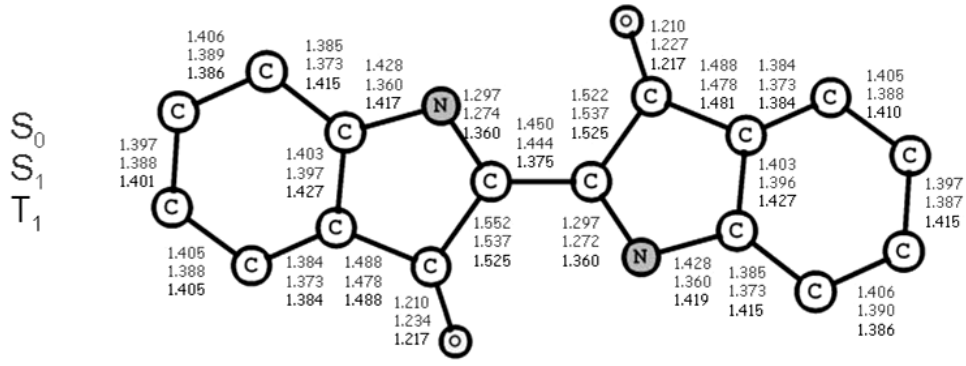

Figure 23 - Bond length (in Å) calculated for DHI using DFT calculations (B3LYP 6-31G** level) for the electronic ground (S_0) and first singlet (S_1) and triplet excited (T_1) states.[52]

The energy difference between the HOMO and LUMO orbitals (vertical transition) has a value of 3.01 eV which agrees well with the energy obtained for the, also vertical, transition (wavelength maxima) in methanol, 3.1 eV, see Table 4. However, and by comparison with the experimental S_0-T_1 energy gap of 2.28 eV, Scheme 16, theory seems to fail since now the energy gap is predicted to be 1.13 eV which is less than a half of the experimental value and much close to that found for indigo triplet state.[50,109] Further studies on the (theoretical) location of the triplet state, namely using different basis set, should provide a more accurate location of the (predicted) triplet state of DHI.

Figure 24 shows the ground-state optimized geometries for DHI together with the molecular contours of the relevant molecular orbitals (HOMO-1, HOMO, LUMO, LUMO+1). From these DFT calculations, the HOMO orbital shows a clear non-bonding character imparted by the non-bonding orbitals in the carbonyl oxygen. In contrast, the LUMO orbital shows a π-antibonding character; these results in a HOMO→LUMO n,π* transition which is in agreement with the experimental data found in toluene (with water). However, like experimentally found in methanol, the lowest lying excited state is of π,π* origin. In Figure 24, the molecular contours in the HOMO-1 are localized along the π-orbitals of the carbon atoms of the six- and five-member rings. This is compatible with a π,π* transition (involving the HOMO-1 and the LUMO and LUMO+ 1 orbitals) which corroborates the finding that in methanol the lowest lying transition is of π,π* origin.

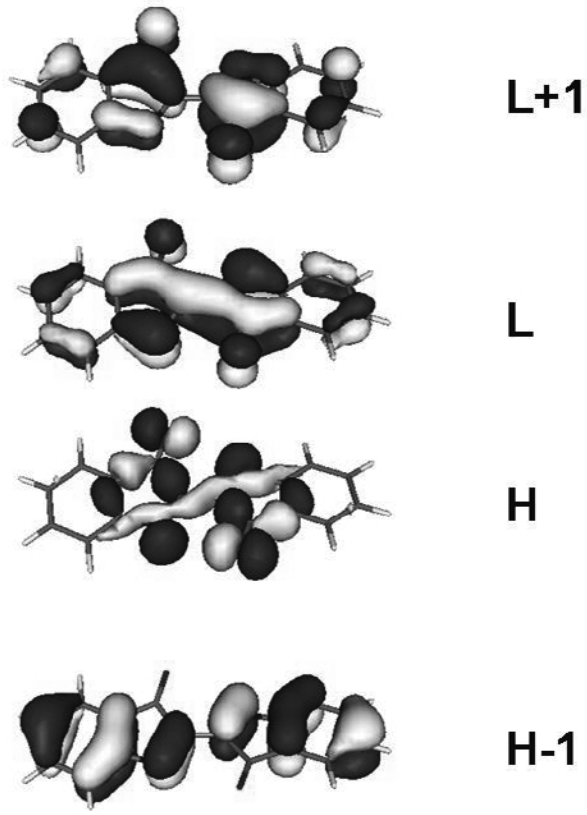

Figure 24- B3LYP 6-31G**optimized ground-state molecular structures and for the HOMO, HOMO-1, LUMO and LUMO+1 molecular orbital contours for DHI.[52]

It is now worth to return to the different geometries displayed by the S_0, S_1 and T_1 states. In the case of S_0 the predicted (more stable) geometry shows a deviation from planarity of 19.72º (dihedral angle between the N-C-C-N bonds) whereas in S_1 and T_1 the more stable geometry is now close to planarity.

The bond length in Figure 23 show that contrary to what has been described with indigo, where DFT calculations show that there is basically no change in the bond length of the six-member rings (of indigo)[109], in the case of DHI there is a difference between the bond length values of the more peripheral bonds of these 6-member rings and those more closed to the five-member rings, indicating less delocalization to the outer bonds. As with indigo[109], the anti-bonding character of the C=O bond is increased in DHI upon going from the S_0 to the S_1 state, which is mirrored by a lengthening of the bond (from 1.210 Å to 1.234 Å). However, the most significant and interesting change in bond length occurs in the central CC bond where the bond distances decrease on going from S_0 to T_1 (0.075 Å) indicating a gain of the double bond character in T_1. The change in this central CC bond length upon going from S_0 to S_1 is insignificant (0.006 Å) indicating that the single bond character of this bond allows the existence of different conformers both in the ground and singlet excited state, as discussed previously in section 3.4.

Again with indigo others have found that, with similar DFT calculations, the $S_0 \rightarrow T_1$ transition causes a significant increase in the length of the CC central bond (from 1.361 to 1.423 Å) resulting in the change of this carbon-carbon bond from a double (S_0) to a single bond (T_1) character.[109] This seems to be in line with the absence of phosphorescence[10] with indigo, not only because of the small S_0-T_1 energy gap, 1.04±0.10 eV[50] (which from the golden rule for the radiationless transitions would favour this channel of deactivation), but also because of the single bond character of the carbon-carbon bond in indigo, allowing a loose bolt effect of this central bond (acting as a stretching or twisting vibration mode promoter of an efficient radiationless transition), that would promote the coupling between the T_1 and S_0 nonradiative modes[114] turning on the $T_1 \sim\sim\rightarrow S_0$ into a very efficient process.

In contrast with indigo is DHI, where theory predicts the opposite situation, Figure 23, i.e., in the triplet state of this oxidized form of indigo the central carbon-carbon bond has now a double bond character. This would explain the observation of phosphorescence since the now more rigid (absence of rotation around the central carbon-carbon bond) together with the high S_0-T_1energy gap value, 2.28 eV (Scheme 15), would decrease the coupling between the nonradiative modes of T_1 and S_0, favouring the radiative channel.[114]

4.7 – CONCLUSIONS

In aqueous solution or in protic solvents, DHI has the tendency to extract hydrogen from the media giving rise to the neutral blue indigo. Depending on the solvent, dehydroindigo displays different spectral and photophysical properties.

The photophysics of DHI is remarkably different from the neutral indigo keto (blue) form and also from the reduced indigo leuco form. In marked contrast to what has been found for keto-indigo, where the internal conversion channel dominates >99% of the excited state deactivation, or with the fully reduced leuco-indigo, where fluorescence, internal conversion and singlet-to-triplet intersystem crossing coexist, in the case of DHI in toluene and benzene, the dominant excited state deactivation channel involves the triplet state. Triplet state yields (ϕ_T) of 70-80%, with negligible fluorescence ($\leq$ 0.01%) are observed in these solvents. In methanol the ϕ_T value decreases to ~15%, with an increase of the fluorescence quantum yield to 2%, which makes these processes competitive with the $S_1 \sim\sim\rightarrow S_0$ internal conversion deactivation process. The data are experimentally compatible with the existence of a lowest lying excited state of n,π^* origin in

toluene (due to hydrogen bonding with the water molecules) and of π,π^* origin in methanol.

This gives further support to the fast deactivation, via the radiationless internal conversion channel, of indigo which must be operative in this neutral form through intramolecular proton transfer from the N-H to the C=O groups.

Time resolved fluorescence decays reveal a fit to a triple exponential decay law, compatible with the presence of rotational isomerisation.

DFT calculations (B3LYP 6-31G** level) were performed in order to characterize the electronic ground (S_0) and excited singlet (S_1) and triplet (T_1) states of DHI. The HOMO-LUMO transition was found to go along with an $n \rightarrow \pi^*$ transition of the oxygen nonbonding orbitals to the central CC and adjacent C-N bonds. Calculations also revealed that in S_0 the two indole-like moieties deviate from planarity from ca. 20º, whereas in S_1 and T_1 the predicted structure is planar; a gradual decrease of the carbon-carbon central bond distance is seen on the order S_0, S_1, T_1.

5. An Indigo Polymer

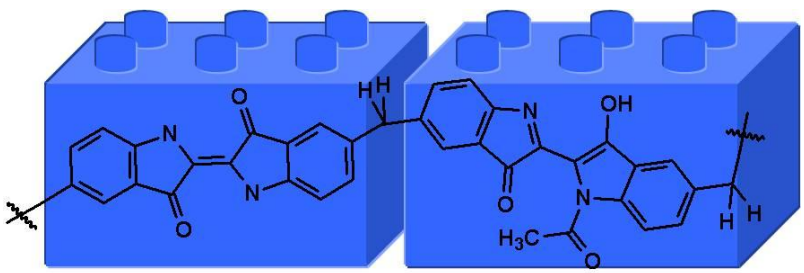

Due to the low solubility of indigo in the majority of organic solvents the idea of a polymer built of indigo has probably never been properly equated. Albeit the pioneer work of G. Heller[115] in 1903 who prepared a polymeric indigo but could not realize the polymeric nature of the dye[116], the first report of a detailed characterization of a polymer of indigo is dated from 1990 with the work of Tanaka *et al.*[117] who prepared a polymer with indigo units in the main skeleton, and found that the polymer was insoluble but possessed a fraction that was attracted to a permanent magnet therefore displaying magnetic properties. More recently Voss *et al.*[116] prepared and characterized two similar statistical copolymers made of indigo and N-acetylindigo with defined structures in solution and solid state.

With the recent recognition of the potential relevance and importance of organic conjugated polymers for photovoltaic applications, including isoindigo based conjugated polymers[118,119], a polymer of indigo, if displaying similar properties to its monomeric unit, is of relevance since it would potentially generate long lived and stable charged species (whose radiative deactivation is negligible) a requisition which is mandatory for this type of applications.

The polymer studied in this section is a 5,5'-methylene-bridged polymeric indigo, a statistical copolymer consisting of indigo (keto structure) and N-acetylindigo units (consisting of N-acetyl-donor units and indolone acceptor units), see Scheme 17.

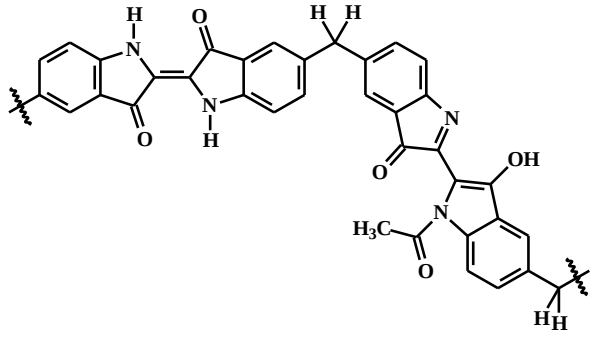

Scheme 17 – Structure of 5,5'-methylene-bridged polymeric indigo.

5.1 - SPECTRAL AND PHOTOPHYSICAL PROPERTIES

As expected, the polymer presents solubility similar to that of indigo, i.e., good solubility in dimethylsulfoxide (DMSO), dimethylformamide (DMF) and dioxane. The absorption and fluorescence, together with the fluorescence excitation spectra in DMSO, are shown in Figure 25. A good overlap between the absorption and the excitation is observed thus attesting the purity (and potentially little polydispersity) of the polymer.

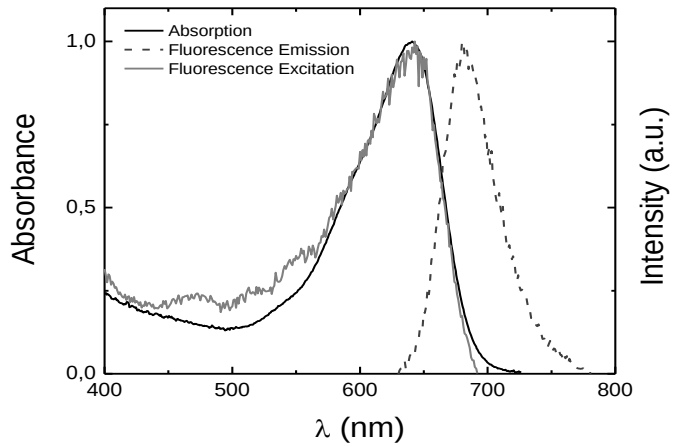

Figure 25- Absorption, fluorescence emission and excitation spectra of the indigo polymer in DMSO, T= 293K.

In Table 6 the spectral and photophysical data for the polymer and indigo itself are given. From data in Table 6 it can be seen that the absorption wavelength maxima is, for the polymer, red-shifted (20 nm in DMF) relative to that observed for indigo. The same happens with the emission maxima, but now with a red-shift of 19 nm (this value can be higher – up to 44 nm- depending on the solvent).

Table 6- Spectral and photophysical properties including quantum yields (fluorescence, ϕ_F, internal conversion, ϕ_{IC}, triplet formation, ϕ_T, and sensitized singlet oxygen formation, ϕ_Δ), lifetimes (τ_F,), rate constants (k_F, k_{NR}, k_{IC}, k_{ISC}) for the polymeric indigo and indigo itself in different organic solvents at T=298 K.

	λ_{abs}^{max} (nm)	ε_S $(M^{-1}cm^{-1})$	λ_{fluo}^{max} (nm)	Δ_{SS} (nm)	ϕ_F	τ_F (ns)	ϕ_T	ϕ_Δ	ϕ_{IC}	k_F (ns^{-1})	k_{NR} (ns^{-1})	k_{IC} (ns^{-1})	k_{ISC} (ns^{-1})
Polymer													
DMSO	630	-	681	51	0.00027	0.040	0.006	-	-	0.00675	24.99	24.84	0.15
DMF	630	-	672	42	0.00037	0.050	0.006	-	0.9936	0.00740	19.99	19.87	0.12
Indigo													
Dx	600	17710	637	37	0.0025	0.126[a]				0.0198	7.92		
DMF	610	22140	653	43	0.0023	0.140	0.0066[b]	0.0012	0.991	0.0164	7.12	7.12	0.0084

(a) value taken from ref.[10]

(b) Data taken from[50]

$$k_F = \frac{\phi_F}{\tau_F} \; ; \; k_{NR} = \frac{1 - \phi_F}{\tau_F} \; ; \; k_{IC} = \frac{1 - \phi_F - \phi_T}{\phi_F} \; ; \; k_{ISC} = \frac{\phi_T}{\tau_F} \; ; \; \phi_{IC} = 1 - \phi_F - \phi_T$$

The absorption spectrum of the polymer shows, besides the red-shift relative to indigo, a higher inhomogeneous broadening of its visible band, a situation which is common to observe in a polymer when compared to its oligomeric counterpart.[120,121] Indeed, the well-defined conjugation length of an oligomer results in a smaller inhomogeneous broadening of the absorption spectra.[122] The Stokes shift (Δ_{SS}) is, with the polymer, comparable to that found with indigo, Table 6. However, whilst with indigo this relatively small value for Δ_{SS} has been suggested to be related to the fact that the absorption is due to the *keto* neutral form, whereas the emission band would result from the convoluted emission of this instantaneously formed species with that resulting from proton transfer (from the N-H to the C=O group which could be intra or –assisted by the solvent– intermolecular), in the case of the polymer the significant Δ_{SS} value suggests to be the result of a different geometry in the ground and excited states.

Another interesting point is the fact that in the emission (Figure 26), the *Full-Width Half*-Maximum (FWHM) is smaller with the polymer than with indigo - albeit the fact that this difference is small- which shows that the emission of the polymer is more localized. This decrease in the FWHM of the polymer suggests that now the emission is solely due to the emission of a single species (chromophoric unit), in contrast to what is observed with indigo.

In contrast to what is observed with indigo, where only with biexponential decay laws (with decay profiles emission wavelength dependent) the decays could be properly fitted,[10,49] now the decays are basically single exponential (see Figure 27). Indeed, as can be seen in Figure 28, the decays of indigo change when collected along the band, mirroring the same decay times but different pre-exponential factors. As mentioned above, this has been consistently linked from various studies to intra- or intermolecular proton transfer between the N-H and C=O groups of indigo.[48,49,57]

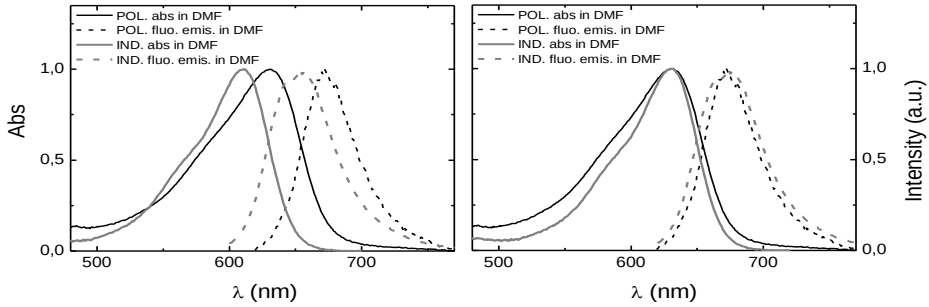

Figure 26- Absorption and fluorescence spectra for indigo and the indigo polymer in DMF. In the **left panel** the spectra are normalized at its intensity/abs maxima, whereas in the **right panel** the absorption spectra of indigo and of its polymer are (artificially) set to have the same maxima and the same is valid for the emission spectra, where now the differences in the inhomogeneous broadening can be better visualized.

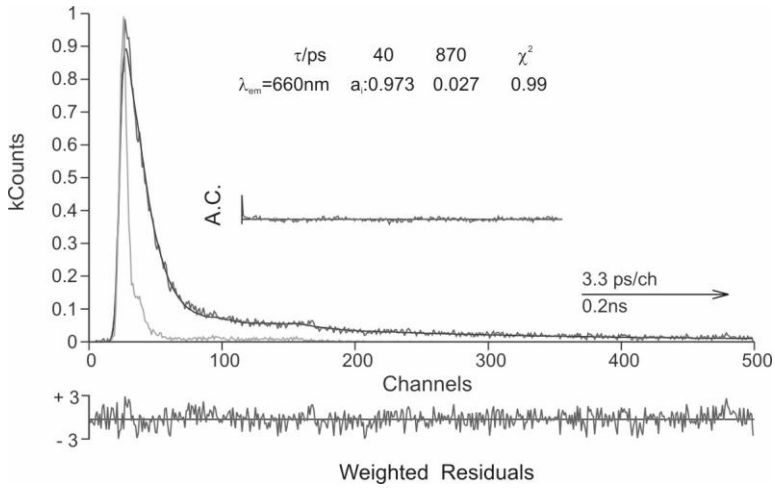

Figure 27- Fluorescence decay and pulse instrumental response for indigo polymer in DMF at T=293K. Shown as insets are the decay times and pre-exponential factors. Also shown are the weighted residuals, autocorrelation functions (A.C.) and the χ^2 values for a better judgment of the quality of the fits.

Another peculiarity is the short value of the fluorescence lifetime (~40-50 ps), displayed by the polymer, in comparison with that of indigo itself, where values between 130-140 ps (Table 6, Figure 27 and refs.[10,49,123]) could be found suggesting that, as with other organic conjugated polymers[124], on-chain energy migration, along chromophoric units (of different segmental size), is responsible for the excited state deactivation of the polymer. Also, the absence of a rising component (which is present in indigo and was associated to an instantaneously formed species which further transfers its proton in the excited state from the N-H to the C=O group) indicates that, in the polymer, either this process compete (inefficiently) with energy migration or that it is purely absent.

It is worth stating that the decay of the polymer is not single exponential. Indeed, an additional long-lived component is needed to properly fit the decays; however, this component is relatively insignificant since the associated pre-exponential factor represents less than 3% of the (concentration) species generated at time zero. The need (and presence) of this additional component is suggested to be related to some of the polydispersity associated to the polymer or, given the different chromophoric contributions to the structure of the polymer to a partial emission of these two partially isolated units, indigo (keto structure) and tautomeric N-acetylindigo.

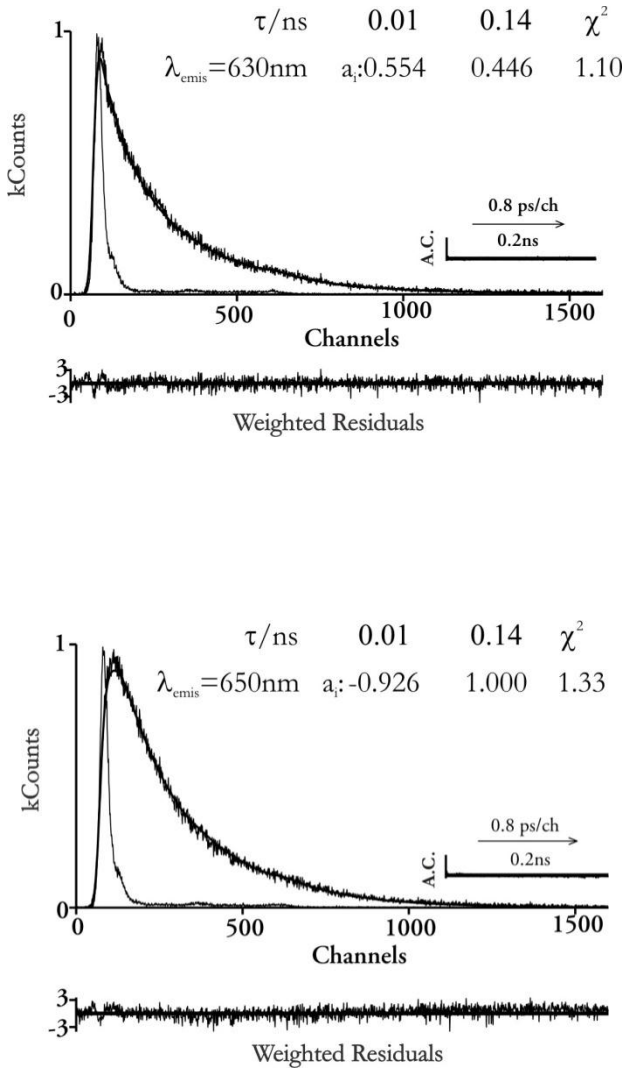

Figure 28- Fluorescence decay and pulse instrumental response for indigo in DMF, collected at two different emission wavelengths at T=293K. Shown as insets are the decay times and pre-exponential factors. Also shown are the weighted residuals, autocorrelation functions (A.C.) and the χ^2 values for a better judgment of the quality of the fits.

5.2- PHOTOACOUSTIC EXPERIMENTS

Like with the parent indigo it was not possible to observe any triplet-triplet transient signal, and time resolved photoacoustic calorimetry (PAC) was the solution found to characterize the triplet state of this polymer.

In the case of systems with negligible volume changes, as it is the present case, time-resolved PAC measures directly the heat released in the decay of transients formed by pulsed laser excitation. In a typical PAC experiment the amount of energy released through the radiationless channels together with the lifetimes associated to these processes is obtained.[50,125] In order to obtain these values for an unknown sample, the photoacoustic wave is first obtained - under identical conditions, including the same optical density at the excitation wavelength- for the solvent and for a reference compound, which decays totally through radiationless processes during a time shorter than the transducer resolution (< 10ns). From the deconvolution of sample and reference signals, the fraction(s) of heat released in the formation of the sample transient(s) are obtained. Since it was previously established that more than 99.9% of the *quanta* loss in indigo are from radiationless processes[50], indigo itself was used as the photoacoustic reference for these experiments. In practical terms, the experimental procedure consists in measure the reference, sample and solvent photoacoustic signal at the same conditions at different energies; the experiment are carried in order to avoid or minimize bi-photonic effects. In the current experiment four different laser energies were used to excite the polymer in solution.

As can be observed in Figure 29, where the waves of a typical PAC experiment are presented - solvent, reference (indigo in the present case) and the polymer-, the PAC wave of the polymer did not show significant differences

relative to the reference (indigo), either in presence or absence of oxygen. Moreover, since no bi-photonic effects could be detected, there was no justification to obtain the energy released (and deposited as heat) by extrapolation to excitation energy values of zero (usual procedure used in our lab for these experiments)[50] and therefore the value was obtained as the mean value of four different experiments giving a quantum yield value for the energy released in the form of heat, $\phi_1 = 0.997 \pm 0.02$.

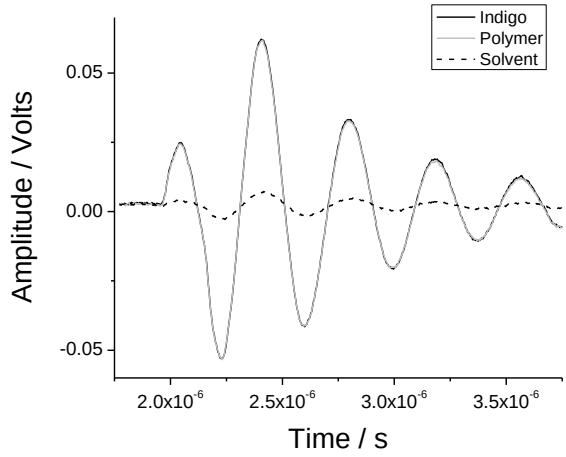

Figure 29 - Example of a typical PAC experiment with the waves for 100% laser intensity: reference wave (indigo, full black line), sample wave (full grey line); sample and reference in DMF (solvent) at 293 K.

In the case of indigo (and the same occurs with the polymer, see Table 6), the triplet is formed very rapidly (within a few hundred ps for indigo and 40-50 ps for the polymer) thus contributing to a prompt heat released fraction (ϕ_1); moreover its decay in degassed solutions is much slower ($\tau_T \sim 30\mu s$[10] in the case of indigo) than the time window of our experiment and is not detected by the

transducer used. The value of ϕ_1 corresponds to the energy fraction deposited in the S_1-S_n decay and T_n-S_1 intersystem crossing. Thus, with the ϕ_1 value measured by PAC, the knowledge of the energies of the excited states involved (S_1 and T_1), and the quantum yield of fluorescence (ϕ_F) it is possible to determine the quantum yields of the nonradiative processes.[50]

The energy balance for the formation of the triplet state requires that the energy of the laser pulse ($E_{h\nu}$) minus the sum of the energies released as heat in the formation of the triplet ($\phi_1 E_{h\nu}$) and the energy lost radiatively ($\phi_F E_{\nu max}$), must equal the energy stored in the triplet state according to the following equation:[50]

$$\phi_T \cdot E_T = (1-\phi_1) \cdot E_{h\nu} - \phi_F \cdot E_{\bar{\nu}\max} \qquad (3)$$

where $E_{\bar{\nu}\max}$ is the energy of fluorescence (taken as the energy at the maximum fluorescence intensity considered as the Gaussian center value of the fluorescence emission band) and $E_{h\nu}$ (the energy of the laser pulse) equal to 2.33 eV. In the case of the polymeric indigo, and assuming the value of the triplet energy of indigo, 134.7 kcal mol^{-1} (1.05 eV), and the values of ϕ_F=0.00037 (Table 6) together with the energy of the singlet state ($E_{\nu max}$) 42.43 kcal mol^{-1} (1.84 eV) from Eq. 3, a value of ϕ_T= 0.0060 was obtained; a value which is very similar to that found for indigo (0.0066)[50].

Summarizing: the quantum yield of fluorescence decreases one order of magnitude in the polymer when compared to indigo, Table 6; this, together with the value for the intersystem crossing yield (0.0066 for indigo vs. 0.0060 for the polymer) leads to an even higher ϕ_{IC} value for the polymer, thus showing that the process behind this decay route is more efficient in the polymer.

5.3 - STABILITY TOWARDS LIGHT

Indigo and the polymeric indigo were irradiated with λ_{exc}= 335 nm at different time intervals and the UV/Vis absorption spectra was obtained, Figure 30. From the plots in Figure 30, the ϕ_R was obtained for indigo in DMF (0.0078) – which compares well to the previously published value[101]- and for polymeric indigo (0.0030), respectively. This value is significantly lower than that of indigo (~2.7 times) which indicates that the polymer indigo has additional stabilization routes towards (photo)degradation. It is worth noting that although not investigated for the current polymer, the major product resulting from the photodegradation of indigo was found to be isatin.[101]

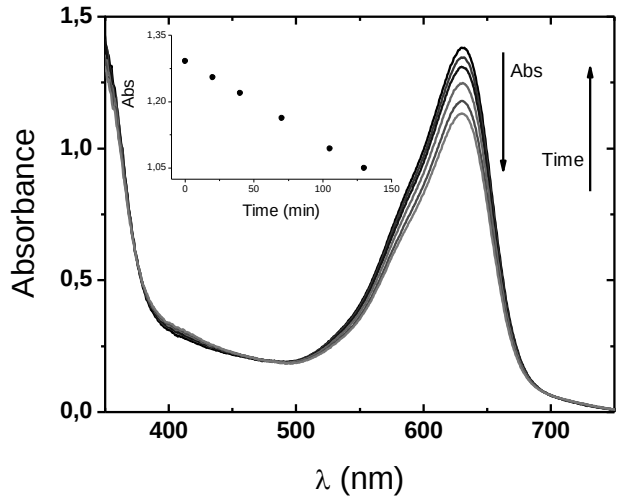

Figure 30 – Polymeric indigo in DMF, irradiated at 335nm and 293K, followed by UV-Vis absorption; as inset is plotted the variation in absorbance at 630nm, for the initial times, from which, comparing with indigo under the same experimental conditions, the ϕ_R value could be obtained.

5.4 – CONCLUSIONS

A comprehensive investigation of the solution photophysics of a polymeric indigo was performed in organic solvents and further compared with indigo.

The spectral and photophysical differences between the two were not significant, with exception to time resolved fluorescence, where polymer (mainly) decays single exponentially (in contrast with indigo, found to be biexponential), with a decay time value of 40-50ns and an even more efficient $S_1 \sim\sim\rightarrow S_0$ internal conversion deactivation channel, related to an efficient energy migration within a energetic ladder of the polymer chromophoric segments, in contrast with indigo where intra-or inter- molecular proton transfer[35,48,49,54,126,127] (between N-H and C=O groups) was attributed to the efficiency of this specific channel.

Relatively to the behaviour under light excitation, the polymer presented a photoreaction quantum yield (ϕ_R) of 0.003, which is lower than the previously determined for indigo in the same solvent (ϕ_R=0.0078).

The overall data suggests that although the polymer and indigo have a close finger-print, the former is more stable which is likely to be due to the additional intramolecular energy transfer processes (within different chromophoric units) found with the polymer.

6. Thioindigo

Thioindigo is the sulphur derivative of indigo, presenting a completely different spectral and photophysical behaviour, when compared with indigo itself, with fluorescence dominating the deactivation of the first excited singlet state (50-70 % of the *quanta* loss, depending on the solvent), with the $S_1 \sim\sim\rightarrow S_0$ internal conversion and $S_1 \sim\sim\rightarrow T_1$ deactivation channels representing, in equivalent values, the remaining quanta loss.

Starting in the 1950's and ending in the year of 1994, George Wyman devoted almost his entire scientific career to the study of indigo derivatives, namely thioindigo.[45,128,129] The idea is due to him that the "photostability of *trans* indigo was due to a very fast proton transfer in the singlet excited state rather than stability imparted to it by hydrogen bonds in the ground state".[47,129] However, there are differing views regarding this mechanism.[48,49,56,57] The experimental conditions at the time did not allow fluorescence of indigo to be detected and thus thioindigo with significant fluorescence yields was selected to provide information on this; on his final and seminal 1994 work Wyman was still embracing this idea: "In sharp contrast with the strongly fluorescent thioindigos, indigo dyes showed no detectable emission".[129] Indeed, the neutral (keto) form of indigo displays fluorescence but with a very low quantum yield.[10,130] It is also worth noting that alkyl substitution at the nitrogen atom allows *cis-trans* photoisomerization of indigo itself to take place.[131,132]

Thioindigo was found to be prone to suffer *cis-trans* isomerisation induced by light, and whose relative proportion was found to be dependent on the solvent, temperature and irradiation wavelength.[133] Indeed the strong dependence on the media can be shown with the example of the wavelength maximum of absorption in chloroform to be 546 nm (*trans* form, where the *cis* form is obtained by irradiating at the trans wavelength maxima leading to a *cis* form with maxima at

~500 nm) whereas it changes to 640 nm in a solution of sulphuric acid, where it only exists in the *trans* form in virtue of the fact that in this solvent media the dye exists in the form of a hydrogen-bonded complex (between S-H and C=O) which precludes, similarly to indigo, isomerization into the *cis* configuration.[133,134] In the case of benzene as solvent the *trans* form was found with a wavelength maxima of 543 nm (which matches our value in Table 7) and the *cis* form at 484 nm.[45]

Moreover, the subsequent investigations by Wyman lead to the conclusion that the *trans* isomer was more fluorescent than the *cis*, and this was due to the fact that the *trans*-thioindigo had a coplanar structure whereas the *cis*-isomer was non-coplanar.[135]

Also in the case of thioindigo Wyman's and co-workers studies showed fluorescence (ϕ_F= 0.56) to be in competition with *cis-trans* photoisomerization ($\phi_{trans \rightarrow cis}$= 0.041 and $\phi_{cis \rightarrow trans}$ = 0.45) and a lifetime of 13.4 ns (although reported to be with great uncertainty) was reported in benzene.[45]

Later on, with degassed benzene solutions, (higher) values of ϕ_F= 0.71 and intersystem crossing yield, ϕ_T=0.23 were reported, together with an also higher value for the *trans*→*cis* isomerization, $\phi_{trans \rightarrow cis}$=0.11.[136] In this same work evidence was given for the *trans-cis* photoisomerization to occur through the triplet state.[136]

The overall data constitute a revision of part of the data provided by George Wyman and his co-workers during the period from 1951 to 1994, giving further convincing evidence that the excited state proton transfer in indigo is the most likely mechanism for its (photo)stability.

An additional thioindigo derivative (Ciba Brilliant Pink - CBP) was also investigated.

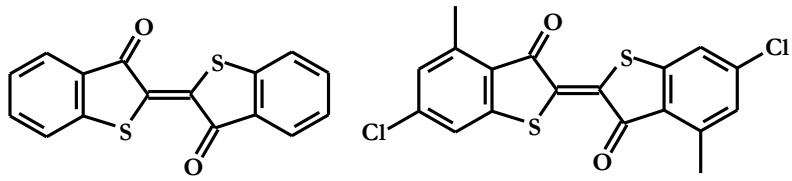

Thioindigo **Ciba Brilliant Pink**

Scheme 18 – Structures of Thioindigo and Ciba Brilliant Pink

6.1 – SPECTRAL AND PHOTOPHYSICAL DATA

The absorption and fluorescence (emission and excitation) spectra of thioindigo and CBP in toluene are shown in Figure 31. A good overlap between the absorption and the excitation spectra is observed thus attesting the purity of the compounds, which was also observed in the other solvents (benzene and dioxane). Observation of the spectra in Figure 31 reveals, for both compounds, the absence of a mirror-image relationship between the absorption and fluorescence spectra which is in contrast with the situation observed with indigo.[10]

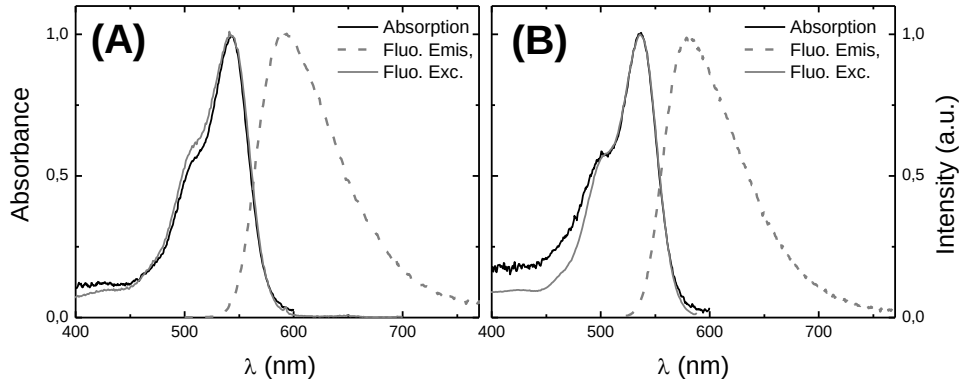

Figure 31- Absorption and fluorescence (emission and excitation) spectra of **A)** thioindigo and **B)** ciba brilliant pink, in toluene, T=293K.

Figure 32 shows the transient triplet-triplet spectra for thioindigo and **CBP** in toluene. Besides the intense transient maxima at 580 nm a depletion band is observed at 540 nm (matching the visible absorption band in Figure 31).

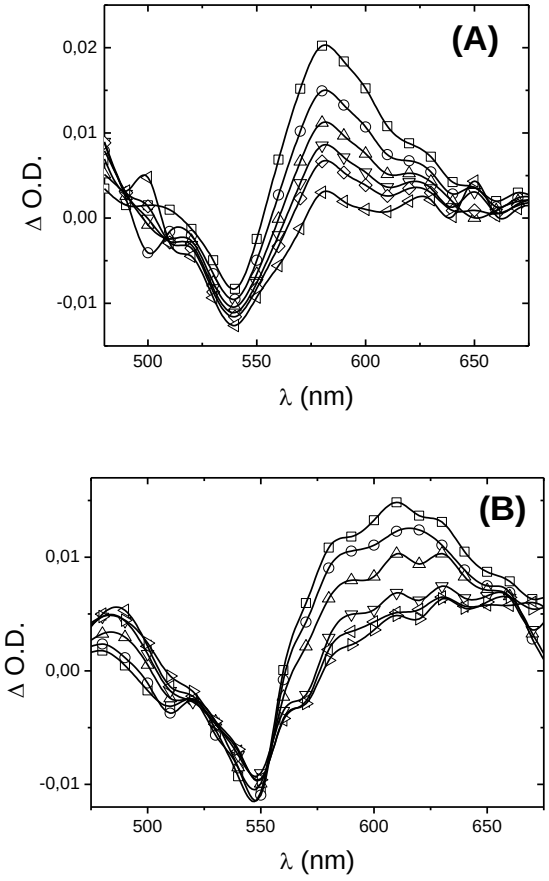

Figure 32- Transient triplet-triplet absorption spectra in toluene of **A)** thioindigo and **B)** ciba brilliant pink, T=293 K.

In Tables 7 and 8 the spectral and photophysical data for thioindigo, ciba brilliant pink and indigo itself are presented, these data provide the basis for a direct comparison between the excited state behaviour of thioindigo (and **CBP**) with indigo. Those values compare well with those previously published by Kirsch in 1975, where ϕ_F = 0.71 and τ_F=13,4ns for thioindigo in benzene were obtained.[136]

Table 7- Spectroscopic properties for thioindigo and ciba brilliant pink in dioxane, toluene and benzene at 293 K. For indigo the same parameters (obtained in previous works[10,48-50]) are also presented in DMF for comparison effects.

Compound /solvent	λ_{max}^{Abs} **(nm)**	λ_{max}^{Fluo} **(nm)**	Δ_{SS} **(nm)**	ε_{SS} **(M^{-1} cm^{-1})**	$\lambda_{max}^{T_1 \rightarrow T_n}$ **(nm)**	ε_{TT} **(M^{-1} cm^{-1})**
thioindigo						
Dioxane	536	595	59	12070 (+/- 390)	590	12295 (+/- 30)
Toluene	542	591	49	14120 (+/- 40)	580	15811 (+/- 290)
Benzene	543	600	57	13640 (+/- 60)	580	14668 (+/- 380)
CBP						
Dioxane	530	572	42	7504 (+/- 190)	610	11253 (+/- 850)
Toluene	537	580	43	7288 (+/- 330)	610	11044 (+/- 580)
Benzene	537	580	43	5973 (+/- 360)	620	13931 (+/- 1650)
indigo*						
DMF	610	653	43	22140	~640	ND

* for indigo data is taken from reference [10]

Table 8- Photophysical properties including quantum yields (fluorescence, ϕ_F, internal conversion, ϕ_{IC}, triplet formation, ϕ_T, and sensitized singlet oxygen formation, ϕ_Δ), for thioindigo and ciba brilliant pink in dioxane, toluene and benzene at 293 K. The same parameters (obtained in previous works[10,48-50]) are also presented for indigo in DMF.

Compound/ Solvent	ϕ_F	ϕ_T	ϕ_Δ	ϕ_{IC}*	$\tau^{T_1 \rightarrow T_n}$ (ns)	τ_F (ns)	k_F* (ns^{-1})	k_{NR}* (ns^{-1})
Thioindigo								
Dioxane	0.54± 0.005	0.071±0.018	0.058±0.008	0.39	328	12.0	0.045	0.038
Toluene	0.69±0.013	0.126±0.001	0.12± 0.005	0.18	428	12.3	0.056	0.025
Benzene	0.72±0.045	0.122±0.004	0.11±0.015	0.16	389	12.2	0.059	0.023
CBP								
Dioxane	0.707± 0.02	0.189±0.014	0.058±0.006	0.10	372	10.39	0.068	0.028
Toluene	0.704±0.03	0.280±0.011	0.15± 0.002	0.016	374	10.37	0.068	0.028
Benzene	0.732±0.005	0.243±0.009	0.13± 0.011	0.025	308	10.28	0.071	0.026
Indigo								
DMF	0.0023	0.0066	0.0012	0.996	~ 30 μs	0.140	0.016	7.13

*ϕ_{IC}= 1-(ϕ_F + ϕ_T); $k_F = \frac{\phi_F}{\tau_F}$; $k_{NR} = \frac{1-\phi_F}{\tau_F}$

In the case of **TI** the values compare well with those previously reported by Kirsch and Wyman for this same compound in benzene solution: ϕ_F = 0.71 and τ_F=13.4 ns.[136]

From Table 7 it can be seen that the wavelength absorption maxima of thioindigo and **CBP** is blue-shifted (~70 nm) relative to indigo. The same happens with the emission but now with a blue-shift of 50-60 nm (depending on the solvent). In contrast with this the Stokes shift (Δ_{SS}) is, for thioindigo and **CBP**, approximately identical to that found with indigo, Table 7. With indigo this has been suggested to be related to the absorption being due to its keto (neutral) form, whereas the emission band would result from the convoluted emission of this, instantaneously formed, species together with that resulting from excited state proton transfer (from the N-H to the C=O group which could be intra or –assisted by the solvent– intermolecular)[35,48,49,54,57,127]; the biexponential nature of the decays in indigo further confirms the existence of these two excited state species.[48,49,137] However, in the case of thioindigo the significant Δ_{SS} value is more likely linked to a change in geometry upon going from the ground to the excited state.[45] This would imply, as suggested by Wyman, that there is some deviation from planarity in the S_1 state of thioindigo (with a geometry between *trans* and *cis* forms).[135] Indeed, thioindigo was found to be prone to suffer *cis-trans* isomerisation induced by light, whose relative proportion was found to be dependent on the solvent, temperature and irradiation wavelength.[133] In the case of benzene as solvent the *trans* form was found with a wavelength maxima of 543 nm (which matches our value in Table 7) and the *cis* form at 484 nm (not detected under our experimental conditions).[45] Moreover, Wyman also concluded that the *trans* isomer was more fluorescent than the *cis*, and that was due to the fact that the *trans*-thioindigo had a coplanar structure whereas the *cis*-isomer was non-coplanar.[135] With thioindigo Wyman's and co-workers showed fluorescence to be

in competition with *cis-trans* photoisomerization ($\phi_{trans \rightarrow cis}$= 0.041 and $\phi_{cis \rightarrow trans}$ = 0.45)[45] and intersystem crossing yield (a ϕ_T=0.23 was reported); an upper value for the *trans→cis* isomerization was reported later $\phi_{trans \rightarrow cis}$=0.11[136] and in this same work evidence for the *trans-cis* photoisomerization to occur through the triplet state was given.[136] Photoisomerization is indeed a feature of not only **TI** but also of indigo but in its leuco form as was showed in chapters 2 and 3.[137,138]

It is also worth noting that the absence (or a very small) Δ_{SS} value would basically imply that the same geometry is present both in the ground and first excited singlet state.

Triplet lifetimes in the ns and microsecond time-scale have been obtained, Table 8. The direct comparison of the quantum yields for fluorescence, internal conversion and intersystem crossing between **TI** (and **CBP**) and indigo shows that in the case of the sulphur derivatives the fluorescence quantum yield dominates and is the major deactivation channel of the excited state in these compounds in clear contrast with indigo. Moreover the triplet intersystem crossing yield is also an effective deactivation channel for the excited state of **TI** and **CBP** with 7-28 % of the *quanta* loss (depending on the compound and solvent) which again is in clear contrast with the behaviour found for indigo where the dominant deactivation is made through the internal conversion channel. Singlet oxygen yields values for **TI** and **CBP** are similar to those found for the intersystem crossing yields thus validating these and showing that sensitization of singlet oxygen is also an efficient excited state process with these compounds.

The overall comparison between indigo and **TI** (or **CBP**) shows that when proton transfer in the excited state is allowed, this opens an efficient radiationless channel (internal conversion) that dominates over all the other deactivation processes. However when the proton transfer in the excited state is precluded, either by sulfur substitution of the N-H group or by reduction of the

carbonyl group (leuco form), fluorescence, intersystem crossing and photoisomerization become efficient deactivation pathways.

6.2 – LOW TEMPERATURE AND AGGREGATE FORMATION

At 293K the gradual increase of concentration in thioindigo, does not produce significant changes in the absorption and fluorescence emission bands; however, in the excitation band, collected at the emission maximum, for higher concentrations it is visible the formation of two new bands (max@515nm and 550nm), indicating of the possible occurrence of aggregation.

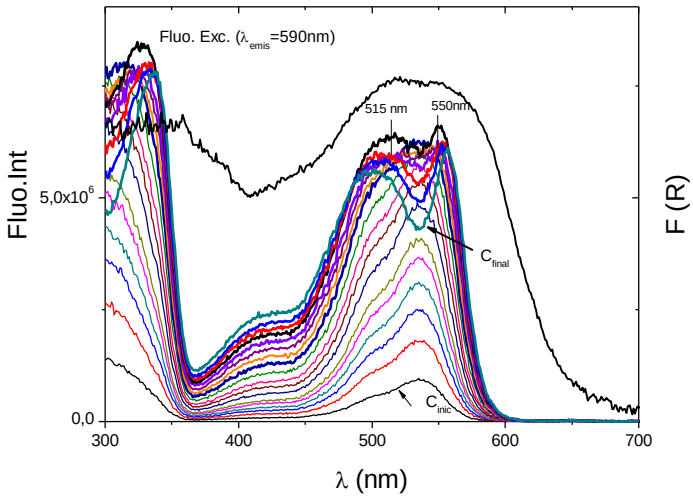

Figure 33 - Evolution of fluorescence excitation spectra of thioindigo in dioxane, with the concentration increasing, and diffuse reflectance (Kubelka-Munk scale) spectrum of solid thioindigo, T =293K. C_{ini} and C_{final} refer to initial and final concentrations respectively.

The fluorescence emission spectra of **TI** at low temperature (77K) was obtained in toluene at two different concentrations (1×10^{-5} M and 2×10^{-4} M), see Figures 34, and 35. For **TI**, at the lowest concentration value, there is a red-shift of the absorption at 77K (here seen by the excitation spectra) relative to the room temperature situation. However, for the high concentration solution, where the presence of dimer/aggregation formation is seen at room temperature (see Figure 35), no red-shift between 293 K and 77K temperatures is observed. Moreover, a narrowing of the fluorescence emission band can be observed at 77K, and there is a clear increase of the half-width of the absorption band of the high concentrated solution at 77K, together with an additional appearance of a vibronic peak at ~510 nm, see Fig. 34. The above results strongly suggest the presence of J-type aggregate/dimers for **TI** at 77K.

Very interesting is to observe what happens with **CBP** under the same experimental conditions. Figure 34 shows that for **CBP** there is a less pronounced difference for the wavelength absorption maxima at 77K vs. 293 K, and equal (10nm) to both concentrations; it should be noted that the high concentration is very close to the saturation limit concentration (which would lead to precipitation). The comparison between **TI** and **CBP** strongly suggests that the methyl groups in **CBP** preclude the formation of dimers or higher order aggregates.

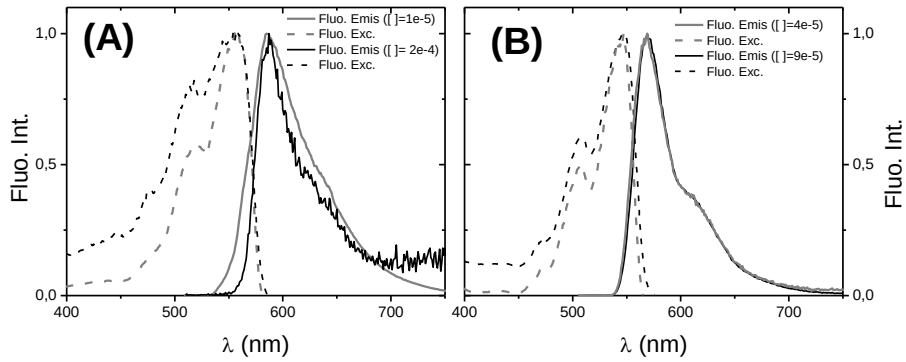

Figure 34 - Fluorescence emission and excitation spectra of **A)** thioindigo and **B)** ciba brilliant pink in toluene, in different concentrations, at 77K.

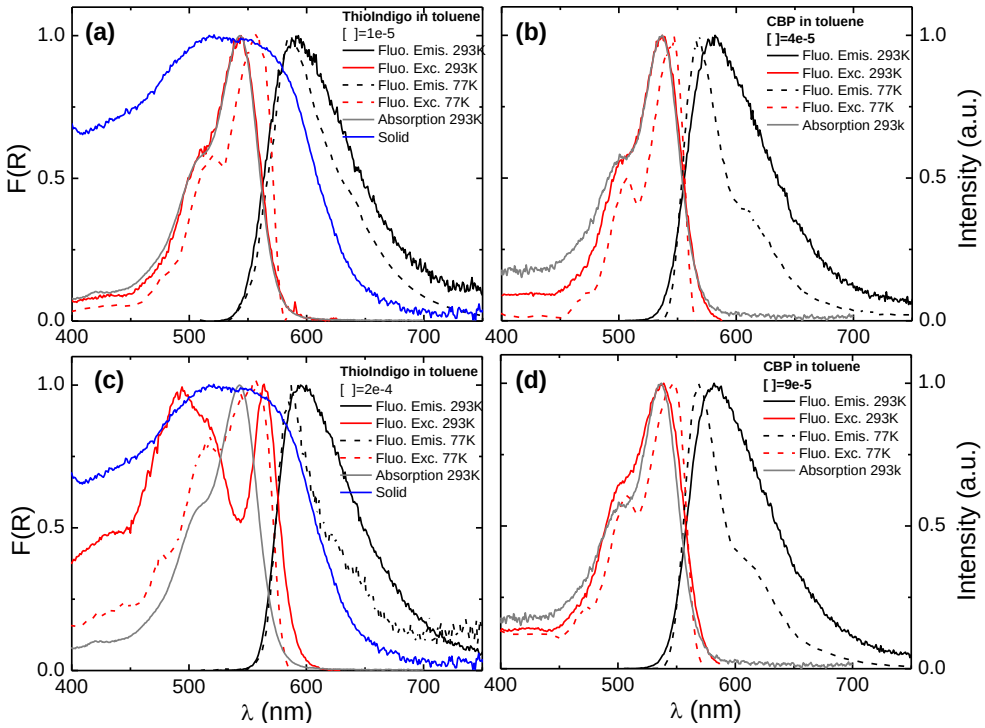

Figure 35 - Low and room temperature absorption and fluorescence spectra of **TI** (left panels) and **CBP** (right panels) in toluene at two different concentrations together with the diffuse reflectance spectrum (Kubelka-Munk scale) of solid thioindigo (in blue in the left panels); top hand panels: low concentrated solution, low hand panels: high concentrated solution.

6.3 - COMPARISON OF THIOINDIGO/CBP WITH INDIGO

Comparison of the solution behaviour (spectra and photophysics) of **TI** (and **CBP**) with indigo gives additional and relevant information in which regards the excited state characteristics of this blue dye. Indeed, in contrast with indigo but similarly to the two other forms of indigo, leuco[58] indigo and dehydroindigo (DHI)[52], where internal conversion looses importance as the main deactivation

pathway, **TI** and **CBP** display significant fluorescence quantum yield values. It is worth noting that with the leuco and DHI forms of indigo, the excited state proton transfer process is absent. Moreover, whereas in the case of leuco indigo the species decays basically with a single exponential decay law (and the same happens with several other derivatives)[10,52] , in the case of DHI due to the single bond character between the two indole moieties, there is possibility of more than one conformer leading to more complex decays.[52] The decays of **TI** and **CBP** are now clearly single exponential (see Table 8) in clear contrast to the behaviour found for indigo where only with biexponential decay laws (with decay profiles dependent on the emission wavelength when collected along the band, mirroring the same decay times but different pre-exponential factors) the decays could be properly fitted.

Also worth noting is the high value of the fluorescence lifetime (~12 ns) for **TI** when compared to indigo itself, where values between 130-140 ps (Table 8 and refs.[10,48,49]) could be found.

7. MAYA BLUE

&

MAYA PINK

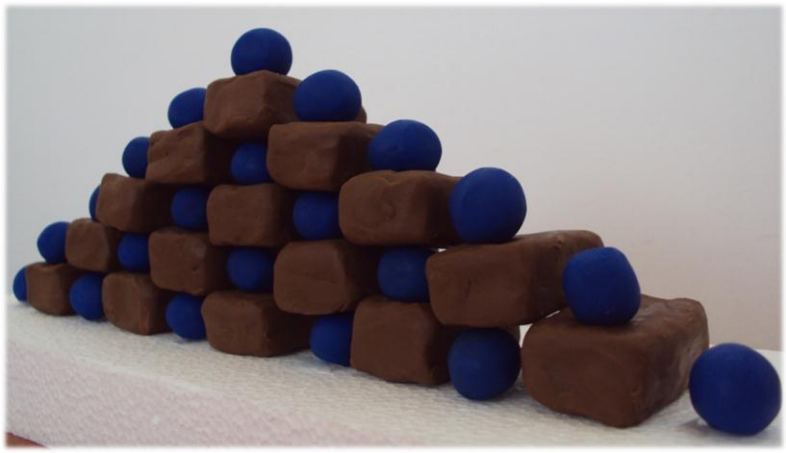

From the earliest days of civilization clays have been used, and became familiar mostly because of their use as raw material to porcelain. In industry they are very appreciated for their properties to absorb not only inorganic but also organic materials, providing novel functional organic/inorganic hybrid materials. One off the oldest and intriguing hybrid is Maya Blue. A mixture of indigo (organic) with attapulgite (inorganic), made by the Mayans in Chichen Itza, Yucatan (Mexico), in which Maya Blue was found in mural paintings, sculptures and other objects.[69,70]

Clay minerals are classified not only by the differences in the layered structures but also by the types of substituted metals, amounts and kinds of exchangeable ions within the interlayers, and the impurities present.

For many time the truly nature of this blue that persists for so long and resists to the most adverse conditions has been an enigma. In 1931, Merwin during the analysis of such mural paintings identified the blue and brilliant pigment Maya Blue[73], which due to its high stability was believed to be an inorganic dye. In 1966 Van Olphen[75], established that Maya Blue was an organic/inorganic hybrid made of indigo and a clay: attapulgite, called "White earth" by the ancient Maya people. Later on the existence of other clay, sepiolite, was equated together with attapulgite or even in replacement of this was equated and is still under debate. [76-78,139]

The high stability of Maya Blue was further tested in laboratory where this hybrid compound was found resistant to several oxidizing and reducing agents, organic solvents, strong acids and alkaline, and high temperatures.[73,76,77,81,90,94,99,140] This lead to a renewed and intense research on nowadays on the structure of Maya Blue and the correct recipe used by the ancient Maya civilization on its production, including new hybrids (with different clays)[141] as sources of pigment stabilization. Albeit the numerous studies on this clay, particularly on the past recent years,

there are still some fundamental aspects under debate. Within these we found, among others, the correct location of indigo on the clay structure[71,81,85,90], the influence of iron, aluminium or magnesium ions in forming complexes between indigo and the clay[71,77,140], the remove of the zeolitic water[71,77,81], different forms of indigo (reduced or oxidized)[52,85,94], type of clay used (attapulgite and/or sepiolite).[76-78] More recently the incorporation of other molecules than indigo in sepiolite or attapulgite clays, including thioindigo, Tyrian purple and methyl red, has been reported.[94,95,142,143]

In attempting to unveil Maya Blue structure, experiments were done with indigo, dehydroindigo, thioindigo and ciba brilliant pink mixed with two clays: attapulgite and sepiolite. The recipe used was the one proposed by van Olphen[75], with mass proportions of dye/clay of 2, 5,10 and 20%. All the samples were submitted to acid attack to ensure that only molecules bounded to the clay were in the sample. Figure 36 presents the diffuse reflectance spectra (Kubelka Munk scale) of the compounds isolated and the clays in study.

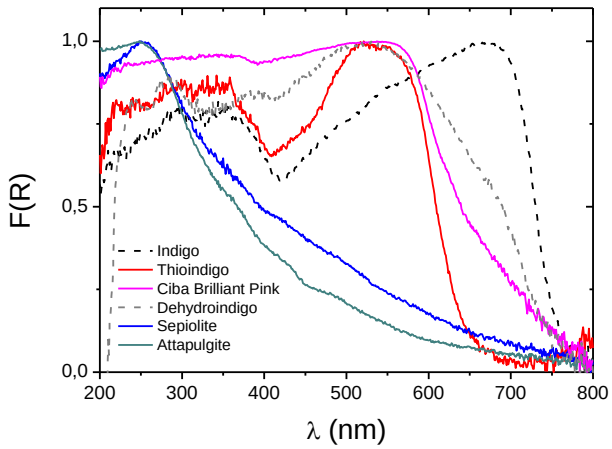

Figure 36 – Diffuse reflectance spectra (Kubelka-Munk scale) of indigo, thioindigo, ciba brilliant pink, dehydroindigo together with the spectra of the sepiolite and attapulgite clays; T=293K

7.1 – INDIGO/ATTAPULGITE AND INDIGO/SEPIOLITE

The recipe of Maya Blue was reproduced with four different dye/clay proportions (weight/weight), 2, 5 10 and 20%, (see Figure 37). All the samples were washed until no traces of indigo could be found in the washing solvent.

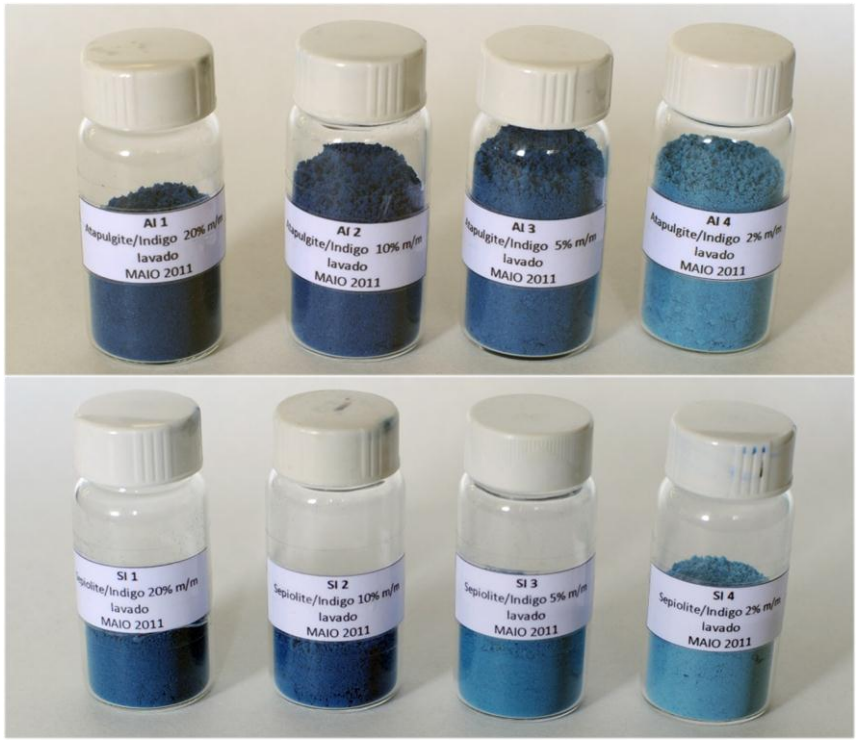

Figure 37 – Photograph of the different mixtures dye/clay studied. **Top:** indigo/attapulgite, 20, 10, 5 and 2% (w/w) counting from the left. **Down:** indigo/sepiolite, 20, 10, 5 and 2% (w/w) counting from the left.

One of the similarities reported for indigo in both clays is that indigo molecules interact directly with the cations (Mg^{2+} for both and maybe also Al^{3+} for attapulgite).[139] A higher confinement and the presence of Al^{3+} in attapulgite can be

responsible for the different behaviour of indigo-attapulgite and indigo-sepiolite complexes.[144] TDDFT (time dependant density functional theory) calculations showed that attapulgite Al^{3+} cations are more likely candidates than Mg^{2+} for bonding with indigo carbonyl.[90]

In Figure 38 are depicted the diffuse reflectance spectra of the washed mixtures, of indigo/attapulgite and indigo/sepiolite. In graphic **A)** the maxima does not change from the indigo alone relative to the mixture; however, there is a broadening when going from the lower proportion of indigo in the clay to the pure indigo, this presumably suggests formation of aggregates. In graphic **B)** a small blue shift, relative to indigo is observed, but the bands of the mixtures remain identical in shape for all indigo/clay proportions.

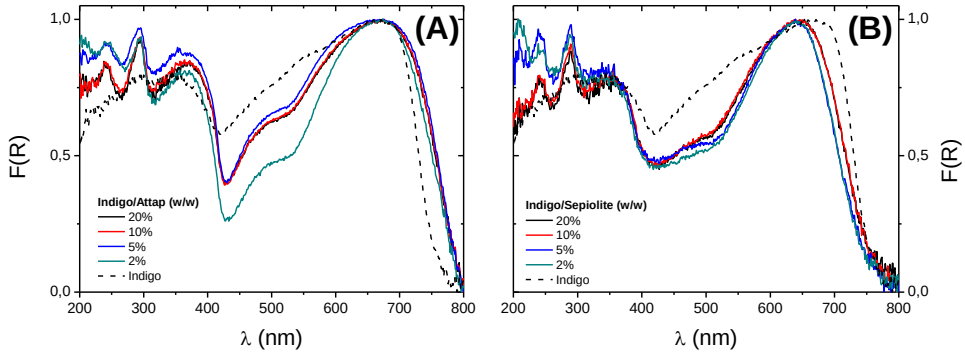

Figure 38 - Diffuse reflectance spectrum (Kubelka-Munk scale) of indigo alone and in four (dye/clay) compositions; **A)** indigo/attapulgite, **B)** indigo/sepiolite T=293K.

The emission spectra of these same proportions are presented in Figure 39. For the mixtures indigo/attapulgite there is a significant red shift of the

wavelength maximum relative to indigo, but the same is not found with indigo/sepiolite. To be noted is the fact that the signal is very weak. For that reason the fluorescence quantum yield, obtained using an integrating sphere, could not be measured once there is a sharp decrease in the fluorescence signal due to losses caused by the integrating sphere. Also due to losses on picosecond TCSPC apparatus, fluorescence lifetimes could not be obtained.

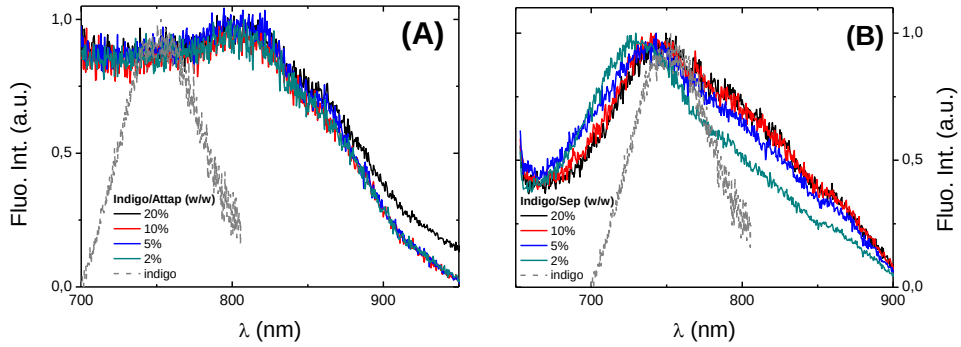

Figure 39 - Fluorescence emission from **A)** indigo (grey line) and indigo/attapulgite (λ_{exc}= 650 nm); and **B)** indigo (grey line) and indigo/sepiolite in all weight/weight proportions (λ_{exc}= 620 nm).

7.2 – THE CONNECTION OF DHI WITH MAYA BLUE

The diffuse reflectance spectra of indigo, DHI and MB are shown in Figure 40 together with the spectra resulting from the subtraction of indigo to MB.

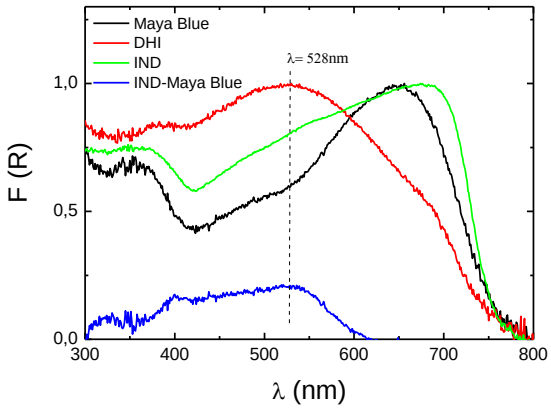

Figure 40 - Kubelka-Munk scale diffuse reflectance spectra of Maya Blue, DHI, IND, and also the difference spectra between IND and MB (IND-Maya Blue).

From these spectra several important observations could be taken. First of all it is clear that the 528nm absorption band maxima for DHI is, in the solid state, strongly red-shifted relative to the solution spectra (Figs 17 – toluene, and 18– methanol, and Table 4). The same happens with indigo shifting from 600-620 nm (Table 2 and refs. [10,30,37,49]and references therein), to 650 nm in the solid state and 680 nm in Maya Blue (Figure 40).

The wavelength maxima of indigo in Maya Blue (resulting from the crushing of synthetic indigo with sepiolite clay which is further heated to 190 ºC for 5 hours) suffers a blue shift when compared to indigo itself. Also worth noting is the observation that indigo in the solid state displays a much more broad visible absorption band than in solution[10] which is clearly related to the stacking of the indigo molecules in the solid leading to aggregate absorption. Very interesting is also the observation that the spectra of indigo in Maya Blue is more sharp and close to that of indigo in solution (exception made to the difference in the wavelength maxima) clearly indicating the nature of the isolated molecules of indigo in sepiolite channels of Maya Blue.

The most interesting feature is, however, the observation that Maya Blue and DHI share a common band at ~ 528 nm. The spectral difference between indigo (in the solid) and Maya Blue leads to a band with maxima and shape very close to that of DHI (in the solid state), Figure 40, clearly suggesting the presence of DHI in Maya Blue in agreement with other recently published studies.[85,87,90,92,93]

An additional relevant piece of information, relative to the contribution of DHI to Maya Blue, is obtained from the fluorescence excitation spectra of Maya Blue collected with a difference of 7 days. As can be seen from Figure 41, the fluorescence excitation spectra of Maya Blue present two bands: one at 650 nm which matches with that present in the solid state spectra of indigo in Maya Blue and an additional at 550 nm, which is close to that found for DHI in the solid state (~ 528 nm).

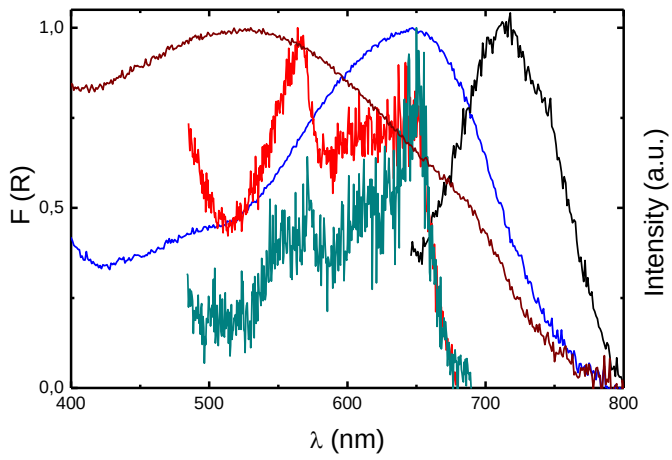

Figure 41- Diffuse reflectance spectra (Kubelka-Munk scale) for Maya Blue (blue trace) and DHI (brown trace) together with fluorescence emission spectra (black trace) and fluorescence excitation spectra collected with 7 days of difference (olive green trace first, red trace after) for Maya Blue. All the spectra (absorption and fluorescence) are normalized.

It is interesting to note that the excitation spectra is more sharp than the solid state absorption suggesting, once again, that the fluorescence comes, indeed, from individual molecules found inside (or at the surface) of the channel clays. However, the most interesting finding in these spectra is that when collected with an interval of 7 days, the 550 nm band (DHI) contribution increases relative to the 650 nm (indigo) band. Although further and detailed studies are needed, this clearly suggests that, albeit not significant, there is, with time, a conversion (most likely inside the clay channels) of indigo into DHI.

Some recent studies indicate that DHI contributes to the greenish colour of Maya Blue.[85,87,93] Electrochemical data suggests that formation of MB involves a significant reorganization of zeolitic water and/structural water of the clay what allows the formation of DHI, and its amount is dependent of the thermal treatment used for sample preparation, being ~20% the maximum DHI/indigo relationship estimated.[85,87,93]

7.3- THIOINDIGO: A FLUORESCENCE PROBE TO MAYA BLUE

Indigo is a very poor fluorescent dye presenting strong limitations in the investigation of its photophysics when in the form of Maya Blue; thioindigo, the sulphur derivative, with its high fluorescence quantum yield was found an additional and important element for the study of this organic/inorganic hybrid. The solid state behaviour of **TI** and **CBP** alone and incorporated in attapulgite clays has been investigated by diffuse reflectance, steady-state and time-resolved fluorescence.

The diffuse reflectance spectra of **TI** and **CBP** together with that of indigo are presented in Figure 36, together with the spectra of sepiolite and attapulgite clays. It can be clearly seen that the clays present an absorption band with maxima at ~250 nm, a region where the three dyes have insignificant absorption. As it happens in solution, the absorption spectra in the solid state of **TI** and **CBP** are blue shifted relative to indigo.

When the mixture of thioindigo and attapulgite is took out of the furnace there is a surprisingly, and visible to the naked eyed, difference from the starting material (thioindigo), that changed from reddish to bright blue (Figure 42). This change is also referred by Manciu *et al.* [142]and Pollete-Niewold *et al.*[94] that attributes this difference to a structural change caused by the interaction with the clay, namely with silanol groups. Manciu also refers that the change is dependent on the temperature.[142]

The colour presented by the different mixtures is the first indication that the environment probed by **TI** and **CBP** in the clays is not identical. Indeed, **TI** changes from a reddish to a bluish colour when incorporated in attapulgite[145] whilst **CBP** remains pink. Moreover, there are also differences when **TI** is mixed with different clays; in fact, thioindigo in sepiolite now turns violet, see Figures 42 and 43.

Figure 42- Photograph of thioindigo (down), and thioindigo mixed with attapulgite (top left) and sepiolite (top top right), in a 20% proportion w/w.

Figure 43 - Photograph of ciba brilliant pink (down), and CBP mixed with attapulgite (top left) and sepiolite (top right), in a 20% proportion w/w.

The absorption spectra of thioindigo in attapulgite (with a 10 percent weight of TI added to attapulgite) are shown in Figure 44 B). The spectra with different degrees of added dye is shown in Figure 44 A).

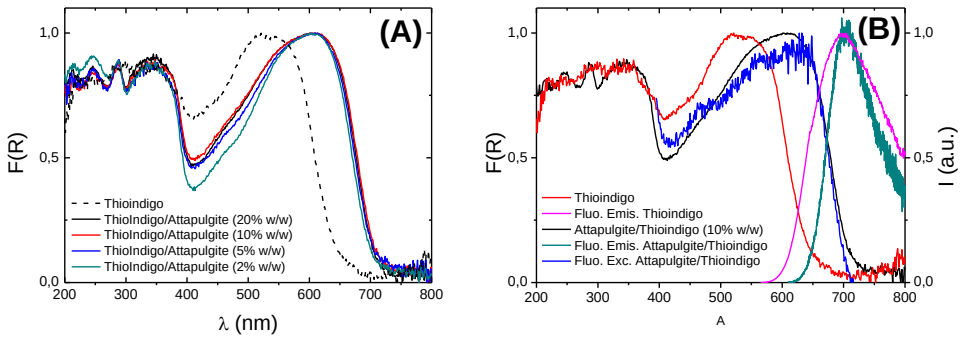

Figure 44 – A) Diffuse reflectance spectra (Kubelka-Munk scale) of thioindigo, and mixtures of thioindigo/attapulgite in different weight percentage proportions, after acid attack, **B)** Diffuse reflectance spectra (Kubelka-Munk scale) of thioindigo alone and in a 10% weight mixture with attapulgite, together with the fluorescence emission and excitation spectra of the compound alone and in the mixture, T=293K.

The **TI** samples were submitted to acid attack with nitric (or sulphuric) acid in order to assure that all the **TI** is indeed attached (incorporated into cavities or bonded) to the attapulgite this avoiding an efficient acid attack. From Figure 44 B) it can be seen that the solid state spectrum of **TI** is clearly blue-shifted relative to that of **TI** when incorporated in attapulgite. This indicates that the environment now probed by **TI** is different to that in the solid (where dimers or higher levels of aggregation are likely to be present) or in solution where the absorption maximum is found at ~540 nm. It is also worth noting that the absorption wavelength

maxima (and shape of the spectra) of **TI** when incorporated with attapulgite does not change with the level of addition of the former in the mixture (Figure 44 A).

Figure 45 shows the emission spectra of thioindigo in attapulgite obtained with λ_{exc}= 515nm (where the absorption - see Figure 44 A), mainly results from thioindigo) and with λ_{exc}= 600 nm (where the absorption is now the result of thioindigo with attapulgite; again see Figure 44 A)). As can be seen from Figure 45, the emission band (and maxima at 703 nm) is independent of both 1) the amount of the thioindigo added to attapulgite and 2) the excitation wavelength. In the case of **TI** in the solid (powder) an emission maximum at 700 nm is observed. This shows that with attapulgite **TI** presents an emission wavelength maximum (703 nm) red-shifted relative to the solution spectra (~590-600 nm), see Table 9, once more giving strong support for the different environment felt by **TI** when mixed/incorporated with attapulgite relative to solution and solid (powder). Moreover, this red shift again suggests that, at a molecular level, **TI** appears as isolated units when incorporated into the clay, whereas in the (solid) powder it appears as a dimer (or aggregate) structure.

Fluorescence excitation spectra of the mixtures TI/attapulgite are presented in Figure 46. In there it can be seen that the fluorescence excitation spectra collected at 710nm is, in shape and maxima, also found to be independent of the thioindigo/attapulgite composition.

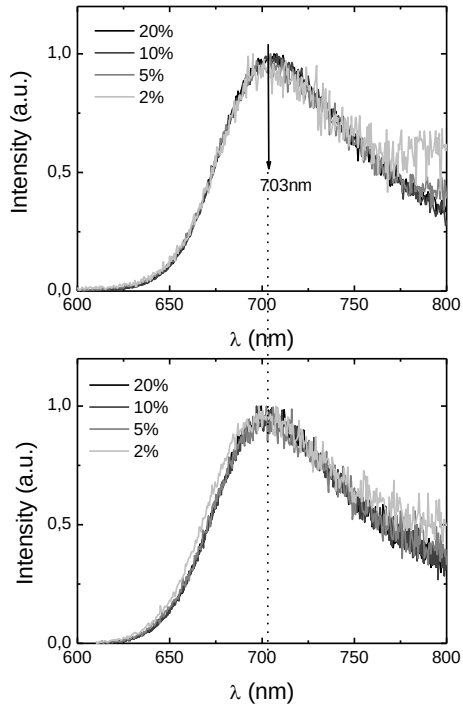

Figure 45 - Fluorescence emission spectra from thioindigo/attapulgite in all weight proportions,T=293K. Top λ_{exc}= 515 nm, down spectra λ_{exc}= 600 nm.

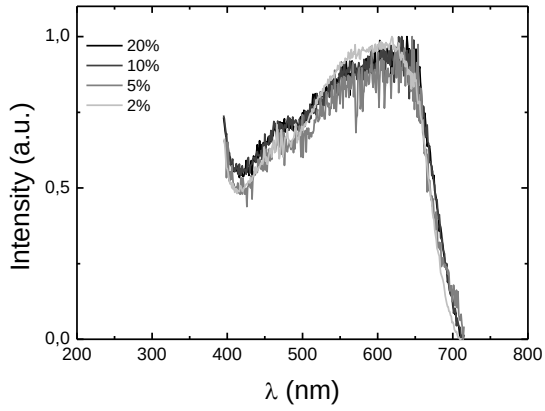

Figure 46 - Fluorescence excitation from the mixture thioindigo/attapulgite in different proportions, after acid attack, T=293K.

7.4 – CIBA BRILLIANT PINK AND ITS INTERACTION WITH THE CLAYS

Previously **CBP** has shown, in solution, a very close behaviour to that presented by thioindigo. However, when incorporated in the clays (attapulgite and sepiolite), there is no such similarity. Figure 47 presents the absorption spectra of CBP/attapulgite with different percentages of the dye in the composition (Fig. 47 A)), together with the spectra of the solid (Fig. 47 B)).The most relevant aspect to be emphasized is the fact that the spectra of **CBP** is broad with an absorption from 200 to 800 nm and a peak at ~550 nm; however, when incorporated in attapulgite, the spectra are now clearly sharper with a defined wavelength maxima at 536 nm. As with **TI** this points once more to the existence of isolated units of the dye when incorporated with the clay by opposition to the situation in the solid powder state.

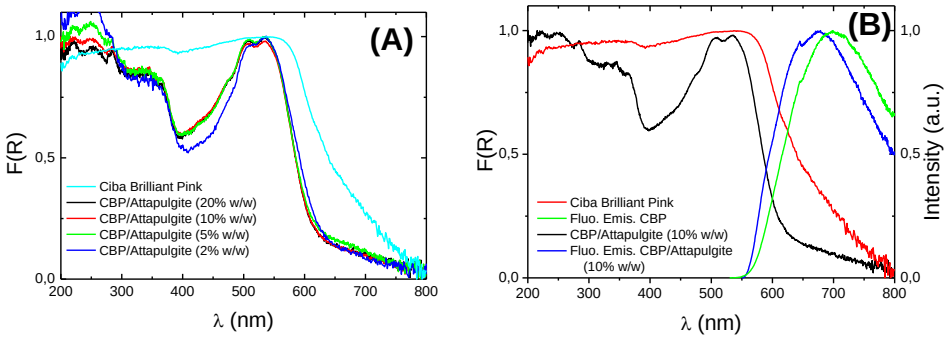

Figure 47 – A) Diffuse reflectance spectrum (Kubelka-Munk scale) of CBP, and mixtures of CBP/attapulgite in different weight percentage proportions, after acid attack, **B)** Diffuse reflectance spectrum (Kubelka-Munk scale) of CBP and in a 10% weight mixture with attapulgite, together with the fluorescence emission and excitation spectra of the isolated compound and incorporated in the mixture, T=293K.

The fluorescence behaviour of **CBP** in both clays is not as coherent as it happens with thioindigo. The different proportions of dye/clay have different wavelength maximum, and the fluorescence excitation do not match the absorption, as can be seen in Figure 48. This is consistent with previous works that conclude that thioindigo derivatives (namely 4,4',7,7'-tetrachlorothioindigo) do not bind to palygorskite as strongly as indigo.[146] They also assume the possibility of reaction between the hydroxy groups of guest and host, but without involvement of the palygorskite channels.

The fluorescence quantum yield of **TI** in attapulgite was found to be independent of the amount of compound incorporated into the mixture presenting a value of ~0.0067 (with an associated error of ~ 20%). This value is higher, although not significantly, than that found for **TI** in the solid state (ϕ_F=0.0015, Table 9) which once more supports (now from a photophysical perspective) the existence of isolated **TI** units in the clay in contrast with the solid (powder) behaviour where dimers and/or higher order aggregates are likely to be present.

Indeed, what comes out immediately from the observation and comparison of data in Tables 8 and 9 is the fact that, upon going from solution to the solid, there is a clear increase of the radiationless contribution. Indeed a general increase of the nonradiative rate constant in solid state is observed and is a consequence of the quenching of fluorescence by molecular aggregation.[147]

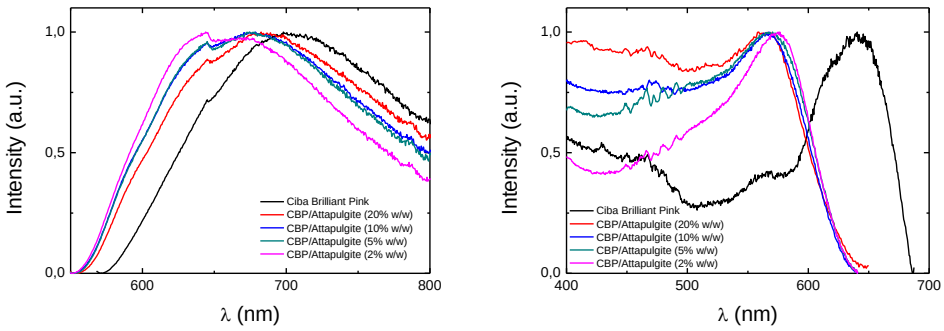

Figure 48 – Fluorescence emission and excitation from the mixture ciba brilliant pink/attapulgite in different proportions, T=293K.

Table 9- Spectral and photophysical properties of indigo, **TI** and **CBP** in the solid state (powder and incorporated in attapulgite), T=293K.

	λ_{max}^{Abs} (nm)	λ_{max}^{Fluo} (nm)	Δ_{ss} (nm)	ϕ_F	τ_F (ns)	k_F (ns^{-1})	k_{NR} (ns^{-1})
Thioindigo	517	697	180	0.0015	0.790*	0.0019	1.263
CBP	550	700	150	0.0023	0.220**	0.0105	4.535
Indigo	675	740	75	$\leq 10^{-4}$	ND	ND	ND
Thioindigo/Attapulgite (20% w/w)	609	703	94	0.0067	0.170	0.0394	5.843
CBP/Attapulgite (20% w/w)	535	700	165	0.0030	0.310**	0.0097	3.216

*major component of a biexponential decay
** major component of a triexponential decay
ND not determined

With **CBP**, a different behaviour is observed, in which the ϕ_F for the different **CBP**/attapulgite mixtures is found to be ~ 0.0030; a value that is close to that found for **CBP** in the solid state (0.0023), see Table 9. This can obviously be

related to steric constrains -promoted by the additional methyl groups- blocking the incorporation, within the clay channels, of **CBP**. This would indicate that **CBP**, differently from **TI** (and presumably indigo), should be found at the surface of the clay channels.

7.5 – TIME RESOLVED DATA

Further and strong additional support from the above analysis comes from time-resolved behaviour of **TI** and **CBP**. In contrast with the solution behaviour, where **TI** was found to decay monoexponentially, the fluorescence decays of **TI** in the solid state (obtained with ps time resolution) were found to fit with a biexponential decay law with decay times of 310 ps and 790 ps (see Figure 49). However, when **TI** is incorporated in attapulgite the fluorescence decays are now (again if compared with solution) single exponentials with a decay time of ~170 ps (see Table 9 and Figure 50).

The environment probed by **TI** is obviously different when incorporated in the clay than when found in solution; nonetheless, the most interesting aspect worth emphasizing is the single exponential nature of the decay when **TI** is incorporated into the clay structure which provides, once more, evidence for the isolated compound (likely inside the clay tunnels) in attapulgite in contrast with the coexistence of aggregates of different order (likely a monomer and a dimer) in the solid as attested by the biexponential nature of the decays (Figure 49).

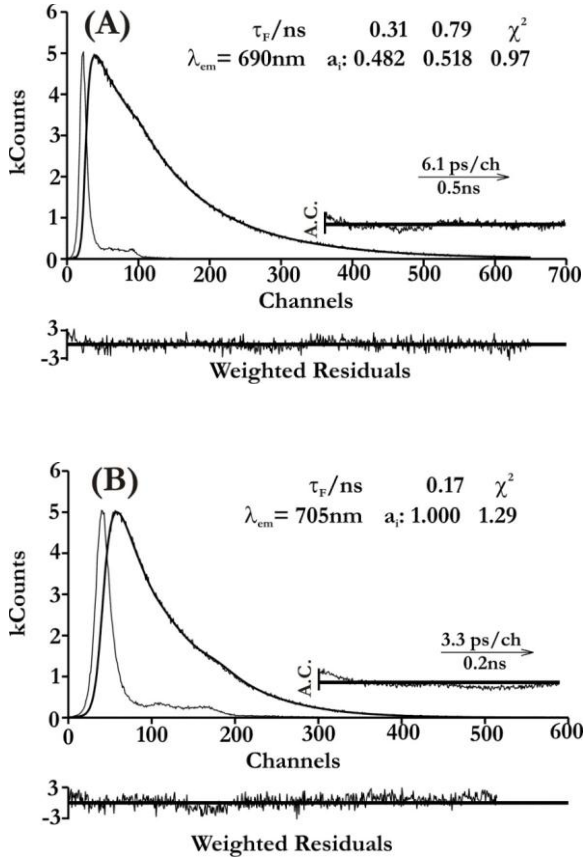

Figure 49- Fluorescence decay of thioindigo **A)** and thioindigo in attapulgite **B)** (20% w/w), at T=293K, with excitation at 450 nm. Shown as insets are the decay times (τ/ns), pre-exponential factors (a_i), and chi-squared values (χ^2). Also shown are the weighted residuals for a better judgment of the quality of the fits.

With the **CBP**/attapulgite mixture unlike with what was observed with **TI**/attapulgite, the decays are always triexponential (Figure 50), with similar values (of decay times and pre-exponential factors) for all **CBP**/attapulgite compositions, further resembling the decay of **CBP** in the solid (powder). The comparison of the two decays in Figure 50 clearly points out for an identical nature of the

environment probed by **CBP**, most likely resulting on contributions from monomer, dimers and other order aggregates. In the case of **CBP**/attapulgite this would mean that **CBP** is at the surface of the clay where it can interact with other **CBP** units.

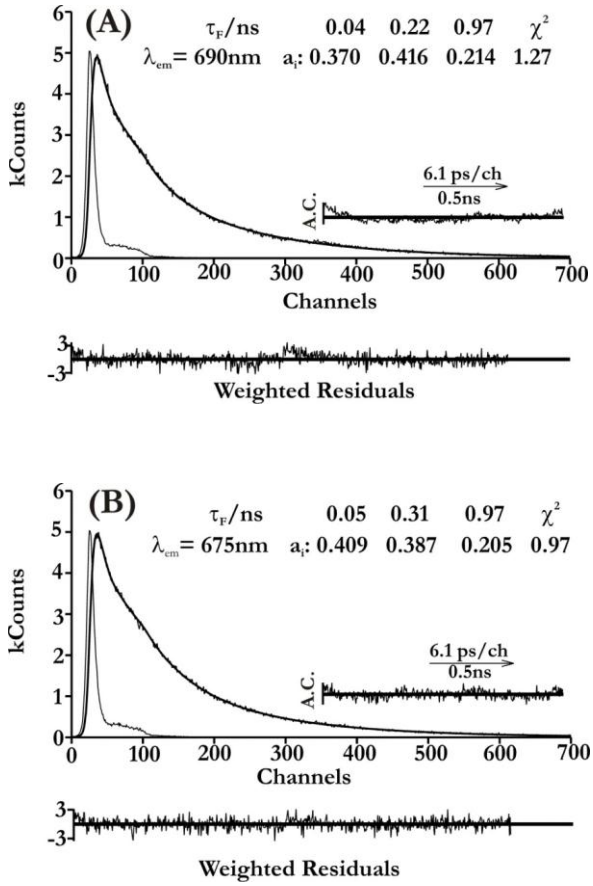

Figure 50 - Fluorescence decay of (top) solid ciba brilliant pink and (bottom) ciba brilliant pink in attapulgite (20% w/w) at T=293K and excitation at 450 nm. Shown as insets are the decay times (τ/ns), pre-exponential factors (a_i), and chi-squared values (χ^2). Also shown are the weighted residuals for a better judgment of the quality of the fits.

Indeed, and as mentioned previously, the exact location of indigo in Maya Blue is still a subject of debate, namely if the dye is found inside the cavities or at the surface of pores of the clay channels, forming a kind of shell. The study with **TI** and **CBP** gives additional clues to this interaction.

Summarizing and giving a more concise picture of the interaction of **TI** and **CBP** with the clays (attapulgite) at a molecular level. A decrease of the fluorescence quantum yield and lifetime in the solid – a consequence of the fluorescence quenching by aggregation or interaction with the clay – was obtained. However, in the case of **TI** the fluorescence decay is single exponential when incorporated in the clay whereas it is triexponential for **CBP** also in the clay. The same **TI** shows a biexponential decay when in the solid (powder) state. This clearly shows a different photophysical behaviour for these two compounds and therefore a different location (or type of interactions) within the clay. The fact that for **TI**/attapulgite the decay is single exponential indicates that the molecule is in an isolated environment (likely inside the clay channels) whereas the double exponential in the solid (powder) suggests the presence of an equilibrium between a monomer and a dimer of **TI**; this is further complemented with the evolution of the excitation spectra in the solid with increasing concentrations of **TI** shown in Figure 32 where at high concentration two bands are seen with maxima at 515 and 560 nm, and at the initial (low concentrations) a single band is observed. These data are also compatible with the biexponential nature of the decays in the solid **TI** (Figure 49).

An additional important result comes from the fluorescence decays of **TI** in sepiolite (Figure 51); now and in contrast with the single exponential nature of **TI** in attapulgite, the decays are now triexponential (with decay times of ~120 ps, ~500ps and ~2.3ns); although the contribution of each component (seen by the pre-exponential values) vary little, the decay times are basically identical. Since the

clay channels in sepiolite have bigger dimensions when compared to attapulgite [86] it is now highly probable that **TI** can be located inside and at the surface of sepiolite giving rise to the multiexponential nature of the decays. It is once more worth remembering that the decays from the various thioindigo/attapulgite mixtures are all single-exponential with approximately identical lifetime values.

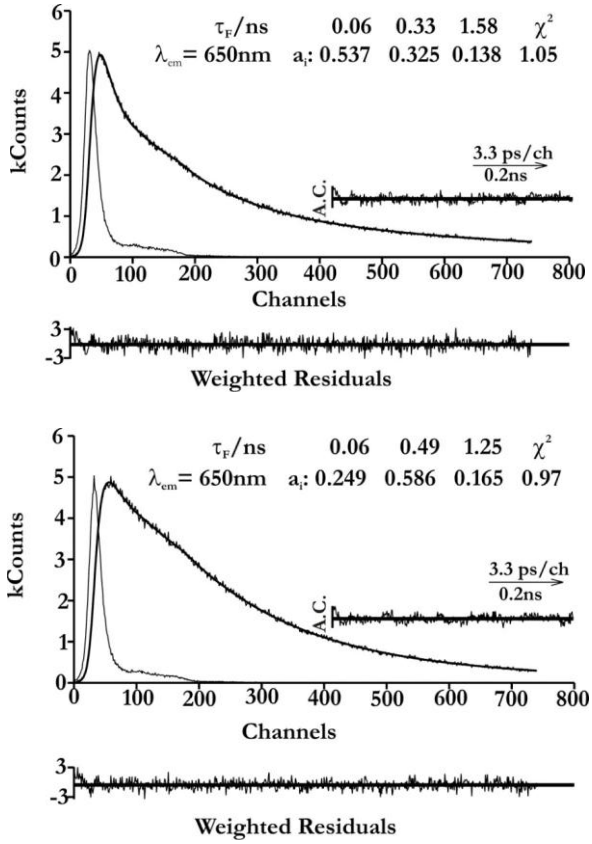

Figure 51 - Fluorescence decays of thioindigo in sepiolite: **top -**2% w/w, **down –** 20% w/w, at T=293K, with excitation at 450 nm. Shown as insets are the decay times (τ/ns), pre-exponential factors (a_i), and chi-squared values (χ^2). Also shown are the weighted residuals for a better judgment of the quality of the fits.

7.6 – SOME NOTES

Another important observation related to the different environment probed by the compounds in each clay (or dye/clay composition) is the colour of the observed complex, as previously mentioned and depicted in Figures 38 and 39. The several proportions also gave different colour hues, see Figures 52 and 53.

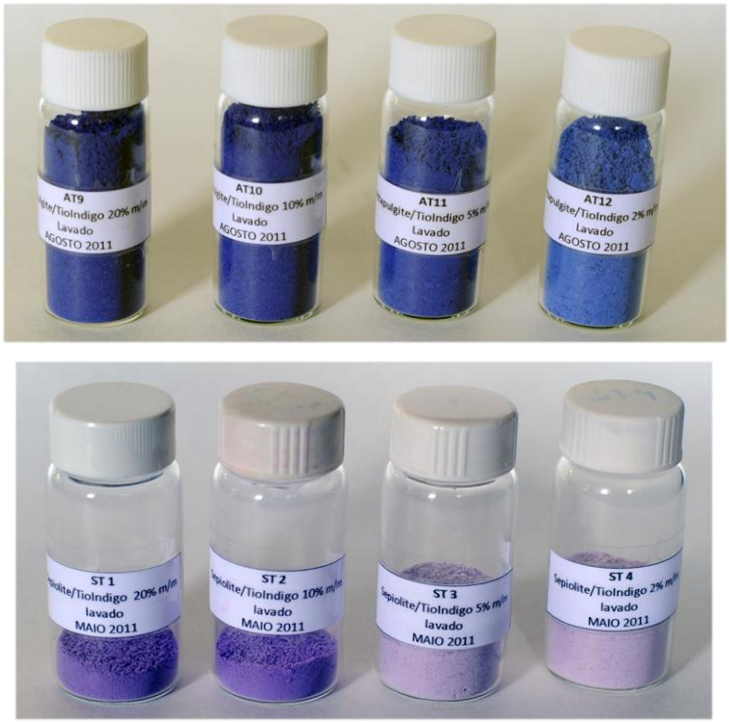

Figure 52 – Photograph of the different (weight/weight) mixtures dye/clay studied. **Top:** thioindigo/attapulgite, 20, 10, 5 and 2% counting from the left. **Down:** thioindigo/sepiolite, 20, 10, 5 and 2% counting from the left.

Attempting to establish an analogy with Zembra purple, the mixture of Tyrian purple with both clays, was also tried but the result, was inconclusive and not satisfactory, since the original colour of the dye vanished, see Figure 54.

Figure 53 – Photograph of the different (weight/weight) mixtures dye/clay studied. **Top:** ciba brilliant pink/attapulgite, 20, 10, 5 and 2% counting from the left. **Down:** ciba brilliant pink/sepiolite, 20, 10, 5 and 2% counting from the left.

Figure 54 – Photograph of the different (weight/weight) mixtures dye/clay studied. **Left:** Tyrian purple/attapulgite, 10, 5 and 2% counting from the left. **Right:** Tyrian purple/sepiolite 10, 5 and 2% counting from the left.

7.7 – MOLECULAR DESIGN

The molecular structure design of attapulgite (or palygorskite), thioindigo and ciba brilliant pink was obtained -aiming to keep the relative molecular dimensions of these structures- in the following manner. The structure of palygorskite was constructed from the American Mineralogist Crystal Structure database with the coordinates given by Chiari *et al.*[82] in cif format which were further converted into xyz coordinates and plotted in the VMD molecular graphics software (available at http://www.ks.uiuc.edu/Research/vmd/). The structure of thioindigo and ciba brilliant pink (in xyz coordinates) was obtained from ChemSpider, further imported to MarvinView (version 5.9.4) and saved in xyz coordinates that were further imported to VMD. This program permits the construction of the overall clay from the basic unit cell together **TI** and **CBP** (with molecular scale dimensions), allowing a clear visualization of the interaction between the host attapulgite with the **TI**/**CBP** guests. Figure 55 shows, in a pictorial manner, the different type of interaction promoted by **TI** and **CBP** with attapulgite. In the case of **TI** the compounds is able to diffuse into the channel cavity whereas in the case of **CBP** due to the methyl (and chlorine) groups it is likely to be found at the surface of the clay cavities where it can be found isolated or as a dimer (see Figure 55).

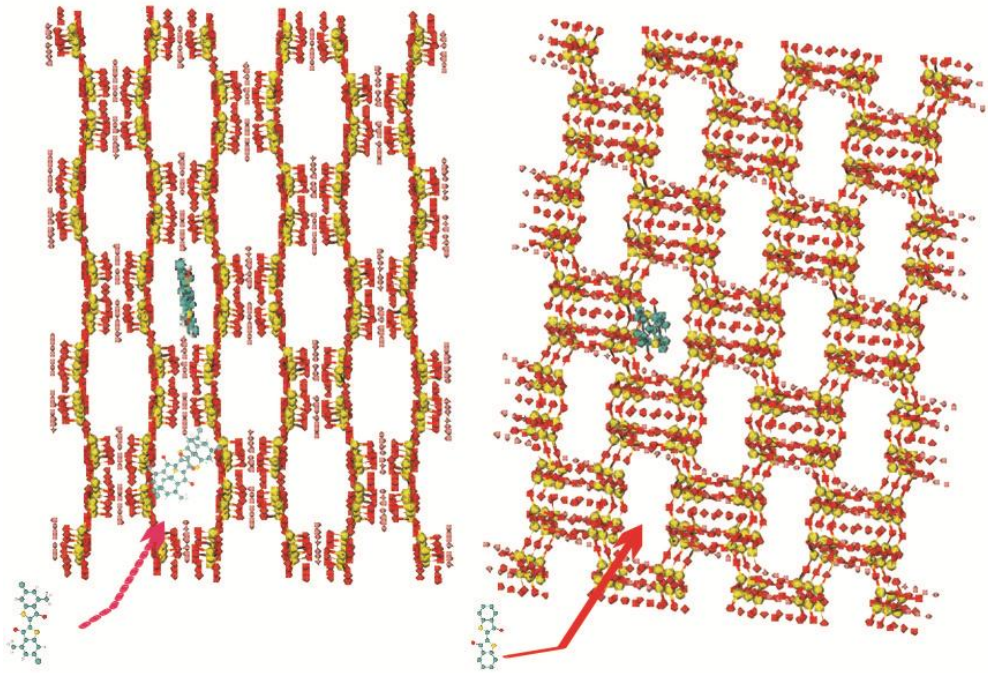

Figure 55- Illustrative picture of the interaction of **CBP** (left hand panel) and **TI** (right hand panel) with attapulgite (palygorskite). For clarity the zeolitic waters are removed. The structure of attapulgite is given in a different perspective in the two panels. The molecular structures of **TI** and **CBP** are also given; in the case of **CBP** the dimer is also presented.

7.8 - CONCLUSIONS

The mixture of indigo, TI and CBP with the typical Mexican clays (attapulgite and sepiolite) provides a unique organic/inorganic hybrid pigments, with characteristic differences, like colour, resistance to degradation and photophysical behaviour.

Based on spectral and photophysical data the interaction between thioindigo (and its derivative ciba brilliant pink) with attapulgite and sepiolite clays has been elucidated, giving further perspectives for the understanding of the structure in Maya Blue. In this work besides revisiting the spectral and photophysical properties of thioindigo –with a comprehensive study of its photophysics in solution- we have extended the study to the solid state by incorporating **TI** (and **CBP)**, in clays of sepiolite and attapulgite. **TI** was found inside the attapulgite clay channels whereas **CBP** is likely to be at the channels surface. When the clay is changed to sepiolite -with higher channel dimensions- both **TI** and **CBP** show similar behavior which indicates that they are probing an identical environment compatible with an interaction with the clay surface.

8. DRAGON'S BLOOD

Dragon's blood is the usual but non-specific name for red-coloured resins obtained from species of *Dracaena* (Dracaenaceae), *Daemonorops* (Palmae), *Croton* (Euphorbiaceae) and *Pterocarpus* (Fabaceae).[148,149] The red resin is collected from natural exudates that appear in injured areas on the stem and branches of *Dracaena* spp. or from a brittle red layer formed outside the scaly fruits of *Daemonorops* spp..[150] This resin has most variable uses; some examples are: dying wool, glue pottery, breath freshener, lipstick, pigment in paints, and more recently is used as a varnish for violins, in photoengraving, as an incense resin, and as body oil.[148,151]

To the name "Dragon's blood" different mythological origins have been given The Greek says that when Ladon (the hundred-headed dragon, guardian of the Garden of Hesperides) was killed, his red blood fall in the ground and in that place trees named as "Dragon trees" grew up. [148] The Indians talk about a struggle between a dragon and an elephant that during (and consequence of) the fight lead to a mixture of the blood of the two creatures, resulting in a magical substance ("Dragon's blood") with medicinal properties.[148]

Brockmann and Junge[152] studied the compounds in dragon's blood resins associated to the red colour, and attributed the colour to a flavylium: dracorhodin; a flavylium which could be considered as belonging to the group of compounds known as anthocyanins. Dracorhodin (quinoidal base of 7-hydroxy-5-methoxy-6-methylflavylium) was isolated and characterized from a commercial source of powdered dragon's blood resin that was probably obtained from a species of *Daemonorops*.[153] More recently, another flavylium, there Christianized as dracoflavylium (4',7-dihydroxy-5-methoxyflavylium) was isolated and characterized from *D. draco*.[149,154] The chemical structures of these compounds are presented in Scheme 19.

Dracorhodin

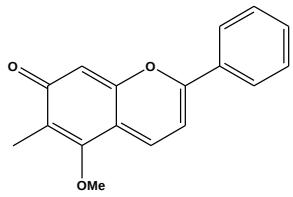

Dracorubin

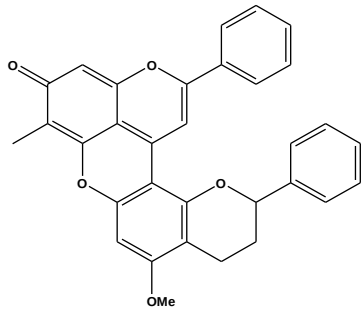

Dracoflavylium

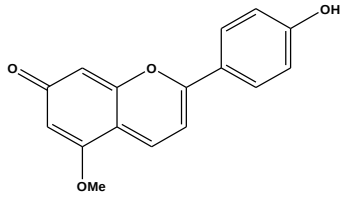

4',7-Dihydroxyflavylium

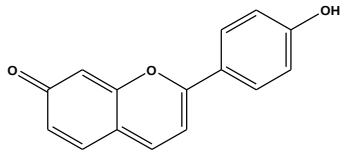

Scheme 19 – Structures for the quinoidal bases responsible for the red colour in Dragon's blood resins from species of *Daemonorops* and *Dracaena*[149] , formed upon deprotonation of the respective flavylium cations.

FLAVYLIUM IONS

Flavylium cations are constituted by a carbon skeleton of 2-phenyl-1-benzopyrylium, Scheme 20, and can be related to anthocyanins, the natural colorants responsible for the reds, blues and purple in nature.[155]

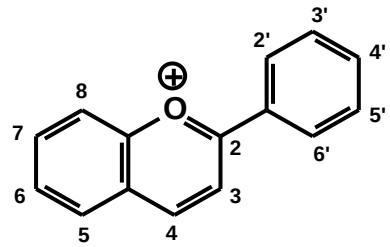

Scheme 20 – Structure of 2-phenyl-1-benzopyrylium – Flavylium ion.

In aqueous solutions, flavylium salts exhibit a complex network of reactions, depicted in Scheme 21 for the particular case of 4',7-dihydroxyflavylium. The equilibrium species at sufficiently acidic pH values is the flavylium cation, $\mathbf{AH^+}$. When the pH is increased, two reactions take place: i) proton transfer to form the quinoidal base **A** and ii) hydration, through position 2, to afford the hemiketal **B**. The proton transfer is faster than the hydration but in many cases the other basic species are more stable at the equilibrium, than **A**, which means that **A**, formed as kinetic product during the first stages of the equilibration process, later disappears (totally or partially) to give the equilibrium distribution of the species. The *cis*-chalcone (**Cc**) is formed from **B** by a tautomeric process and the *trans*-chalcone (**Ct**) results from the isomerisation of the former species. In basic media, ionized species can be formed: the (ionized) quinoidal base $\mathbf{A^-}$ and anionic **Ct**

(**Ct^{n}**) and **Cc** (**Cc^{n-}**) species. The relevant contribution for colour is given by the **AH^{+}** and the quinoidal bases **A** and **A^{-}**. [156-159]

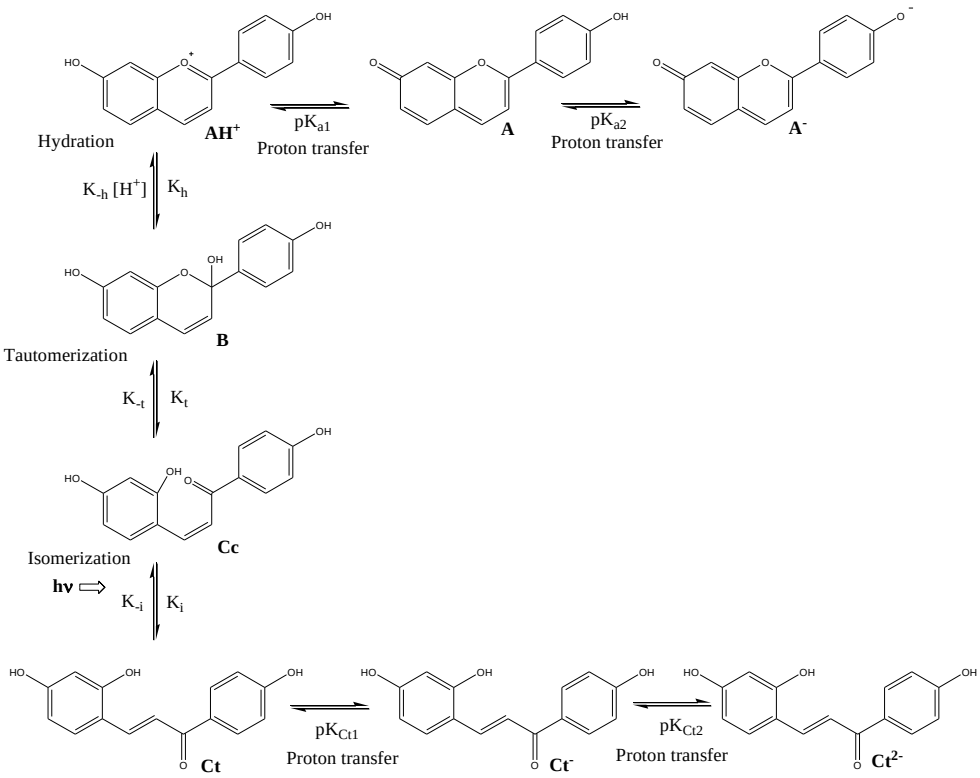

Scheme 21 – Chemical network reaction of 4',7-dihydroxiflavylium (DHF)[159]

8.1- DRACORHODIN

Dracorhodin (Scheme 22), the main constituent from dragon's blood resin, was separated by HPLC-DAD from a commercial sample of *Daemonorops draco* from Zecchi (Florence, Italy), as described in ref[149]. This natural flavylium compound is a potent pharmaceutical substance due to its biological and pharmacological activities such as antimicrobial, antiviral, antitumor and cytotoxic activity.[160] Scheme 22 shows the structural transformations that occur in aqueous solutions.

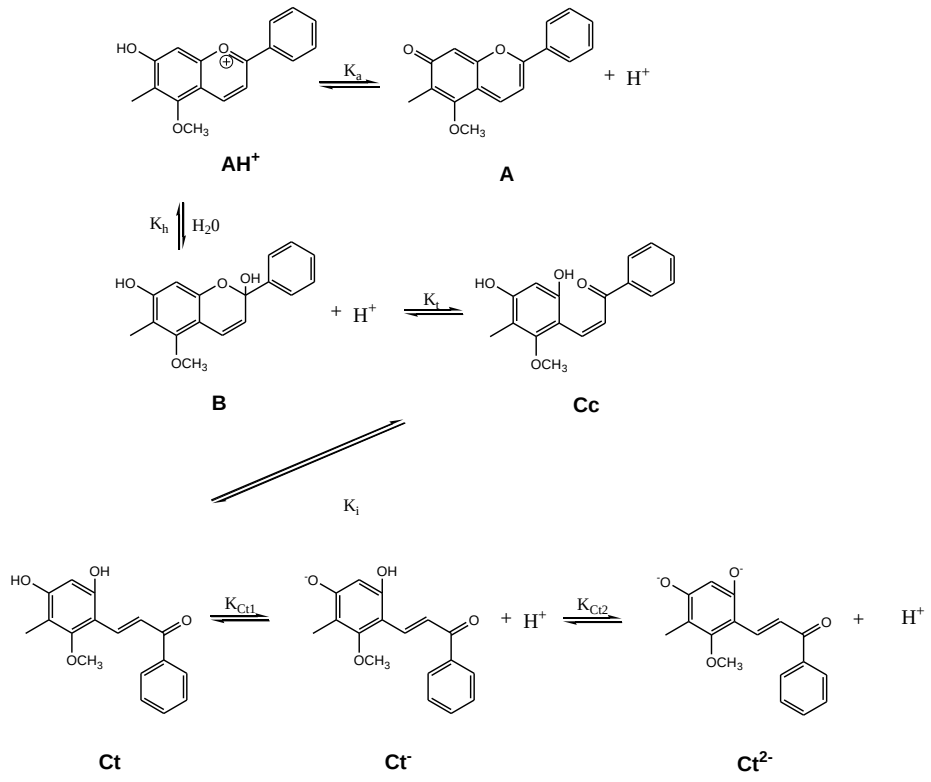

Scheme 22 - Multiple structural transformations/equilibria of dracorhodin in solution.

In order to further understand the chemistry and pH (colour) dependence of dracorhodin, a complete characterization of the equilibrium and of the transient species was carried out in acidic and basic media.

8.1.1 - ACIDIC MEDIA

The compound 7-hydroxy-5-methoxyflavylium presents different forms which are reversibly interconverted by pH modifications (Scheme 22): the flavylium cation (**AH^+**), the quinoidal base (**A**) formed by deprotonation of the flavylium cation, the hemiketal species **B**, obtained by hydration in the 2 position of the flavylium cation, the *cis*-chalcone **Cc**, formed from the hemiketal **B** through a ring opening tautomeric process and the *trans*-chalcone **Ct**, obtained from **Cc** via a *cis-trans* isomerisation reaction. Under basic conditions, **Ct** can deprotonate to form **Ct^-** and **Ct^{2-}** (the deprotonated **Cc** forms that are also formed as transient species were omitted for simplification).

In Figure 56 the spectral variations of dracorhodin obtained upon pH jumps from a stock solution at pH1 to higher pH values are depicted.

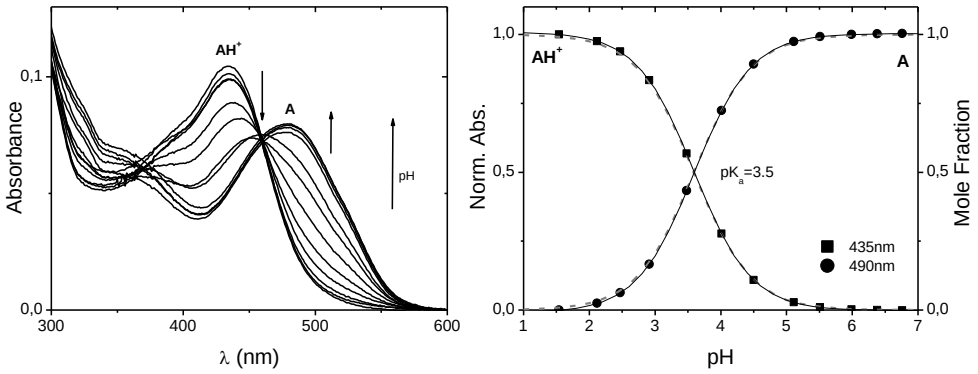

Figure 56 - Left: Spectral variations occurring immediately (ca. 1 min) upon a pH jump from equilibrated solutions of dracorhodin at pH 1.0 to higher pH values; Right: calculated pK_a=3.5 upon fitting (full line) of the absorbance at 435 and 490nm, and mole fraction distribution of the species, the former superposes the absorption fit (dotted grey line).

At very acidic pH values the absorption band of the dracorhodin cation, λ_{max}=435nm, **AH$^+$**, is dominant; by increasing the pH a new band at λ=480 nm is obtained owing to the formation of the red quinoidal base **A** (pK_a=3.5). The spectra obtained at thermal equilibrium is shown in Figure 57 (left), with a pK'_a=3.2. The flavylium cation is again the dominant species at more acidic pH values but for higher pH values an equilibrium is established between the base **A** and the *trans*-chalcone **Ct**.

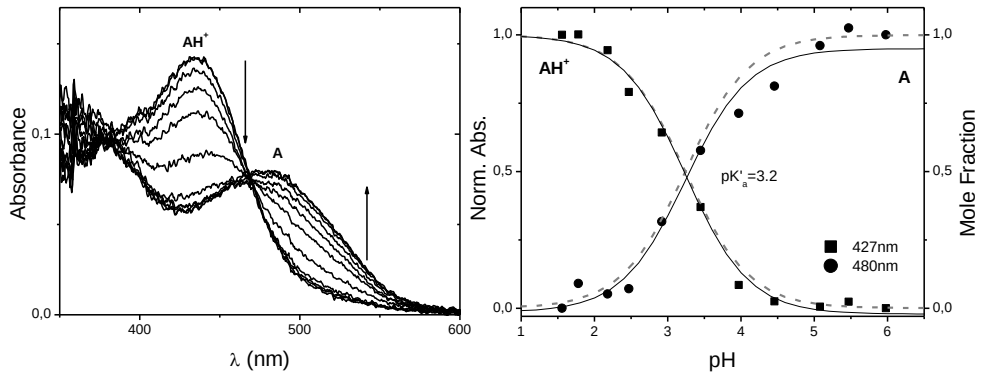

Figure 57 - Left: Spectral variations after thermal equilibrium (one day) upon a pH jump from equilibrated solutions of dracorhodin at pH 1.0 to higher pH values; Right: calculated pK'_a =3.2 upon fitting (full line)of the absorption at 427 and 480nm, and mole fraction distribution of the species (dotted grey line).

8.1.2 - BASIC MEDIA

By carrying out a titration starting from Ct^{2-} back to acidic medium, and monitoring the spectra after approximately one minute; the pK_a values of the *trans*-chalcone could be measured: pK_{Ct2}= 10.2 (Ct^-/Ct^{2-}) and pK_{Ct1}=8.7 (Ct/Ct^-) were obtained (Figure 58).

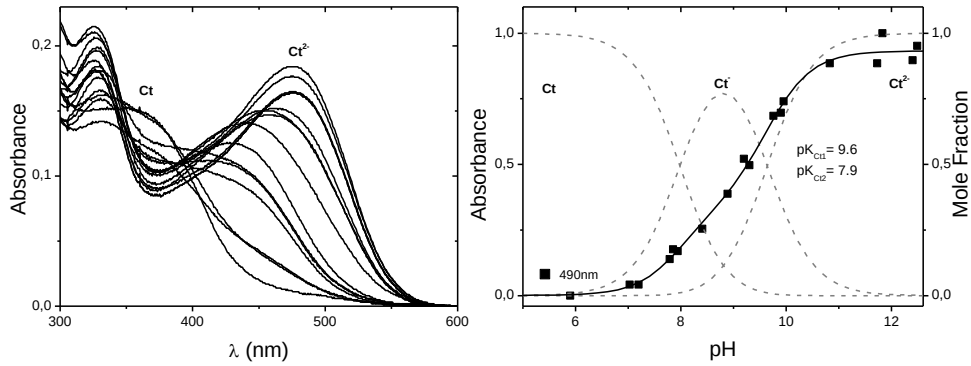

Figure 58 - Spectral variations of the *trans*-chalcone species of dracorhodin, taken immediately upon a pH jump from the equilibrated solutions at pH 12.0 to lower pH values (Left). Right: pK_{Ct1} =9.6 and pK_{Ct2} =7.9 upon fitting (full line) of the absorption at 490nm and 350nm, and mole fraction distribution of the species (dotted grey line).

8.1.3 - pH JUMP EXPERIMENTS

A series of pH jump experiments were performed on dark-equilibrated solutions, from pH=1 (**AH**$^+$) to the pH range 2-6. For each jump, depending on the final pH, **AH**$^+$ becomes **A** (partial or totally), and after that occurs a spectral evolution corresponding to a partial conversion to **Ct**. First-order kinetic laws were observed, see Figure 59. The flavylium cation, which is in fast equilibrium with the quinoidal base formed immediately upon the pH jumps, is transformed in the *trans*-chalcone (**Ct**). From the linear fit of the $\ln(A-A_{eq})$ at the absorption maximum (475nm in this case) *versus* the time evolution (in seconds), it is possible to obtain the kinetic constant (k_{obs}) for each pH jump.

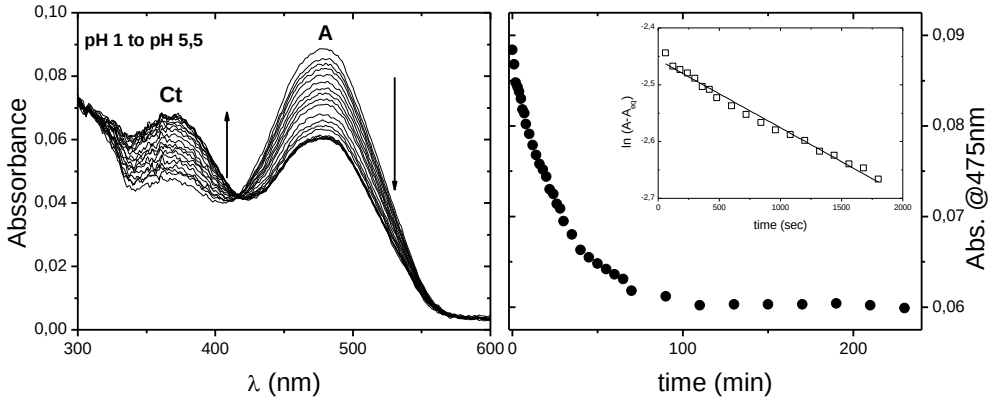

Figure 59 – Left: spectral changes occurred after a pH jump from pH=1 to 5.5 for dracorhodin. Right : evolution of the absorbance at 475nm with time; shown as inset is the presentation and fit of the logarithm of absorption value at 475nm - from this fit the value of k_{obs} is obtained.

The overall kinetic mechanism for dracorhodin can be described as in Eq. 4.

$$\mathbf{A} \underset{}{\overset{K_a}{\rightleftharpoons}} \mathbf{AH^+} \underset{K_{-h}[H^+]}{\overset{K_h}{\rightleftharpoons}} \mathbf{B} \overset{K_t}{\rightleftharpoons} \mathbf{Cc} \underset{K_{-i}}{\overset{K_i}{\rightleftharpoons}} \mathbf{Ct} \qquad (4)$$

The steady state approach can be applied to the species **B** and **Cc** leading to Equation 5 where the observed rate constant presents a bell shape curve when plotted as a function of pH, in this plot k_{-i} is a limit for low pH and zero an upper limit for high pH values. Representation of k_{obs} for several pH jumps, as a function of pH leads to a bell-type curve, Figure 60.

$$k_{obs} = \frac{\frac{[H^+]}{[H^+]+Ka} \times k_i K_T K_h + k_{-i}[H^+]}{[H^+] + \frac{k_i K_T}{k_{-h}}} \qquad (5)$$

8.1.4 – NETWORK OF CHEMICAL REACTIONS

Following Scheme 22, and the data obtained until this point, the present system can be accounted for by the following set of equations, assuming that at the equilibrium the concentration of the hemiketal and *cis*-chalcone species can be neglected, as the experimental data suggests:

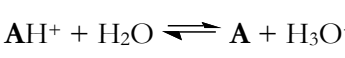

$$k_{a1} = \frac{[A]\,[H^+]}{[AH^+]} \qquad (6)$$

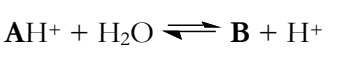

$$k_h = \frac{[B]\,[H^+]}{[AH^+]} \qquad (7)$$

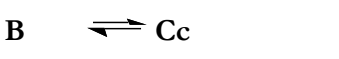

$$k_t = \frac{[C_c]}{[B]} \qquad (8)$$

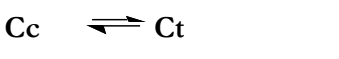

$$k_i = \frac{[C_t]}{[C_c]} \qquad (9)$$

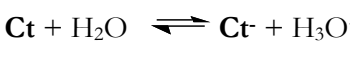

$$k_{Ct1} = \frac{[Ct^-]\,[H^+]}{[Ct]} \qquad (10)$$

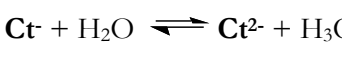

$$k_{Ct2} = \frac{[Ct^{2-}]\,[H^+]}{[Ct^-]} \qquad (11)$$

Considering that at the equilibrium the concentration of **B** and **Cc** is negligible (as observed experimentally), C_o is the sum of the concentration of all species at the equilibrium

$$C_0 = [AH^+] + [A] + [Ct] + [Ct^-] + [Ct^{2-}] \qquad (12)$$

It can be easily demonstrated that the mole fraction distribution of each species at the equilibrium is given by:

$$\frac{[AH^+]}{C_0} = \frac{[H^+]^3}{D} \quad (13)$$

$$\frac{[A]}{C_0} = \frac{k_a [H^+]^2}{D} \quad (14)$$

$$\frac{[Ct]}{C_0} = \frac{k_h k_t k_i [H^+]^2}{D} \quad (15)$$

$$\frac{[Ct^-]}{C_0} = \frac{k_h k_t k_i k_{Ct1} [H^+]}{D} \quad (16)$$

$$\frac{[Ct^{2-}]}{C_0} = \frac{k_h k_t k_i k_{Ct1} k_{Ct2}}{D} \quad (17)$$

with

$$D = [H^+]^3 + (k_a + k_h k_t k_i)[H^+]^2 + k_h k_t k_i k_{Ct1}[H^+] + k_h k_t k_i k_{Ct1} \quad (18)$$

the calculated equilibrium constants are the following:

$$k'_a = 10^{-3.2}; k_{a1} = 10^{-3.5}; k_{Ct1} = 10^{-7.9}; k_{Ct2} = 10^{-9.6}$$

If sufficient kinetic data were collected the value of $k_h k_t k_i$ could be obtained from a fitting with eq. (5) which together with the above equilibrium constants would allow calculation of the mole fraction distribution of species through eqs. (13) – (18). Nevertheless, analysis of the spectral data in Fig. 57 indicates that the final equilibrium for pH>5 contains ca. 70% A and 30% Ct.

8.1.5 - EXCITED STATE CHARACTERIZATION

The UV-Vis titration (Figure 56), revealed the existence of one acid/base equilibrium. A very similar pK_a value of 3.3 was obtained with the fluorescence emission titration made immediately after the pH jump from the equilibrated solutions of dracorhorin at pH=1, Figure 60. This shows that the equilibrium is restricted to two species and that the $pK_a=pK_a^*=3.2 \pm 0.2$.

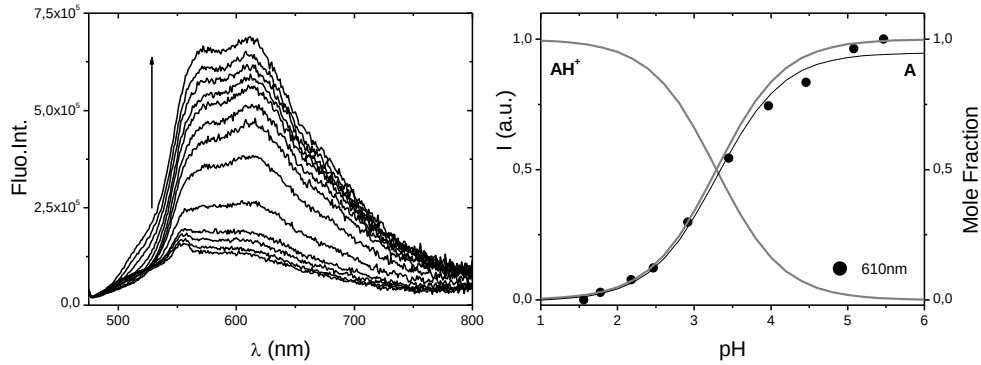

Figure 60 – Fluorescence emission evolution with pH, λ_{exc}= 465nm – isosbestic point from Figure 57, and immediately upon the pH jump. The right plot is the mole fraction distribution of the **AH⁺** and **A** species (dotted grey line) and emission fit (black line) at 610nm, with $pK_a^*=3.3$.

The fluorescence decays collected at the maximum emission wavelengths and pH values where the two dominant species prevail are presented in Table 10. The fluorescence quantum yields, determined in the same conditions of Figure 60, for **AH^+** was 4.42×10^{-4}, and 1.93×10^{-3} for **A.**

Table 10 – Time resolved fluorescence data for dracorhodin in aqueous equilibrated solutions, collected at 615nm with λ_{exc}=451nm and T=293K. Also shown are the chi-square ($\chi2$) values for a better judgment of the quality of the fittings.

pH/form	τ_1 (ns)	τ_2 (ns)	τ_3 (ns)	a_1	a_2	a_3	$\chi2$
1.66 (AH^+)	0.02	0.08	0.40	0.684	0.290	0.026	1.15
5.91 (A)	0.01	0.08	0,41	0.397	0.590	0.013	1.12

From Table 10 it can be seen that there are two main species responsible for the decay: a shorter with ~10ps and a longer with 80ps It can also be observed, that upon going from pH 1.66 to 6, there is an increase of the relative contribution from the 80ps species, with a concomitant decrease of the contribution of the ~10ps species. It can therefore be concluded that **AH^+** decays with a lifetime of 10 ps and **A** with 80ps. The additional third decay time has a negligible contribution. At alkaline pH values where the ionized *trans*-chalcone **(Ct^{2-})** (12.24) is dominant, the fluorescence decay, although not strictly single exponential, has its major component with a decay time of ~ 10 ps, see Figure 61.

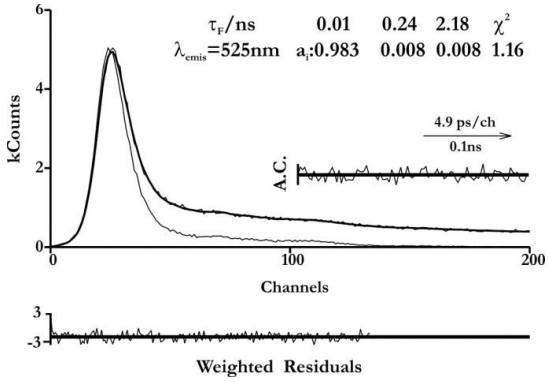

Figure 61 - Fluorescence decay of the ionized *trans*-chalcone (Ct^{2-}) at T=293K, with excitation at 451 nm. Shown as insets are the decay times (τ/ns), pre-exponential factors (a_i), and chi-squared values (χ^2). Also shown are the weighted residuals for a better judgment of the quality of the fits.

8.1.6 - CONCLUSIONS

Dracorhodin has been extracted from *Daemonorops draco* , the species **AH^+** and the quinoidal base **A** are the responsible for the colour of this compound, being yellow at strong acidic conditions, and orange at moderate acidic pH values. The titration at ca. 1 min after the pH jumps provided a pK_a of 3.5 for the equilibrium **$AH^+ \leftrightarrow A$**, with fluorescence quantum yields of 4.42×10^{-4} (**AH^+**) and 1.93×10^{-3} (**A**), and a pK_a^*=3.2. After thermal equilibrium a pK_a'=3.2 was determined, and the **AH^+** and **A** species decay with fluorescence lifetimes of respectively ~10 ps and 80 ps, indicating that fluorescence is not an effective deactivation channel. The ionized *trans*-chalcone was also investigated, pK_{Ct1} =9.6 and pK_{Ct2} =7.9 values were determined, the **Ct^{2-}** was found to have a major component of 10 ps.

8.2 – 4',7-DIHYDROXY-5-METHOXYFLAVYLIUM – DRACOFLAVYLIUM

The complex network of chemical reversible reactions of 4',7-dihydroxy-5-methoxyflavylium – identified as the major red colourant in samples of dragon's blood resins, and named as dracoflavylium (**DRF**) – was previously published by M. J. Melo *et al.*. [154] which have determined all the equilibrium constants, that enables a complete characterization of the system. In this chapter dracoflavylium was studied in an organic solvent – Dimethylformamide (DMF) - and different environments were used (acidic and basic) by the addition of some drops of HCl 1M and NaOH 1M. Very curiously is to observe that under alkaline conditions a blue colouration was obtained contrasting with the reddish colour of $\mathbf{A}^-$ in aqueous solution, see Figure 62.

Figure 62 – Picture of Dracoflavylium dissolved in: DMF with some drops of HCl 1M (Yellow); neutral DMF (Orange); DMF with some drops of NaOH 1M (Purple blue).

8.2.1 - SPECTRAL DATA

In homogeneous aqueous solution Dracoflavylium exhibits three forms in the ground state, the cation (**AH$^+$**), the quinoidal base (**A**) and the anion (**A$^-$**), with well defined pK_a values: pK_{a1}=4.0 and pK_{a2}=7.5.[154] The network of chemical reactions is depicted in Scheme 23.

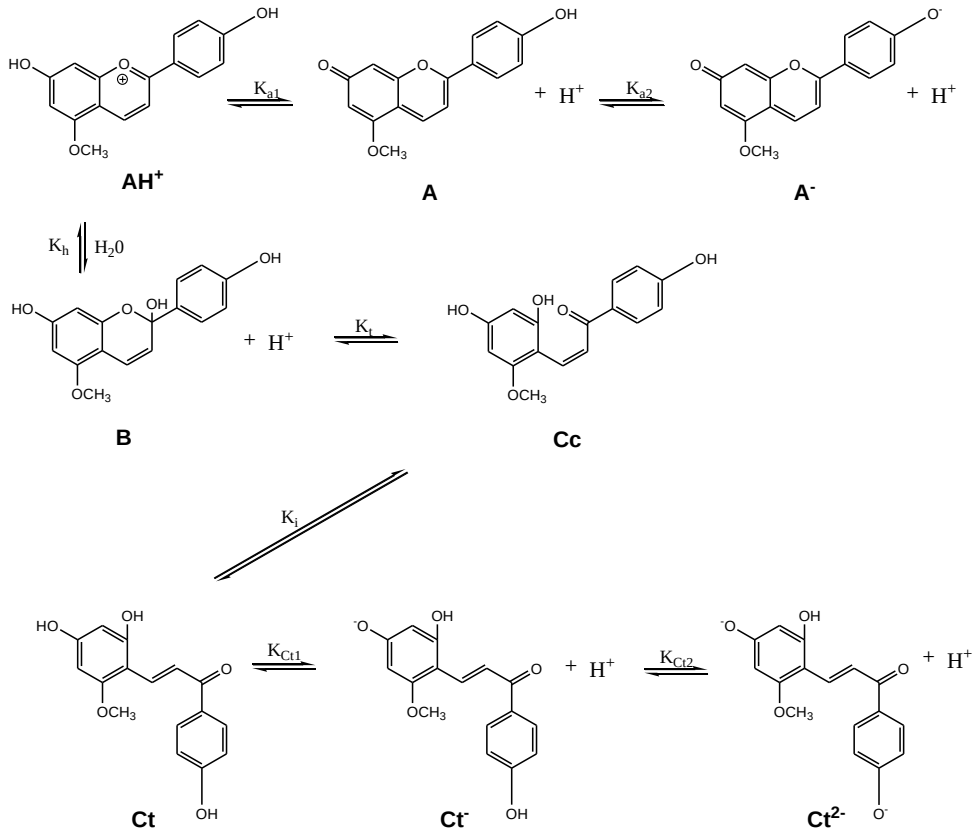

Scheme 23 – Network of chemical reactions for dracoflavylium.[154]

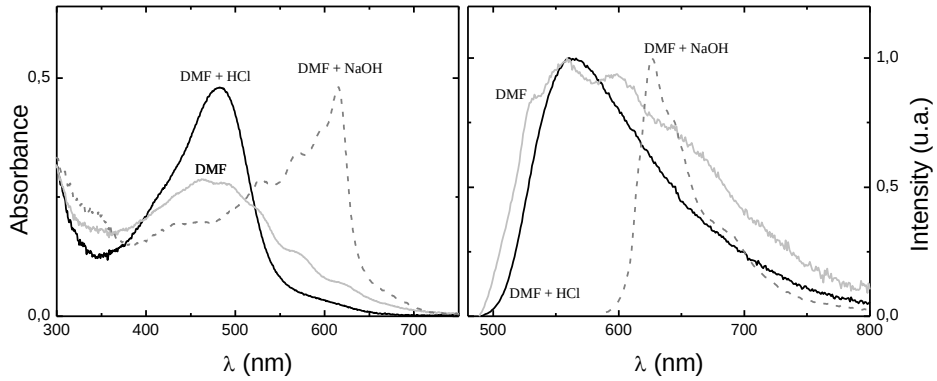

Figure 63 – Absorption (left) and fluorescence emission spectra (right) of Dracoflavylium in DMF in different environments.

From Figure 63 a red shift of the absorption and fluorescence bands when going from the neutral and acidified DMF to the alkaline solution can be observed; this red shift is more pronounced in the absorption (~135nm) than in the fluorescence spectra (~65nm). It is also visible that the spectrum is, in pure DMF, are in both cases more broad. In Figure 64 the absorption, emission and excitation fluorescence spectra for Dracoflavylium in the neutral, basified and acidified DMF are shown; from the spectra it can be seen that for all solvent environments there is a match between the absorption and excitation spectra.

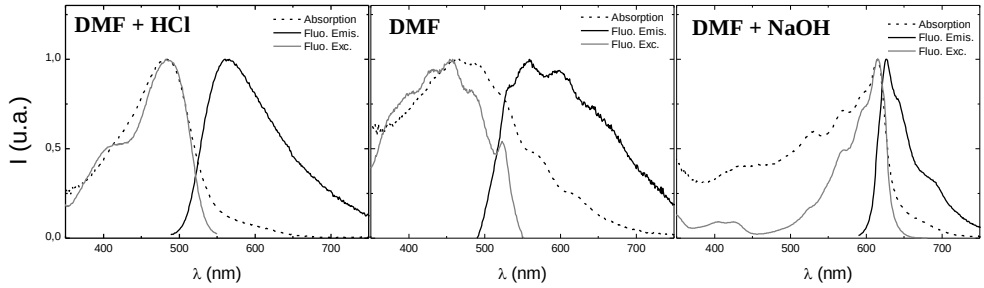

Figure 64 - Absorption, emission and excitation fluorescence spectra for Dracoflavylium in acidic DMF, DMF, and basic DMF, at T=293K.

Comparison of the absorption spectra of **DRF** in DMF, with the spectra published (in water)[154] and here reproduced (Figure 65), shows that there is no complete overlap between the spectra in the organic solvent and in aqueous solution.

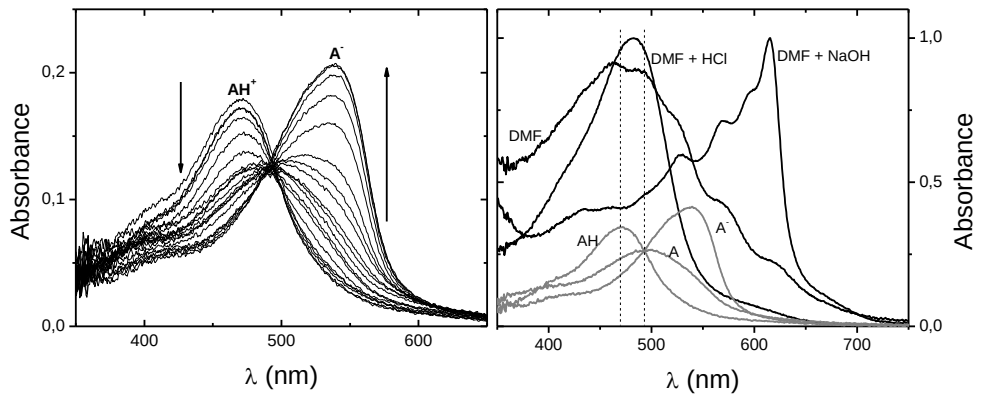

Figure 65 - Spectral variations occurring immediately (ca. 1 min) upon a pH jump from equilibrated solutions of dracoflavylium at pH 1.0 to higher pH values, (left panel)in aqueous solution; overlap of the three species in DMF – black line, and in aqueous solution – grey line, (right panel), T=293K.

8.2.2 - EXCITED STATE CHARACTERIZATION

From Table 11 it can be seen that fluorescence is not the most important route for the excited state deactivation. In addition, no transient triplet states or efficient singlet oxygen sensitization could be obtained which points out to internal conversion as the main deactivation route for the different species of Dracoflavylium in DMF (neutral, basified and acidified).

Table 11- Absorption and emission maxima together for dracoflavylium in DMF, DMF with HCl, and DMF with NaOH.

Solvent	λ_{max}^{Abs} **(nm)**	λ_{max}^{Fluo} **(nm)**	Δ_{SS} **(nm)**	ϕ_F
DMF + HCl	481	563	82	0.00232
DMF	463	559	96	0.00144
DMF + NaOH	614	626	12	0.00632

Time resolved fluorescence data reveals that the decays can only be properly fitted with sums of three exponentials in the different solvent environments (see Table 12). The data also reveal some differences in the obtained decay times and pre-exponential factors in neutral, acidified and basified DMF.

Table 12 – Time resolved fluorescence data for dracoflavylium in DMF, DMF with HCl and DMF with NaOH, collected at 560nm for DMF+HCl, and DMF,and 525nm for DMF+NaOH; λ_{exc}=392nm and T=293K.

Solvent	τ_1 (ns)	τ_2 (ns)	τ_3 (ns)	a_1	a_2	a_3	$\chi 2$
DMF + HCl	0.03	0.24	1.42	0.380	0.445	0.176	1.18
DMF	0.02	0.19	0.66	0.528	0.383	0.088	1.18
DMF + NaOH	0.01	0.13	0.50	0.559	0.299	0.142	1.20

The data suggest that in neutral, acidified and basified DMF a more complex network of reactions is present and the initial intention of isolation the **AH**$^+$ (neutral and acidified DMF) and **A** (alkaline DMF) was found unsuccessful.

8.2.3 - CONCLUSIONS

4',7-dihydroxy-5-methoxyflavylium, Dracoflavylium, when dissolved in dimethylformamide, and later submitted to the addition of HCl and NaOH showed three distinct colours, that beside the spectral differences, photophysically behave similarly.

9. Brazilwood

During the Middle Age period, original from the East Indies, under the name *brazil, bresil, brasil, brasilium, brisil, brisiliehout, berzi, verzi or verzino* – and later brazilwood – a wood derived from *Caesalpinia sappan* L. tree, was used to obtain bright reddish-purple colours for textile dyeing, like cotton, woollen cloth, silk and as red ink. This dye, extracted from brazilwood, was exotic and very expensive, and the trading from Asia to Europe very difficult, resulting in the increase of the dye cost.[161,162]

When the Portuguese navigators, in 1500, set foot on land on what is now Brazil, they found abundance of brazilwood, and also found that the tree was very similar to the one they were used to known from Asia. The name for that land was meant to be "Terra de Vera Cruz" but due to the huge quantity of the tree the name was changed to Brazil.[161] This scandalized the devout, who complained that it amounted, as one member of the Church put it to "preferring a block of wood to the Holy Cross and a red dye to the true blood of Christ".[162]

There is a general consensus that this constitutes a unique case where the name of a country was derived from a tree. There is also an historical connection between the discovery of the new land and the growth of a dyeing industry for wood. Until the Portuguese discovery, the dyestuff was only used for luxury textiles such as velvet. The intensive exploitation of these natural sources lead to a nearly extinction of this tree.[161,162]

Photograph of pieces of brazilwood, and a cotton dyed with brazilwood, taken at Durer'house, Nuremberg. Author's picture.

Brazilin (Scheme 24) is the major compound isolated from Caesalpinia which, upon exposure to air and light, forms the deep red brazilein (Scheme 24 B). This exposure oxidises the second hydroxyl group to a quinoid moiety. The π-electron delocalization created with the conjugated system gives rise to the deep red colour characteristic of brazilwood.[163]

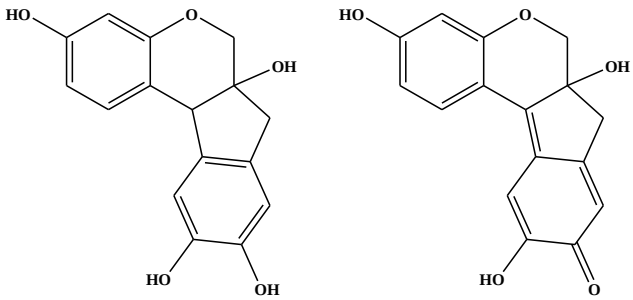

Brazilin **Brazilein**

Scheme 24 – Structures of the major component in brazilwood – brazilin - and its correspondent oxidized and colourant form – brazilein.

The first report of the isolation of brazilin, from brazilwood, was made by Chevreul in 1808 (quoted in refs[164,165]), but no attempt was made to determine its constitution until 1864(quoted in refs[164,165]), when Bolley, as the result of several analysis, suggested the formula $C_{22}H_{20}O_7$ as the result of several analyses. It was Liebermann and Burg who, in 1883, have accurately determined the constitution of brazilin with its empirical formula of $C_{16}H_{18}O_7$.[164,165]

The mechanism of brazilin oxidation was, for that time, already known. Indeed, in 1901, Gilbody refers that "if air is passed through a solution of dilute alkali for a considerable time, the purple colour of the solution gradually changes to a reddish-brown and the brazilein which is first produced is completely oxidized ".[164]

The (correct) structure of brazilin has not always been consensual. In fact, it was Perkin in 1902[166] who proposed a structure that is nowadays accepted. The oxidation to brazilein was, at the time, together with the formation of salts when treated with concentrated mineral acids (a behaviour first observed in 1882), already one of the most interesting known characteristics of brazilin. It was also noted at the time that the obtained orange or red salts could not be regenerated by the action of alkalis to the original colouring matters.[167]

9.1 - BRAZILIN

9.1.1 - PURIFICATION OF BRAZILIN

100 g of Brazilwood chips (from Kremer pigments) were placed in a 1L beaker with 500mL of methanol, and left there for two days, during what, the mixture was occasionally stirred. After this period of time, the liquid became dark red, and the mixture was filtrated; the procedure was repeated twice. The extract was concentrated under reduced pressure, and partitioned in H_2O-MeOH (3 :1, 200mL) and Ethyl Acetate (100mL × 3). A small part of the obtained extract was re-dissolved in methanol and further chromatographed in a silica gel column using as eluent a mixture of $CHCl_3$-MeOH (from 15 :1 to 5 :1), a procedure adapted from Kim *et al.*[168]. However, this procedure proved to be more complex than expected; indeed, at a certain point, all the silica became completely red, see Figure 66, and there was no way to proceed with to the separation of different constituents of the original solution. Due to that, several different portions of the eluted fractions were collected and reduced to dryness. Some of those portions were dissolved in water and acidified with some drops of aqueous HCl 0.1M, and further injected in an HPLC-DAD. Two main fractions were found to elute with different retention times, see Figure 67; one at nine minutes and another at twelve

minutes. Both fractions were found to match with the literature spectra attributed to brazilin.[168-171]

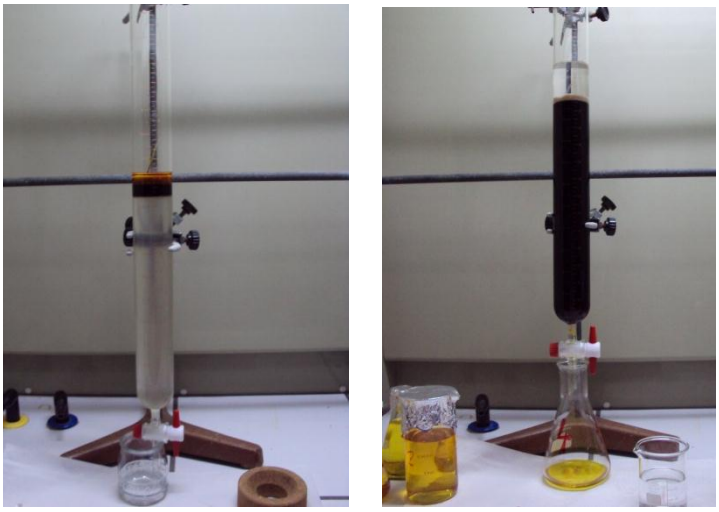

Figure 66 – Pictures obtained at the beginning and at the end of the silica chromatography of brazilwood.

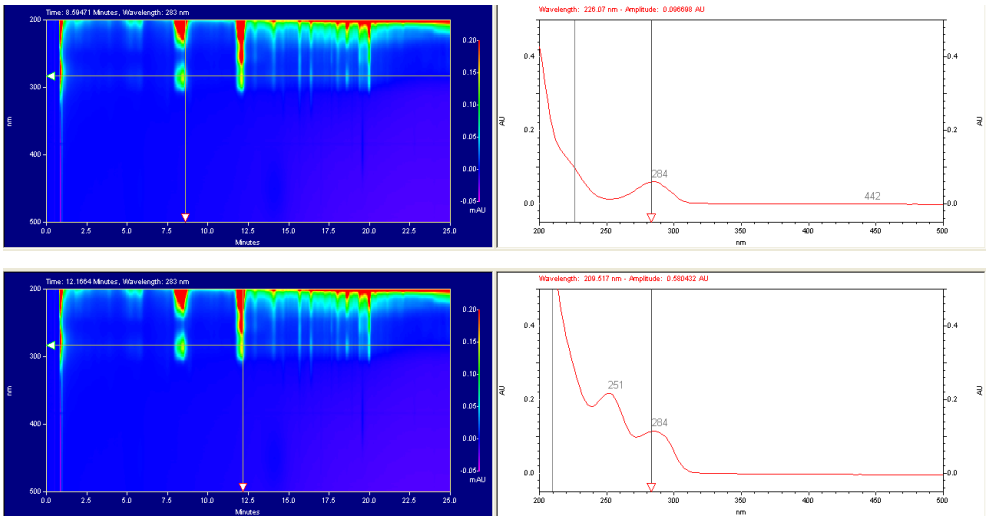

Figure 67 – Chromatogram of the second portion obtained from the silica column (left). Top-right, UV-Vis spectra of the "9 minutes fraction", down-right, UV-Vis spectra of the "12 minutes" fraction.

The ^{1}H NMR spectra of the fraction eluted at nine minutes, matched the one published by Kim[168] for brazilin.

Using the same separation method used to obtain dracorhodin, reported in ref[154] these two fractions appear at five minutes and seven minutes respectively. This method was therefore used to isolate brazilin (the five minute fraction).

9.1.2 - pH BEHAVIOUR

Brazilin was titrated in aqueous solution by several pH jumps starting from acid pH=1 to higher pH values (~12). From Figure 68 it can be seen that for brazilin there is a maximum at 283nm at pH=1, and at pH~6 the maximum is now at 295nm; at pH up to 10 the solution became deep red, and a new band at 520nm attributed to de-protonated brazilein is now present. In order to easily identify the species in equilibrium, the acronym BxH (where x stands for the number of protonated hydroxyl groups in brazilin), and BOXxH in brazilein was established, see Scheme 25.

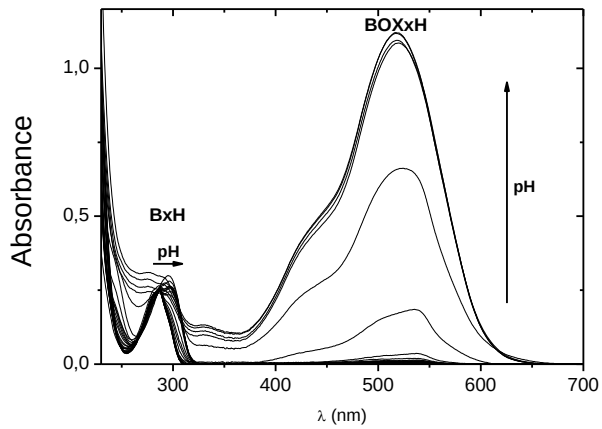

Figure 68 – Changes in the absorption spectra, occurred upon the pH jumps from equilibrated stock solutions of brazilin at pH=1 to pH=12, T=293K.

The brazilin used in this experiment (Figure 68) was previously purified and its structure proved by NMR; however, it still shows the presence of a small amount of brazilein. The titration curve was built by plotting the change in absorbance (at the brazilin absorption wavelength maximum) at different pH values (using pH jumps from a stock solution at pH=1), and is depicted in Figure 69. Two different processes occur with increasing pH: (i) change in the band around 280nm until pH<10 and (ii) formation of an absorption band centred at ~500nm for pH>10. The first process is illustrated in detail in Fig. 69 and corresponds to deprotonation of **brazilin** with two measurable pK_a values of pK_{a1}=6.6 and pK_{a2}=9.4 for pH<10, see Scheme 25. The second process should correspond to the third deprotonation of **brazilein** followed by fast oxidation to full deprotonated brazilein. This is further confirmed by the appearance of the same band around 520nm upon titration of brazilein (see Figure 76).

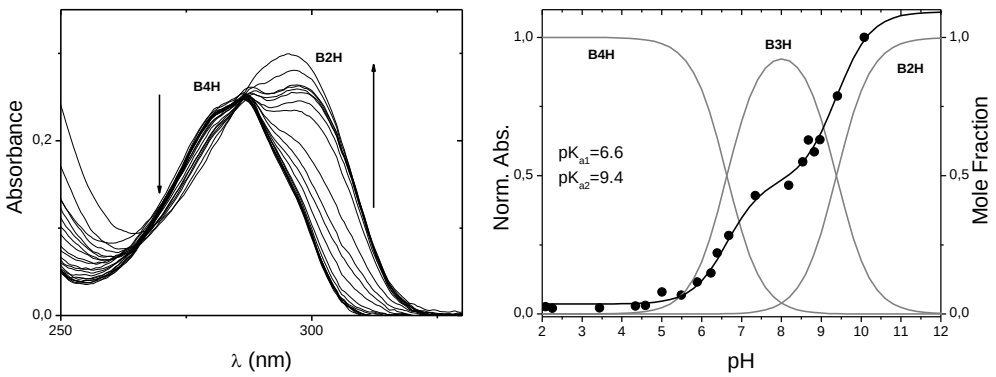

Figure 69 – Left : spectral variations occurred upon a pH jump from equilibrated solutions of brazilin at pH=1 to alkaline pH values. Right : calculated pK_a upon fitting of the absorbance at 295nm (black line), and mole fraction distribution of the species (grey line).

As can be seen from Figure 68, at very acidic pH values a single (and dominant) species exists with an absorption maxima at 284 nm; upon increasing the pH, a new band (with λ_{max} =295nm) gradually appears.

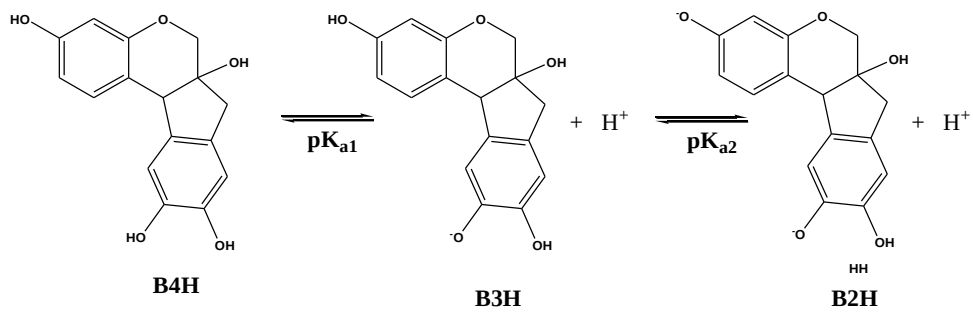

B4H **B3H** **B2H**

Scheme 25 – Structural changes of brazilin with pH

Part of the existent literature report studies on haematoxylin and haematein, the main colourants of logwood, and structurally very similar to brazilin and brazilein, see Scheme 26. These studies make mention to the fact that the fast oxidation of haematoxylin is an obstacle to the titration of the reduced form.[172,173] However, in the present case, this did not constitute a problem, since the stock aqueous solution of brazilin was kept unaffected during the time of the titration.

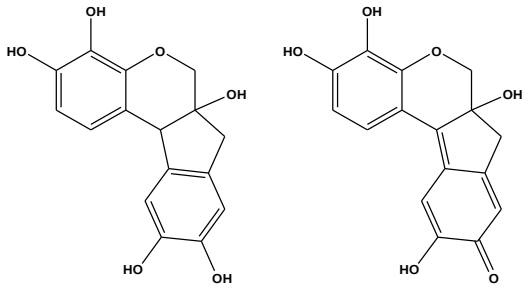

Scheme 26 – Structures of haematoxylin and haematein, the main dye constituents obtained from logwood.

9.1.3 - SPECTRAL DATA

Figure 70 presents the absorption, fluorescence emission and excitation spectra of brazilin at pH=1. From the spectra it can be seen that there is an almost perfect match between the absorption and fluorescence excitation spectra, thus attesting the purity of the investigated brazilin.

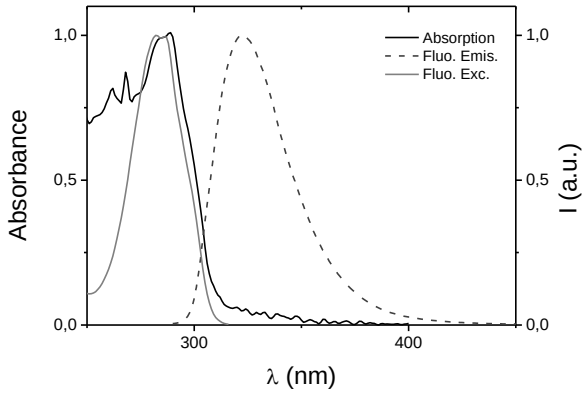

Figure 70 – Absorption and fluorescence emission and excitation spectra of brazilin in HCl 0.1M, T=293K.

Table 13- Spectral and photophysical properties of brazilin at pH=1, T=293K

	λ_{max}^{Abs} **(nm)**	λ_{max}^{Fluo} **(nm)**	Δ_{SS} **(nm)**	ε_{SS} (M^{-1} cm^{-1})	ϕ_F	τ_F (ps)
Brazilin	284	323	39	6160	0.330	260

Considering the dyes studied until now, brazilin presents the highest fluorescence quantum yield value. Moreover, the fluorescence decay is single exponential (Figure 71), reinforcing the idea that at lower pH values this species (brazilin) is dominant, see Table 13. Moreover it can be observed from Figure 70 and table 13 that the Stokes shift is not considerably high, thus showing that there are no significant structural changes between the ground and first singlet excited states.

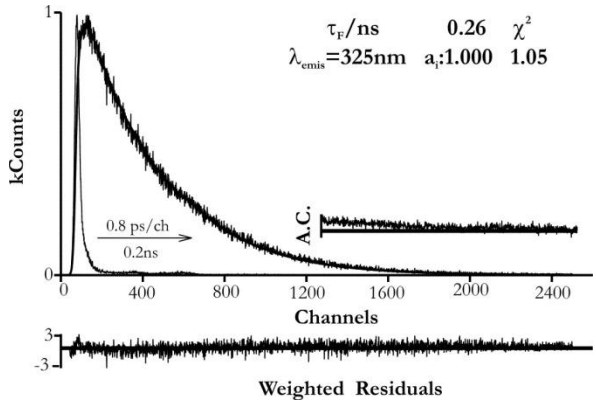

Figure 71 - Fluorescence decay of brazilin in HCl 0.1M, at T=293K, with excitation at 282 nm. Shown as insets are the decay times (τ/ns), pre-exponential factors (a_i), and chi-squared values (χ^2). Also shown are the weighted residuals for a better judgment of the quality of the fits.

9.1.4 - EXCITED STATE CHARACTERIZATION

The fluorescence titration curve for brazilin was obtained using 290 nm as the excitation wavelength (isosbestic point of the ground state titration curves) and the results are depicted in Figure 72.

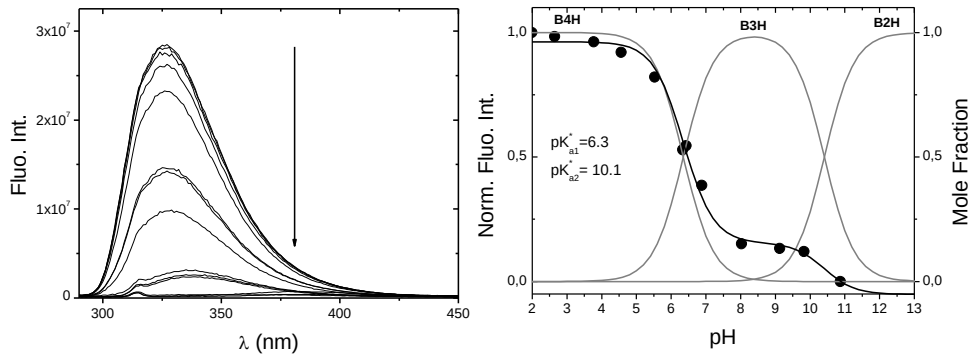

Figure 72 - Left : spectral variations occurred upon a pH jump from equilibrated solutions of brazilin at pH 1 to higher pH values. Right : calculated pK^*_a from the fitting of the emission at 350nm (black line), and mole fraction distribution of the species (grey line).

At pH=1 a fluorescence emission maximum at 323 nm is observed with a quantum yield of 0.330 (Table 13); upon going to alkaline pH values, the fluorescence emission gradually decreases and a very weak band at ~400nm appears (Figure 72). From the fluorescence titration curves, two pK^*_a values were obtained: $pK_{a1}{}^*$=6.3 and $pK_{a2}{}^*$=10.1; these values are very close to the obtained ground-state pK_a values -pK_{a1}=6.6 and pK_{a2}=9.4- see above Figure 69. This supports the fact that there is little change in the charge distribution between the S_0 and S_1 states.

The variation of the decay profiles with the pH was also investigated, with pH jumps from a stock solution of brazilin at pH=1. As seen in Figure 71, the acidic species decays mono-exponential, and at pH ~4 a second component begins to appear leading to biexponential decays (with decay components of 20 ps and 260 ps) until pH~9 is reached where it turns on again to be single exponential but now with a dominant value of 20 ps. The decay times were found constant all over the pH range whereas the associated pre-exponential factors vary reciprocally as illustrated in Figure 73. From the pre-exponential dependence with pH a titration curve could be constructed (similar to that obtained from the steady-state data in Figure 72), from which a pK_a=6.3 is obtained, see Fig. 73. Also from Figure 72 it can be seen that the B2H species has a very low fluorescence, and for that reason and also due to some signal loss occurred in the ps-TCSPC apparatus, we were unable to properly collect a decay and therefore to obtain its fluorescence lifetime.

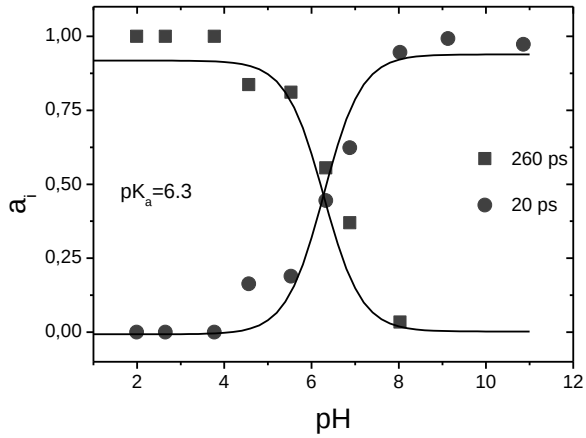

Figure 73 – Plot of pre-exponential coefficients (a_i) associated to brazilin decay times of 20 and 260 ps as a function of the pH (after pH jump from a stock solution in HCl 0.1M), collected at λ_{emis}=325nm and with excitation at λ=282nm, T=293K.

9.1.5 – INFLUENCE OF LIGHT AND OXYGEN IN THE OXIDATION OF BRAZILIN

Using a ND-YAG laser, with λ_{exc}=266nm, the irradiation of aerated and degassed solutions of brazilin at pH=1.5, was performed, see Figure 74. It can be seen that irradiation promotes the increase of the absorption band centred at 445nm (attributed to brazilein); however, this increase is more pronounced for aerated than it is for degassed solutions, Fig.74 D.

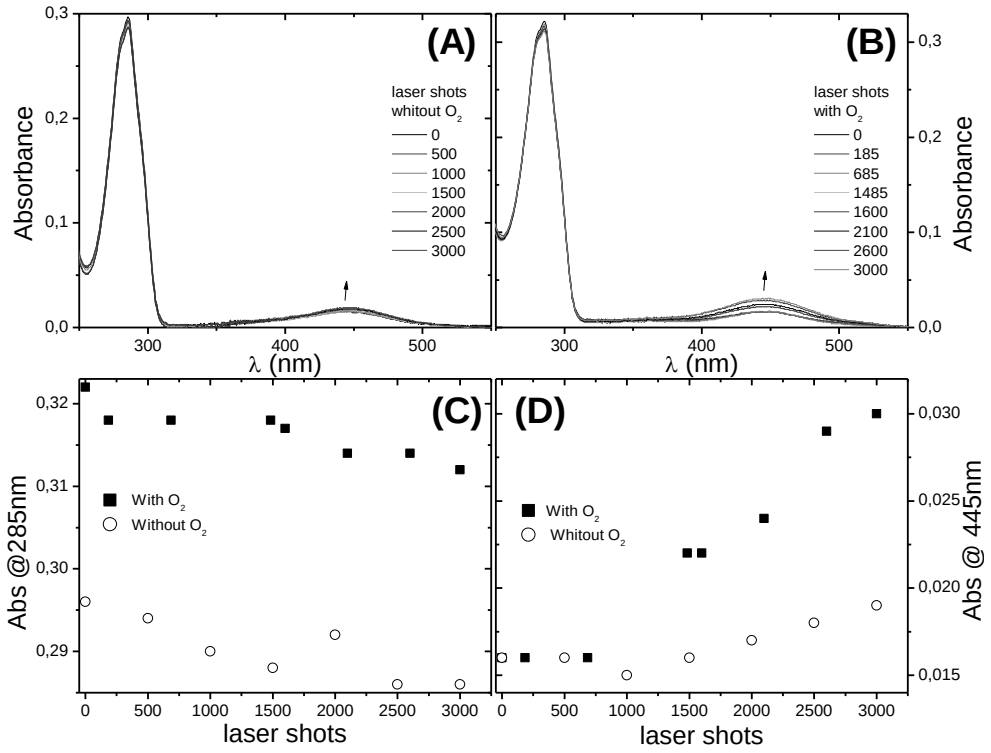

Figure 74 – Top: spectral observed changes occurred in brazilin aqueous solutions at pH=1.5, upon laser irradiation (266nm) with a different number of laser shots – **(A)** degassed solution, **(B)** aerated solution. **Down:** representation of the changes occurred at **(C)** 285nm (brazilin) and **(D)** 445nm (brazilein), T=293K. The energy of the laser was 13.8 ± 1 mJ.

Taking into account that the formation of brazilein occurs from the oxidation of brazilin it would be expected to see a decrease in the brazilin absorption band (285 nm); in Fig.74C, it can be seen that the decrease indeed occurs, but it is not found proportional to the increase of the brazilein band (D). A plausible explanation can lie in the differences of the molar extinction coefficient of both species, 6160 $M^{-1}cm^{-1}$ for brazilin (Table13) and 4680 $M^{-1}cm^{-1}$ for brazilein (Table 14).

The evolution in the dark (without irradiation) was also followed, Figure 75, again using aerated and degassed solutions of brazilin at pH 1.5.

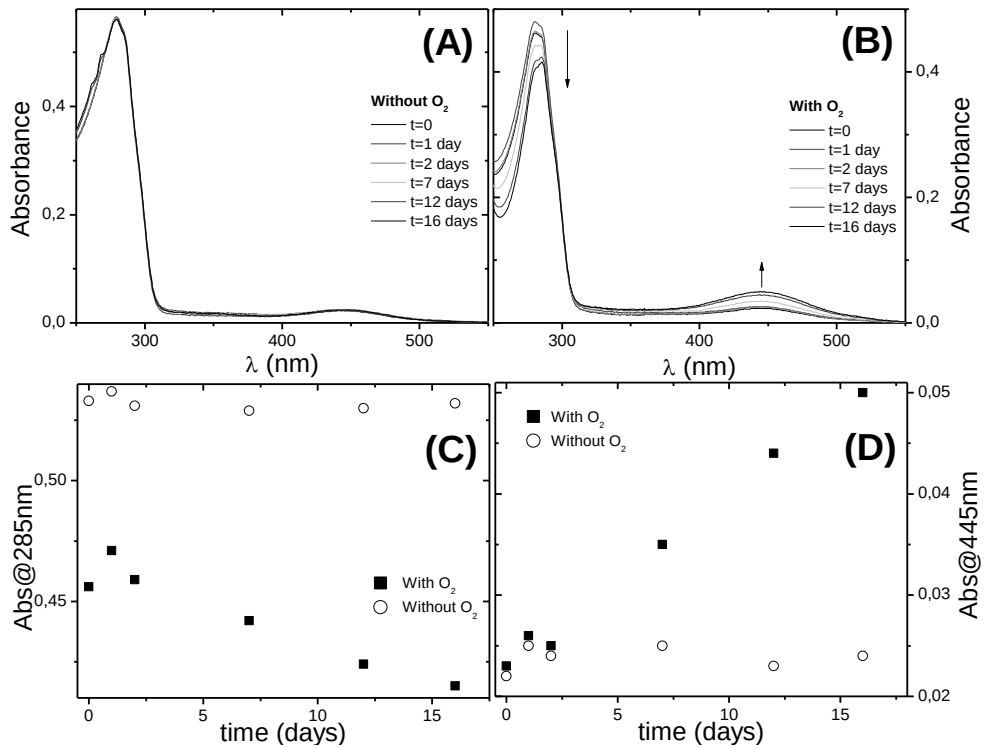

Figure 75 – Top: spectral observed changes occurred in brazilin aqueous solutions at pH=1.5, in the dark– **(A)** degassed solution, **(B)** aerated solution. **Down:** representation of the changes occurred at **(C)** 285nm (brazilin) and **(D)** 445nm (brazilein), T=293K.

From Figure 75 it can be seen that the evolution is very slow, with days being needed in order to observe some significant changes. During the time of the experience those changes were only visible for aerated solutions, (D); for degassed solutions it can be considered that no changes have occurred. Similar to what happened when using laser irradiations, the differences in brazilein absorption band were found much more pronounced than in the brazilin band (Fig. 75, C)).

9.2 - BRAZILEIN

Brazilein was easily isolated by following the procedure described in references [168,174]. Scheme 27 depicts the pH induced changes to brazilein. Once more the acronym BOXxH is used to designate each particular species.

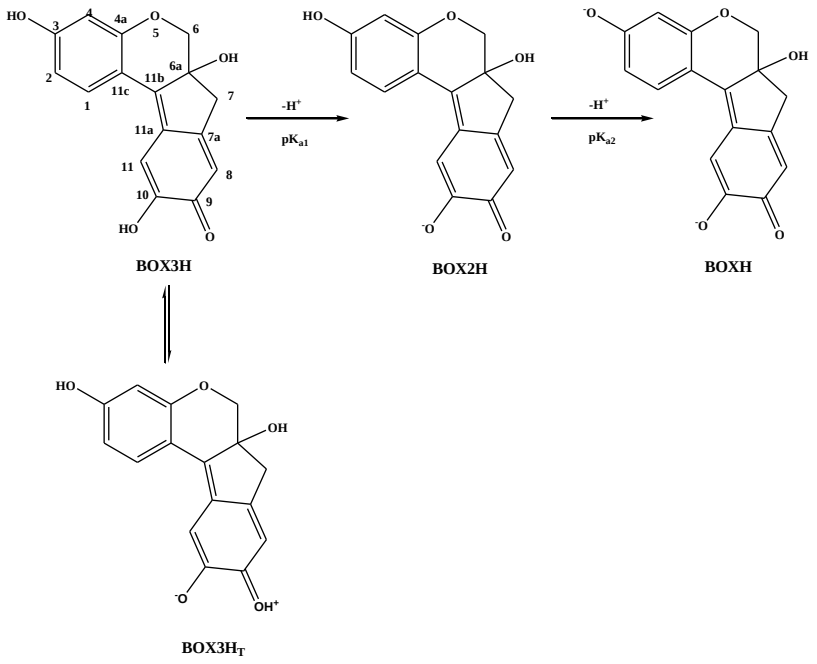

Scheme 27 - Structural changes of brazilein with pH. Numbering is given for the fully protonated form.

9.2.1 - SPECTRAL DATA

Spectral changes occurred for brazilein after pH jumps from equilibrated stock solutions of brazilein at pH=1 are depicted in Figure 76 from which two pK_a were determined: pK_{a1}=5.6 and pK_{a2}=9.3; as expected, these are very close to those obtained for brazilin (6.6 and 9.4 respectively; see above figure 69).

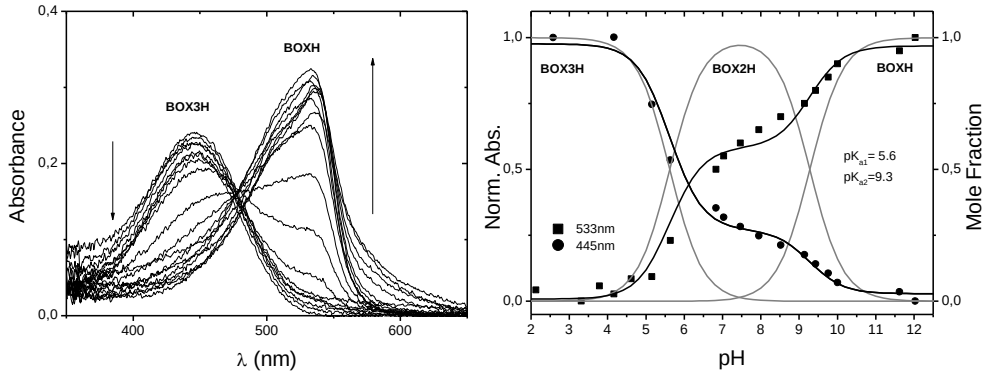

Figure 76- Left : spectral variations occurred upon a pH jump from equilibrated solutions of brazilin at pH=1 to alkaline pH values. Right : calculated pK_a resulting from the fitting of the absorbance at 445 and 553nm (black line), and mole fraction distribution of the species (grey line).

As previously mentioned for brazilin, at alkaline pH values, brazilein solution becomes deep red, with a large increase in the absorption maximum, and which immediately starts to fade, into a colourless solution, see Figure 77. This was previously reported for haematein.[173] This colour fading of the fully protonated form of brazilein corresponds, in principle, to a degradation process involving the breakdown of the carbon skeleton, since the colour almost disappears. For this to be completely proved further studies on the

characterization of the degradation products are needed, but were considered out of the scope of the present thesis.

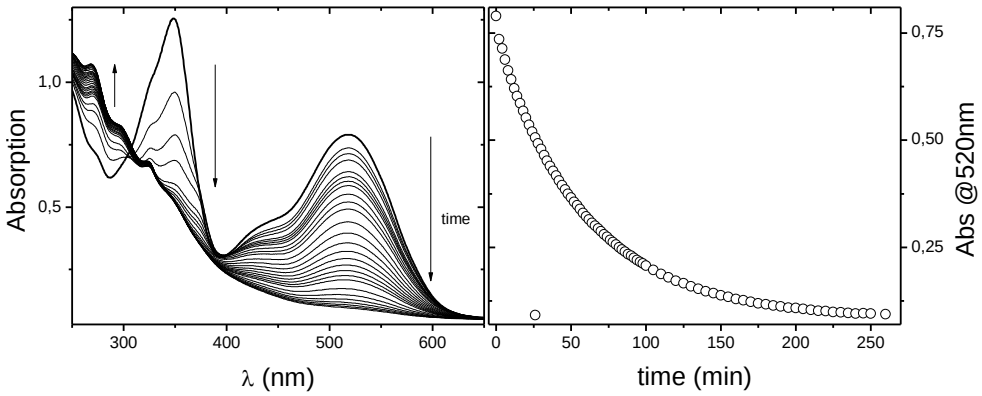

Figure 77- Left: spectral changes after a pH jump from pH=1 to pH=12 of an equilibrated aqueous solution of brazilein, collected for around 270 min. Right: plot of the absorption at 520nm over time, T=293K.

Table 14, summarizes the spectral and photophysical properties of brazilein at pH≈1.5. Comparison with brazilin, Table 13, shows that there is a red shift (both in absorption and fluorescence), and the Stokes shift value is much higher. Another important difference lies in the fluorescence quantum yield value which is found two orders of magnitude lower than that of brazilin.

Table 14- Spectral and photophysical properties of brazilein at pH≈1.5, T=293K

	λ_{max}^{Abs} **(nm)**	λ_{max}^{Fluo} **(nm)**	Δ_{SS} **(nm)**	ε_{SS} (M^{-1} cm^{-1})	ϕ_F
Brazilein	445	570	125	4680	0.00680

9.2.2 – EXCITED STATE CHARACTERIZATION

Due to the occurrence of fading (particularly from pH 7 and above), the emission spectra were collected as fast as possible after a pH jump from an equilibrated solution of brazilein at pH=1 (λ_{exc}=480nm). The emission fluorescence spectra after pH jumps in the range 1 – 12 are depicted in Figure 78. We can see that from pH=1.4 to pH=7.6 the fluorescence intensity increases and for higher pH values it decreases sharply. Two excited state pK_a could be determined, pK^*_{a1}=6.3 and pK^*_{a2}= 9.7, very close to those determined for the ground state, and also to those found for brazilin.

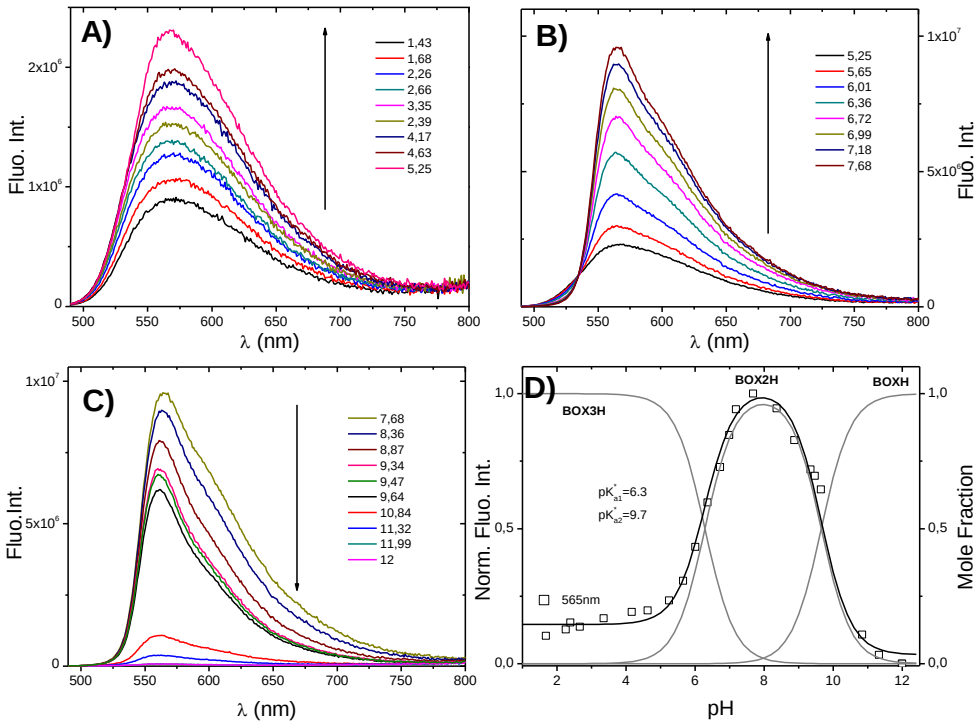

Figure 78 – Fluorescence spectral variations (λ_{exc}=480nm) occurred upon a pH jump from equilibrated solutions of brazilein at pH=1, **A)** to pH=5 and **B)** to pH=8. **C)** spectral variations occurred upon a pH jump from pH=1 to pH between 8 and 12. **D)** calculated pK^*_a upon fitting of the emission at 565 nm (black line), and mole fraction distribution of the species (grey line).

When investigating the fluorescence lifetimes, and in contrast to brazilin, where at pH=1 the decay was found mono-exponential, for brazilein it is biexponential. Observing Figure 78 (panel down right) it is likely that an equilibria at pH below 2 is present. Therefore an attempt to obtain the lifetime of the totally protonated species was tried with the determination of the decay times at pH values below 1, by dissolving brazilein in pure $HClO_4$. A value of 3.89ns was found for pH=-1, see Figure 79. However, with the increase of the pH solution this decay time strongly decreases and the decays becomes bi- and triexponential. Between pH 3 and 4 the decays are biexponential with values of 0.35 and 0.11ns. This is in agreement with Fig. 78D and Scheme 27, where the two decay times should be associated to the BOX3H and BOX2H species. Figure 79 shows the evolution of the first decay time with the pH. Due to the fading, beginning at pH~7, the fluorescence decays could be only collected until this pH value. The data suggests that below pH 1 an additional excited state proton transfer process is occurring which will be further explored in the next section.

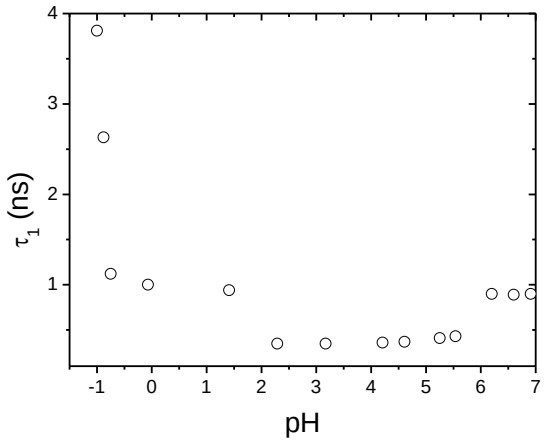

Figure 79 – Variation of the first fluorescence lifetime found for brazilein, along pH, λ_{exc}=450nm, and collected at 565nm, T=293K.

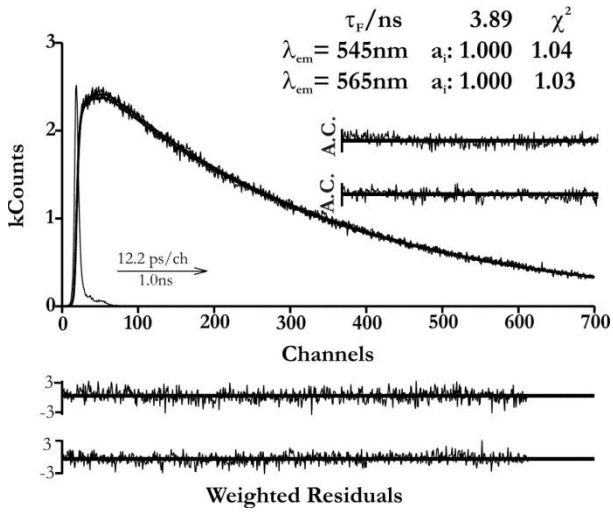

Figure 80 - Fluorescence decay of brazilein in aqueous solution at pH=-1, at T=293K, with excitation at 460 nm, and collected at 545 and 565nm and T=293K. Shown as insets are the decay times (τ/ns), pre-exponential factors (a_i), and chi-squared values (χ^2). Also shown are the weighted residuals for a better judgment of the quality of the fits.

9.2.3 – BRAZILEIN EXCITED STATE INTRAMOLECULAR PROTON TRANSFER

The fluorescence emission spectra collected with λ_{exc}=480nm (isosbestic point from Figure 77) is depicted in Figure 81. Beginning with the most acidic pH value, below 0, a red shift of the fluorescence wavelength maximum is observed together with a decrease in fluorescence intensity), λ_{max}= 543nm for pH=-1 and λ_{max}= 564nm for pH above 1. The changes in the fluorescence intensity can be due to the presence of an intramolecular excited proton transfer process, with the formation (during the decay of the BOX3H species) of the $BOX3H_T$ species.

The fluorescence emission in highly acidic solution (pH<1) is due to the fully protonated BOX3H specie where the excess protons in the solvent blocks any possibility of proton transfer. With an increase of pH (-1<pH<0), it becomes possible for an intramolecular proton transfer to occur from the hydroxyl group from carbon 10 to the carbonil group from carbon 9, forming the $BOX3H_T$ tautomer[175,176] (see Scheme 27). The presence of an intramolecular excited state proton transfer process is therefore a process competing with fluorescence, promoting a strong decrease of the intensity of fluorescence, see in Figure 81.

The excited state lifetime of the species also changed abruptly, decreasing sharply in a similar way to the fluorescence emission. The plot of the fluorescence intensity at 564nm (Fig. 81) matches the evolution of the first fluorescence lifetime (τ_1) with pH, presented in Figure 81.

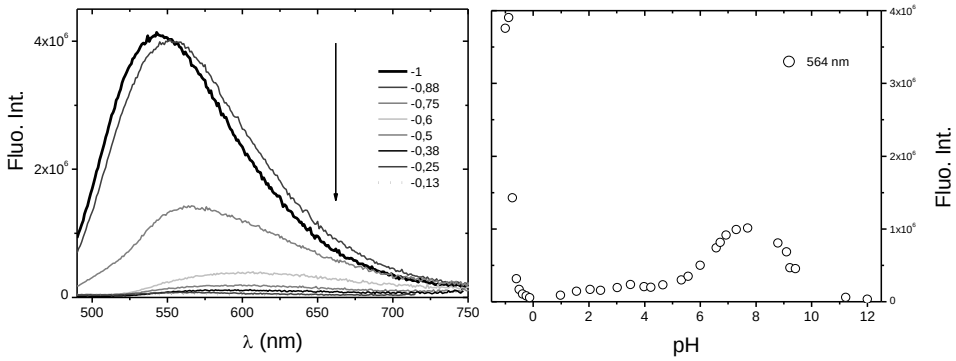

Figure 81 – Fluorescence emission from aqueous solutions of brazilein, from pH=-1 to pH=0, λ_{exc}=480nm, T=293K. R**ight:** plot of the fluorescence intensity at 564nm. Data from pH up to 0 was taken from Figure 79.

The comparison of the absorption spectra of brazilein in an aqueous solution with pH=1.4 with the fluorescence excitation spectrum of a ($HClO_4$) solution at pH=-0.84, Figure 82, can also suggest that the differences in the

fluorescence emission (maxima) which are dependent on the pH (Figure 81), are due to a fully protonated species (BOX3H), giving further support to the existence of an excited state proton transfer.[177-182]

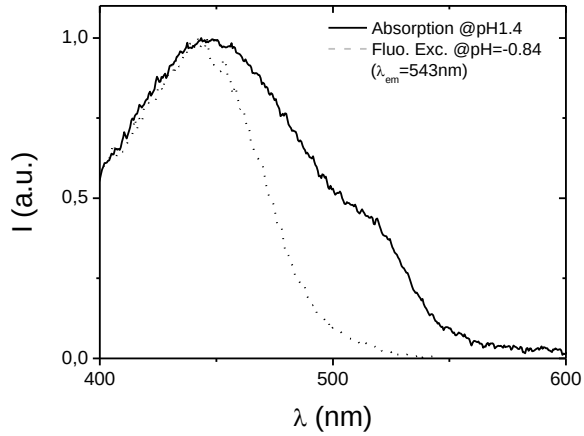

Figure 82 - Absorption of an aqueous solution of brazilein at pH=1.4, and fluorescence excitation spectra collected with λ_{emis}=543nm, of an aqueous solution of brazilein at pH=-0.84, T=293K.

9.3 - CONCLUSIONS

There is still a lot to unveil related to the major dye components of brazilwood, being its interaction and behaviour with mineral salts (such as alumen) probably a crucial step in this study. The fading at basic pH can constitute an additional drawback on the study and conservation (in works of art) of these dyes. Moreover, an additional input as come out from this work consisting in the finding that the oxidation of brazilin into brazilein is not as fast as it is frequent to be mentioned in the literature; indeed, this process was found to be more dependent on the oxygen than on light exposure.

In the ground state two pK_a values were obtained for brazilin (pK_{a1}=6.6, and pK_{a2}=9.4) and brazilein (pK_{a1}=5.6, and pK_{a2}=9.3). Brazilin showed to display a fluorescence quantum yield relatively high (0.330) when compared to brazilein at the same acidic pH value (0.0068). For the excited state two very similar pK_a were also determined for both forms, brazilin (pK^*_{a1}=6.3, and pK^*_{a2}=10.1) and brazilein (pK^*_{a1}=6.3, and pK^*_{a2}=9.7). For brazilein indications were given on the possible presence of excited state proton transfer which could account for the low fluorescence quantum yield and high internal conversion quantum yield.

10. FINAL REMARKS AND FUTURE PERSPECTIVES

Indigo is a mythic molecule with a remarkable history including in the history of chemistry. Amazingly in the XXI century it still harbours mysteries to unveil. In this work some of these have been revealed, namely the chemistry of the reduced (leuco) and oxidized (dehydroindigo), forms of indigo. In the case of indigo and some derivatives, it was found that these display spectral and photophysical properties which are dependent on the position and degree of substitution, with fluorescence and intersystem crossing as important deactivation pathways for the excited state, in contrast with the keto forms where 99.99% of the quanta is lost through the internal conversion channel.

With leuco indigo rotation around the central C-C bond is allowed and the photoisomerization of this form was here investigated and a photoconversion quantum yield of 0.9 was determined for leuco indigo in this process.

The oxidized form of indigo – DHI – was investigated for the first time; it was found that it presents a completely different spectral and photophysical behaviour when compared with keto and leuco indigo; additionally it was also found that, in toluene and benzene, the dominant excited state deactivation pathway involve the triplet state, with negligible fluorescence ($\phi_F \leq 0.01\%$). This gave further support to the fast deactivation, via the radiationless internal conversion channel, of indigo which must be operative in this neutral form through intramolecular proton transfer from the N-H to the C=O groups.

A polymeric indigo has also been investigated in this work. Comparison with indigo revealed that no significant differences exist between the polymer and the monomeric unit. However, the single exponential nature of the polymer (in contrast with the bi-exponential decay in indigo) shows that in the polymer an even more efficient $S_1 \sim\sim\rightarrow S_0$ internal conversion deactivation channel, related to

an efficient energy migration within a energetic ladder of the polymer chromophoric segments, is present.

The ancient Maya civilization technology fabricate what is consensually accepted to be the first organic/inorganic hybrid; this technology was here reproduced using indigo, thioindigo and ciba brilliant pink; the last two have high fluorescence quantum yields and were selected for a more detailed photophysical investigation in solution and when incorporated in two different clays: attapulgite and sepiolite. The obtained hybrid showed a different colour (when compared with the dye in the solid) together with a resistance to degradation towards alkali, acids, organic solvents and light.

Dracorhodin and Dracoflavylium, extracted from dragon's blood resin, have also been investigated in this work. The excited-state characterization was also investigated in DMF and in acid and alkaline DMF. Two species were found to be dominating the excited state, and the major deactivation pathway was again established as associated to the radiationless processes.

From brazilwood two compounds were isolated: brazilin and brazilein (the oxidized form of brazilin). For both species, two pK_a of ~6.5 and 10.0 values were observed. Possible occurrence of excited state intramolecular proton transfer was investigated for brazilein.

11. REFERENCES

(1) Struckmeier, S. *Chem. Unserer Zeit* **2003**, *37*, 402.

(2) Saunders, B. A. C.; Brakel, J. v. The Trajectory of Color. In *Perspectives on Science* Technology, T. M. I. o., Ed., 2002; Vol. 10, nº3.

(3) Finlay, R. *J. World Hist.* **2007**, *18*, 383.

(4) Orna, M. V. *J. Chem. Educ.* **2001**, *78*, 1305.

(5) Pawlak, K.; Puchalska, M.; Miszczak, A.; Rosloniec, E.; Jarosz, M. *J. Mass Spectrom.* **2006**, *41*, 613.

(6) Zarkogianni, M.; Mikropoulou, E.; Varella, E.; Tsatsaroni, E. *Color. Technol.* **2011**, *127*, 18.

(7) Morris, P. J. T.; Travis, A. S. *American Dyestuff Reporter* **1992**, *81*.

(8) Ingamells, W. *Colour for textiles: A user's handbook*; Society of Dyers and Colourists: West Yorkshire, England, 1993.

(9) Clark, R. J. H.; Cooksey, C. J.; Daniels, M. A. M.; Withnall, R. *Endeavour* **1993**, *17*, 191.

(10) de Melo, J. S.; Moura, A. P.; Melo, M. J. *J. Phys. Chem. A.* **2004**, *108*, 6975.

(11) Bender, M. *J. Chem. Educ.* **1947**, *24*, 2.

(12) Balfour-Paul, J. *Indigo*; British Museum Press: London, 1998.

(13) Baeyer, A.; Drewson, V. *V. Ber. Dtsch. Chem. Ges.* **1882**, *15*, 2856.

(14) de Meijere, A. *Ang. Chem. Int. Ed. Eng.* **2005**, *44*, 7836.

(15) Berke, H. *Chem. Soc. Rev.* **2007**, *36*, 15.

(16) Greenspan, A. *Bible Review* **2003**, *19*, 32.

(17) Ziderman, I. I. Purple Dyeing in the Ancient Mediterranean World: Characterisation of Biblical Tekhelet. In *Lecture delivered before the International Conference on Colours in Antiquity* University of Edinburgh, 2001.

(18) Ziderman, I. I. Revival of Biblical Tekhelet Dyeing with Banded Dye-Murex (Ph. trunculus): Chemical Anomalies. In *Dyes in History and Archaeology*; Kirby, J., Ed.; Archetype Publications: London, 2001; Vol. 16/17; pp xvii and 87.

(19) Kokubun, T.; Edmonds, J.; John, P. *Phytochemistry* **1998**, *49*, 79.

(20) Lee, J.-Y.; Shin, Y.-S.; Shin, H.-J.; Kim, G.-J. *Bioresorce Technol.* **2011**, *102*, 9193.

(21) Eisenbrand, G.; Hippe, F.; Jakobs, S.; Muehlbeyer, S. *J. Cancer Res. Clin. Oncol.* **2004**, *130*, 627.

(22) Maugard, T.; Enaud, E.; Choisy, P.; Legoy, M. D. *Phytochemistry* **2001**, *58*, 897.

(23) Bloxam, W. P.; Perkin, A. G. *J. Chem. Soc.* **1910**, *97*, 1460.

(24) McKee, J. R.; Zanger, M. *J. Chem. Educ.* **1991**, *68*, A242.

(25) Brown, T. M.; Cooksey, C. J.; Dronsfield, A. T. *Educ. Chem.* **2001**, *38*, 69.

(26) Christie, R. M. *Colour Chemistry*; Royal Society of Chemistry: Cambridge, 2001.

(27) Reis, A.; Schneider, W. *Z. Kristall.* **1928**, *68*, 543.

(28) Christie, R. M. *Biotechnic & Histochemistry* **2007**, *82*, 51.

(29) SerranoAndres, L.; Roos, B. O. *Chem-Eur J.* **1997**, *3*, 717.

(30) Zollinger, H. *Color Chemistry. Synthesis, Properties, and Applications of Organic Dyes and Pigments*, 3rd ed.; Verlag Helvetica Chimica Acta & Wiley-VCH: Zürich, 2003.

(31) Dilthey, W.; Wizinger, R. *J. Prak. Chem-Leip.* **1928**, *118*, 321.

(32) Luttke, W.; Hermann, H.; Klessing.M. *Angew. Chem. Int. Edit.* **1966**, *5*, 598.

(33) Klessinger, M. *Dyes and Pigments* **1982**, *3*, 235.

(34) Bauer, H.; Kowski, K.; Kuhn, H.; Luttke, W.; Rademacher, P. *J. Mol. Struct.* **1998**, *445*, 277.

(35) Yamazaki, S.; Sobolewski, A. L.; Domcke, W. *Phys. Chem. Chem. Phys.* **2011**, *13*, 1618.

(36) Bauer, H.; Kowski, K.; Kuhn, H.; Luttke, W.; Rademacher, P. *J. Molc. Struct.* **1998**, *445*, 277.

(37) Jacquemin, D.; Preat, J.; Wathelet, V.; Perpete, E. A. *J. Chem. Phys.* **2006**, *124*, 074104.

(38) Perpete, E. A.; Preat, J.; Andre, J. M.; Jacquemin, D. *J. Phys. Chem. A.* **2006**, *110*, 5629.

(39) Sadler, P. W. *J. Org. Chem.* **1956**, *21*, 316.

(40) Friedlander, P. *Ber. Deut. Chem. Ges.* **1906**, *39*, 1060.

(41) H. D. Hartough; Meisel, S. L. *Compounds with condensed thiophene rings*; Interscience Publishers, inc.: New York, 1954.

(42) Jacquemin, D.; Preat, J.; Wathelet, V.; Fontaine, M.; Perpete, E. A. *J. Am. Chem. Soc.* **2006**, *128*, 2072.

(43) Blanc, J.; Ross, D. L. *J. Phys. Chem.* **1968**, *72*, 2817.

(44) Wyman, G. M. *Journal of the Chemical Society D-Chemical Communications* **1971**, 1332.

(45) Wyman, G. M.; Zarnegar, B. M. *J. Phys. Chem.* **1973**, *77*, 831.

(46) Cherepy, N. J.; Sanner, R. D. *Opt. Mater.* **2006**, *28*, 1350.

(47) Wyman, G. M.; Zarnegar, B. M. *J. Phys. Chem.* **1973**, *77*, 1204.

(48) Seixas de Melo, J.; Rondão, R.; Burrows, H. D.; Melo, M. J.; Navaratnam, S.; Edge, R.; Voss, G. *J. Phys. Chem. A.* **2006**, *110*, 13653.

(49) Seixas de Melo, J. S.; Rondão, R.; Burrows, H. D.; Melo, M. J.; Navaratnam, S.; Edge, R.; Voss, G. *ChemPhysChem* **2006**, *7*, 2303.

(50) Seixas de Melo, J. S.; Serpa, C.; Burrows, H. D.; Arnaut, L. G. *Ang. Chem. Int. Ed. Eng.* **2007**, *46*, 2094.

(51) Rondao, R.; Sergio Seixas de Melo, J.; Voss, G. *ChemPhysChem* **2010**, *11*, 1903.

(52) Rondao, R.; Seixas de Melo, J. S.; Bonifacio, V. D. B.; Melo, M. J. *J. Phys. Chem. A.* **2010**, *114*, 1699.

(53) Kobayashi, T.; Rentzepis, P. M. *J. Chem. Phys.* **1979**, *70*, 886.

(54) Iwakura, I.; Yabushita, A.; Kobayashi, T. *Chem. Lett.* **2009**, *38*, 1020.

(55) Iwakura, I.; Yabushita, A.; Kobayashi, T. *Chem. Phys. Lett.* **2010**, *484*, 354.

(56) Elsaesser, T.; Kaiser, W.; Lüttke, W. *J. Phys. Chem.* **1986**, *90*, 2901.

(57) Nagasawa, Y.; Taguri, R.; Matsuda, H.; Murakami, M.; Ohama, M.; Okada, T.; Miyasaka, H. *Phys. Chem. Chem. Phys.* **2004**, *6*, 5370.

(58) Rondao, R.; de Melo, J. S. S.; Voss, G. *ChemPhysChem* **2010**, *11*, 1903.

(59) Nicholson, S. K.; John, P. *Appl. Microbiol. Biotechnol.* **2005**, *68*, 117.

(60) Padden, A. N.; Dillon, V. M.; John, P.; Edmonds, J.; Collins, M. D.; Alvarez, N. *Nature* **1998**, *396*, 225.

(61) Padden, A. N.; John, P.; Collins, M. D.; Hutson, R.; Hall, A. R. *J. Archaeol. Sci.* **2000**, *27*, 953.

(62) Roessler, A.; Crettenand, D. *Dyes Pigment.* **2004**, *63*, 29.

(63) Roessler, A.; Crettenand, D.; Dossenbach, O.; Marte, W.; Rys, P. *Electrochim. Acta* **2002**, *47*, 1989.

(64) Voss, G. *Color. Technol.* **2006**, *122*, 317.

(65) Voss, G. *J. Soc. Dye. Colour* **2000**, *116*, 87.

(66) Interior, M. d. L. d. U. d. B. *Catálogo do Museu dos Lanifícios da Universidade da Beira Interior. Núcleo da Tinturaria da Real Fábrica de Panos*; Museu de Lanifícios da Universidade da Beira Interior: Covilhã, 1998.

(67) Blackburn, R. S.; Bechtold, T.; John, P. *Color. Technol.* **2009**, *125*, 193.

(68) Voss, G.; Schramm, W. *Helv. Chim. Acta* **2000**, *83*, 2884.

(69) Morris, E. H. *The Temple of the warriors* Charles Scribner's Sons: New York, 1931.

(70) Morris, E. H.; Charlot, J.; Morris, A. A. *The Temple of the warriors at Chichen Itzá, Yucatan*; Carnegie Institution of Washington: Washington, 1931; Vol. 1.

(71) Giustetto, R.; Xamena, F.; Ricchiardi, G.; Bordiga, S.; Damin, A.; Gobetto, R.; Chierotti, M. R. *J. Phys. Chem. B* **2005**, *109*, 19360.

(72) Gettens, R. J. *Am. Antiq.* **1962**, *27*, 557.

(73) del Rio, M. S.; Martinetto, P.; Reyes-Valerio, C.; Dooryhee, E.; Suarez, M. *Archaeometry* **2006**, *48*, 115.

(74) Shepard, A. O. *Am. Antiq.* **1962**, *27*, 565.

(75) Van Olphen .H. *Science* **1966**, *154*, 645.

(76) Arnold, D. E.; Branden, J. R.; Williams, P. R.; Feinman, G. M.; Brown, J. P. *Antiquity* **2008**, *82*, 151.

(77) Ovarlez, S.; Chaze, A. M.; Giulieri, F.; Delamare, F. *C. R. Chim.* **2006**, *9*, 1243.

(78) Ovarlez, S.; Giulieri, F.; Chaze, A. M.; Delamare, F.; Raya, J.; Hirschinger, J. *Chem.-Eur. J.* **2009**, *15*, 11326.

(79) JoseYacaman, M.; Rendon, L.; Arenas, J.; Puche, M. C. S. *Science* **1996**, *273*, 223.

(80) Arnold, D. E. *Am. Antiq.* **1971**, *36*, 20.

(81) Chiari, G.; Giustetto, R.; Druzik, J.; Doehne, E.; Ricchiardi, G. *Appl. Phys. A-Mater. Sci. Process.* **2008**, *90*, 3.

(82) Chiari, G.; Giustetto, R.; Ricchiardi, G. *Eur. J. Mineral.* **2003**, *15*, 21.

(83) Fois, E.; Gamba, A.; Tilocca, A. *Microporous Mesoporous Mat.* **2003**, *57*, 263.

(84) Polette, L. A.; Meitzner, G.; Yacaman, M. J.; Chianelli, R. R. *Microchem J.* **2002**, *71*, 167.

(85) Domenech, A.; Domenech-Carbo, M. T.; Pascual, M. *J. Phys. Chem. C* **2007**, *111*, 4585.

(86) Giustetto, R.; Seenivasan, K.; Bordiga, S. *Period. Mineral.* **2010**, *79*, 21.

(87) Domenech, A.; Domenech-Carbo, M. T.; Pascual, M. *J. Phys. Chem. B* **2006**, *110*, 6027.

(88) Giustetto, R.; Chiari, G. *Eur. J. Mineral.* **2004**, *16*, 521.

(89) Giustetto, R.; Levy, D.; Chiari, G. *Eur. J. Mineral.* **2006**, *18*, 629.

(90) Tilocca, A.; Fois, E. *J. Phys. Chem. C* **2009**, *113*, 8683.

(91) Hubbard, B.; Kuang, W. X.; Moser, A.; Facey, G. A.; Detellier, C. *Clay Clay Min.* **2003**, *51*, 318.

(92) del Rio, M. S.; Boccaleri, E.; Milanesio, M.; Croce, G.; van Beek, W.; Tsiantos, C.; Chyssikos, G. D.; Gionis, V.; Kacandes, G. H.; Suarez, M.; Garcia-Romero, E. *J. Mater. Sci.* **2009**, *44*, 5524.

(93) Domenech, A.; Domenech-Carbo, M. T.; del Rio, M. S.; Goberna, S.; Lima, E. *J. Phys. Chem. C* **2009**, *113*, 12118.

(94) Polette-Niewold, L. A.; Manciu, F. S.; Torres, B.; Alvarado, M.; Chianelli, R. R. *J. Inorg. Biochem.* **2007**, *101*, 1958.

(95) Karmous, T.; Ayed, N.; Chelbi, F.; El Hili, A. *Techne* **1996**, *4*, 57.

(96) de Melo, J. S. S.; Rondao, R.; Burrows, H. D.; Melo, M. J.; Navaratnam, S.; Edge, R.; Voss, G. *ChemPhysChem* **2006**, *7*, 2303.

(97) Becker, R. S. *Theory and Interpretation of Fluorescence and Phosphorescence*; Wiley-Interscience: New York, 1969.

(98) Domenech, A.; Domenech-Carbo, M. T.; Pascual, M. *J. Solid State Electrochem.* **2007**, *11*, 1335.

(99) Manciu, F. S.; Reza, L.; Polette, L. A.; Torres, B.; Chianelli, R. R. *J. Raman Spectrosc.* **2007**, *38*, 1193.

(100) del Rio, M. S.; Picquart, M.; Haro-Poniatowski, E.; Van Elslande, E.; Uc, V. H. *J. Raman Spectrosc.* **2006**, *37*, 1046.

(101) Sousa, M. M.; Miguel, C.; Rodrigues, I.; Parola, A. J.; Pina, F.; de Melo, J. S. S.; Melo, M. J. *Photochem. Photobiol. Sci.* **2008**, *7*, 1353.

(102) Valeur, B. *Molecular Fluorescence: Principles and Applications*; Wiley-VCH: Weinheim, 2002.

(103) Seixas de Melo, J.; Moura, A. P.; Melo, M. J. *J. Phys. Chem. A.* **2004**, *108*, 6975.

(104) Seixas de Melo, J. S.; Serpa, C.; Burrows, H. D.; Arnaut, L. G. *Angewandte Chemie-International Edition* **2007**, *46*, 2094.

(105) Pina, J.; de Melo, J. S. S. *Phys. Chem. Chem. Phys.* **2009**, *11*, 8706.

(106) Gorman, A. A.; Lovering, G.; Rodgers, M. A. J. *J. Am. Chem. Soc.* **1978**, *100*, 4527.

(107) Pina, J.; de Melo, J. S.; Burrows, H. D.; Macanita, A. L.; Galbrecht, F.; Bunnagel, T.; Scherf, U. *Macromolecules* **2009**, *42*, 1710.

(108) Haucke, G.; Seidel, B.; Graness, A. *J. Photochem.* **1987**, *37*, 139.

(109) Ngan, V. T.; Gopakumar, G.; Hue, T. T.; Nguyen, M. T. *Chem. Phys. Lett.* **2007**, *449*, 11.

(110) Klessinger, M. *Angew. Chem. Int. Ed. Engl.* **1980**, *19*, 908.

(111) Klessinger, M.; Luettke, W. *Tetrahedron* **1963**, *19, Suppl. 2*, 315.

(112) Malkin, J. *Photophysical and Photochemical Properties of Aromatic Compounds*; CRC Press: Boca Raton: FL, 1992.

(113) El-Sayed, M. A. *Acc. Chem. Res.* **1968**, *1*, 8.

(114) Turro, N. *Modern Molecular Photochemistry*; University Science Books: Sausalito: CA, 1991.

(115) Heller, G. *Zeitschr. Farben- und Textilchem.* **1903**, *2*, 329.

(116) Voss, G.; Drechsler, M.; Eller, S.; Gradzielski, M.; Gunzelmann, D.; Mondal, S.; van Smaalen, S.; Voertler, C. S. *Helv. Chim. Acta* **2009**, *92*, 2675.

(117) Tanaka, H.; Tokuyama, K.; Sato, T.; Ota, T. *Chem. Lett.* **1990**, 1813.

(118) Stalder, R.; Mei, J. G.; Reynolds, J. R. *Macromolecules* **2010**, *43*, 8348.

(119) Mei, J. G.; Graham, K. R.; Stalder, R.; Reynolds, J. R. *Org. Lett.* **2010**, *12*, 660.

(120) Hoffmann, S. T.; Bassler, H.; Kohler, A. *J. Phys. Chem. B* **2010**, *114*, 17037.

(121) de Melo, J. S.; Burrows, H. D.; Svensson, M.; Andersson, M. R.; Monkman, A. P. *J. Chem. Phys.* **2003**, *118*, 1550.

(122) Kersting, R.; Lemmer, U.; Mahrt, R. F.; Leo, K.; Kurz, H.; Bassler, H.; Gobel, E. O. *Phys. Rev. Lett.* **1993**, *70*, 3820.

(123) *Indirubin, the red shade of indigo*; Meijer, L.; Guyard, N.; Skaltsounis, L. A.; Eisenbrand, G., Eds.; Life in Progress Editions: Roscoff, France, 2006.

(124) Pina, J.; de Melo, J. S.; Burrows, H. D.; Maçanita, A. L.; Galbrecht, F.; Bunnagel, T.; Scherf, U. *Macromolecules* **2009**, *42*, 1710.

(125) Schaberle, F. A.; Nunes, R. M. D.; Barroso, M.; Serpa, C.; Arnaut, L. G. *Photochem. Photobiol. Sci.* **2010**, *9*, 812.

(126) Iwakura, I. *Phys. Chem. Chem. Phys.* **2011**, *13*, 5546.

(127) Iwakura, I.; Yabushita, A.; Kobayashi, T. *Bull. Chem. Soc. Jpn.* **2011**, *84*, 164.

(128) Brode, W. R.; Pearson, E. G.; Wyman, G. M. *J. Am. Chem. Soc.* **1954**, *76*, 1034.

(129) Wyman, G. M. *EPA News Lett.* **1994**, *50*, 9.

(130) Miliani, C.; Romani, A.; Favaro, G. *Spectroc. Acta Pt. A-Molec. Biomolec. Spectr.* **1998**, *54*, 581.

(131) Giuliano, C. R.; Hess, L. D.; Margerum, J. D. *J. Am. Chem. Soc.* **1968**, *90*, 587.

(132) Weinstein, J.; Wyman, G. M. *J. Am. Chem. Soc.* **1956**, *78*, 4007.

(133) Wyman, G. M. *Chem. Rev.* **1955**, *55*, 625.

(134) Wyman, G. M.; Brode, W. R. *J. Am. Chem. Soc.* **1951**, *73*, 1487.

(135) Rogers, D. A.; Margerum, J. D.; Wyman, G. M. *J. Am. Chem. Soc.* **1957**, *79*, 2464.

(136) Kirsch, A. D.; Wyman, G. M. *J. Phys. Chem.* **1975**, *79*, 543.

(137) Rondao, R.; de Melo, J. S.; Schaberle, F. A.; Voss, G. *Phys. Chem. Chem. Phys.* **2012**, *14*, 1778.

(138) Rondao, R.; de Melo, J. S.; Melo, M. J.; Parola, A. J. *J. Phys. Chem. A.* **2012**, *116*, 2826.

(139) Raya, J.; Hirschinger, J.; Ovarlez, S.; Giulieri, F.; Chaze, A. M.; Delamare, F. *Phys. Chem. Chem. Phys.* **2010**, *12*, 14508.

(140) del Rio, M. S.; Martinetto, P.; Somogyi, A.; Reyes-Valerio, C.; Dooryhee, E.; Peltier, N.; Alianelli, L.; Moignard, B.; Pichon, L.; Calligaro, T.; Dran, J. C. *Spectroc. Acta Pt. B-Atom. Spectr.* **2004**, *59*, 1619.

(141) Dejoie, C.; Martinetto, P.; Dooryhee, E.; Strobel, P.; Blanc, S.; Bordat, P.; Brown, R.; Porcher, F.; del Rio, M. S.; Anne, M. *ACS Appl. Mater. Interfaces* **2010**, *2*, 2308.

(142) Manciu, F. S.; Ramirez, A.; Durrer, W.; Govani, J.; Chianelli, R. R. *J. Raman Spectrosc.* **2008**, *39*, 1257.

(143) Giustetto, R.; Seenivasan, K.; Pellerej, D.; Ricchiardi, G.; Bordiga, S. *Microporous Mesoporous Mat.* **2012**, *155*, 167.

(144) Ovarlez, S.; Giulieri, F.; Delamare, F.; Sbirrazzuoli, N.; Chaze, A. M. *Microporous Mesoporous Mat.* **2011**, *142*, 371.

(145) Polette-Niewold, L. A.; Manciu, F. S.; Torres, B.; Alvarado, M.; Chianelli, R. R. *Journal of Inorganic Biochemistry* **2007**, *101*, 1958.

(146) Reinen, D.; Kohl, P.; Muller, C. *Z. Anorg. Allg. Chem.* **2004**, *630*, 97.

(147) Peng, Q.; Yi, Y. P.; Shuai, Z. G.; Shao, J. S. *J. Chem. Phys.* **2007**, *126*, 114302.

(148) Gupta, D.; Bleakley, B.; Gupta, R. K. *J. Ethnopharmacol.* **2008**, *115*, 361.

(149) Sousa, M. M.; Melo, M. J.; Parola, A. J.; de Melo, J. S. S.; Catarino, F.; Pina, F.; Cook, F. E. M.; Simmonds, M. S. J.; Lopes, J. A. *J. Chromatogr. A* **2008**, *1209*, 153.

(150) Pearson, J.; Prendergast, H. D. V. *Econ. Bot.* **2001**, *55*, 474.

(151) Baumer, U.; Dietemann, P. *Anal. Bioanal. Chem.* **2010**, *397*, 1363.

(152) Brockmann, H.; Junge, H. *Ber. Deut. Chem. Ges.* **1943**, *76*, 751.

(153) Brockmann, H.; Haase, R. *Ber. Deut. Chem. Ges.* **1936**, *69*, 1950.

(154) Melo, M. J.; Sousa, M.; Parola, A. J.; de Melo, J. S. S.; Catarino, F.; Marcalo, J.; Pina, F. *Chem.-Eur. J.* **2007**, *13*, 1417.

(155) Haslam, E. *Practical Polyphenolics, From structure to molecular recognition and physiological action*; Cambridge University Press: Cambridge, 1998.

(156) Pina, F.; Maestri, M.; Balzani, V. Photochromic systems based on synthetic flavylium compounds and their potential use as molecular-level memory

elements. In *Hanbook of Photochemistry and Photobiology*; Nalwa, H. S., Ed.; American Scientific Publishers, 2003; Vol. 3:Supramolecular Photochemistry; pp 411.

(157) Moncada, M. C.; Pina, F.; Roque, A.; Parola, A. J.; Maestri, M.; Balzani, V. *Eur. J. Org. Chem.* **2004**, 304.

(158) Pina, F.; Melo, M. J.; Parola, A. J.; Maestri, M.; Balzani, V. *Chem.-Eur. J.* **1998**, *4*, 2001.

(159) Pina, F.; Lima, J. C.; Parola, A. J.; Afonso, C. A. M. *Angew. Chem.-Int. Edit.* **2004**, *43*, 1525.

(160) Shi, J. M.; Hu, R. L.; Lu, Y. B.; Sun, C. R.; Wu, T. X. *J. Sep. Sci.* **2009**, *32*, 4040.

(161) Defilipps, R. A. *Archives of Natural History* **1998**, *25*, 103.

(162) Cardon, D. *Natural Dyes: Sources, Tradition, Technology and Science*; Archetype, 2007.

(163) Edwards, H. G. M.; de Oliveira, L. F. C.; Nesbitt, M. *Analyst* **2003**, *128*, 82.

(164) Gilbody, A. W.; Perkin, W. H.; Yates, J. *J. Chem. Soc.* **1901**, *79*, 1396.

(165) Robinson, R. *Bull. Soc. Chim. Fr.* **1958**, 125.

(166) Perkin, W. H. *J. Chem. Soc.* **1902**, *81*, 221.

(167) Engels, P.; Perkin, W. H.; Robinson, R. *J. Chem. Soc.* **1908**, *93*, 1115.

(168) Kim, D. S.; Baek, N. I.; Oh, S. R.; Jung, K. Y.; Lee, I. S.; Lee, H. K. *Phytochemistry* **1997**, *46*, 177.

(169) Karapanagiotis, I.; Minopoulou, E.; Valianou, L.; Daniilia, S.; Chryssoulakis, Y. *Anal. Chim. Acta* **2009**, *647*, 231.

(170) Karapanagiotis, I.; Chryssoulakis, Y. *Annal. Chim-Rome* **2006**, *96*, 75.

(171) Huang, Y. D.; Zhang, J. S.; Pettus, T. R. R. *Org. Lett.* **2005**, *7*, 5841.

(172) Lalor, G. C.; Martin, S. L. *J. Soc. Dye. Colour* **1959**, *75*, 513.

(173) Lalor, G. C.; Martin, S. L. *J. Soc. Dye. Colour* **1959**, *75*, 517.

(174) Berger, S.; Sicker, D. *Classics in Spectroscopy: Isolation and Structure Elucidation of Natural Products*; Wiley-VCH, 2009.

(175) Strandjord, A. J. G.; Barbara, P. F. *J. Phys. Chem.* **1985**, *89*, 2355.

(176) Strandjord, A. J. G.; Courtney, S. H.; Friedrich, D. M.; Barbara, P. F. *J. Phys. Chem.* **1983**, *87*, 1125.

(177) Melo, M. J.; Melo, E.; Pina, F. *Arch. Environ. Contam. Toxicol.* **1994**, *26*, 510.

(178) Pina, F.; Benedito, L.; Melo, M. J.; Parola, A. J.; Bernardo, A. *J. Chem. Soc.-Faraday Trans.* **1996**, *92*, 1693.

(179) Melo, M. J.; Bernardo, M. A.; Melo, E. C.; Pina, F. *J. Chem. Soc.-Faraday Trans.* **1996**, *92*, 957.

(180) Freitas, A. A.; Quina, F. H.; Macanita, A. A. L. *J. Phys. Chem. A.* **2011**, *115*, 10988.

(181) Moreira, P. F.; Giestas, L.; Yihwa, C.; Vautier-Giongo, C.; Quina, F. H.; Macanita, A. L.; Lima, J. C. *J. Phys. Chem. A* **2003**, *107*, 4203.

(182) Pina, F.; Melo, M. J.; Santos, H.; Lima, J. C.; Abreu, I.; Ballardini, R.; Maestri, M. *New J. Chem.* **1998**, *22*, 1093.

12.

Experimental Section

12.1- MATERIALS AND METHODS

Indigo derivatives were provided by Prof. Gundula Voss (University of Bayreuth, Germany)[1], dehydroindigo by Prof. Vasco Bonifácio[2], dracoflavylium and brazilein by Prof. Maria João Melo and Prof. A. Jorge Parola (REQUIMTE-CQFB and Faculty of Sciences and Technology of the New University Lisbon)[3,4], dracorhodin and brazilin were purified by Raquel Rondão at Faculty of Sciences and Technology of the New University Lisbon, the remaining were purchased from Aldrich, Ciba Ltd and Kremer Pigments. The clays were acquired from Tolsa and Kremer Pigments. The synthesis, purification and properties of the samples under study have been described elsewhere.[1-3,5] All the solvents used were of spectroscopic or equivalent grade and were used without further treatment, except for dioxane[6], toluene and methanol (dried and purified by distillation over CaO).[6] For photophysical measurements, solutions were prepared with concentrations ranging from $1x10^{-5}$ to 10^{-6} M.

12.2- CONVERTION TO LEUCO FORM

Leuco species were prepared by adding 2-3 drops of concentrated sodium dithionite/NaOH solution (0.15 g $Na_2S_2O_4$ in 10 mL NaOH (1 M)) to the dye in dioxane, submitted to constant and gentle bubbling with Ar. The solution was left bubbling for a further 20 minutes and then sealed in a proper device described elsewhere.[7]

12.3- MAYA BLUE -TYPE COMPOUNDS SYNTHESIS

Synthesis procedure for the Maya Blue- type compounds followed essentially the one proposed by van Olphen:[8] 2g of clay was mixed with 0.4, 0.2, 0.1 and 0.04g of compound (20, 10, 5 and 2% w/w) in 50mL of water. The mixture was then stirred for 1 hour and further heated, for 5 hours, at 190 ºC. The obtained solid was rinsed with distilled water and acetone until no trace of dye (as followed by the absorption spectra) could be found in the mother waters of the washing solvent. The final step consisted in the acid attack (with concentrated sulphuric or nitric acid), followed by rinsing again with distilled water and acetone; again no traces of indigo could be found in the washing solvent(s). The obtained pigment was then left drying at room temperature.

12.4- ABSORPTION

Absorption measurements were carried out on Shimadzu UV-2100 spectrometer. The molar extinction coefficients (ε) were obtained from the slope of the plot of the absorption with (at least) six solutions of different concentrations versus the concentration (correlation values >0.999).

The solid state spectra were recorded on a Shimadzu UV-2450 by diffuse reflection using an integrating sphere model reference ISR-2200. The samples for the solid state spectra were obtained by mixing the different pigments with barium sulphate. Before spectra of the solid sample were run, a baseline, with barium sulphate, was obtained.

12.5- STEADY-STATE FLUORESCENCE

Fluorescence measurements were recorded with a Horiba-Jobin-Yvon Fluorolog 3-2.2 spectrometer. Fluorescence spectra were corrected for the wavelength response of the system. Solid-state fluorescence emission spectra were obtained using a triangular quartz cell and with a Horiba-Jobin-Yvon integrating sphere.

12.5.1- FLUORESCENCE QUANTUM YIELDS AT ROOM TEMPERATURE

Room temperature fluorescence quantum yields (ϕ_F) were determined by comparison with standards of known quantum yield. The emission quantum yields of these reference compounds should be independent of the excitation wavelength, so the standards can be used in their full absorption range. In practice the quantum yields are determined by comparison of the integrated area under the emission spectra of optically matched solutions of the samples ($\int I(\lambda)^{cp} d\lambda$) and that of the suitable reference compound ($\int I(\lambda)^{ref} d\lambda$). The absorption and emission range of the samples (cp) and reference (ref) compound should match as much as possible. The absorbance values should be kept as lower as possible to avoid inner filter effects. In these conditions, using the same excitation wavelength, the unknown fluorescence quantum yield (ϕ_F^{cp}) is calculated using Equation 19,[9]

$$\phi_F^{cp} = \frac{\int I(\lambda)^{cp} d\lambda}{\int I(\lambda)^{ref} d\lambda} \cdot \frac{n_{cp}^2}{n_{ref}^2} \cdot \phi_F^{ref} \qquad (19)$$

where n_x is the refractive index of the solvents in which the compounds and the reference were respectively dissolved.

In cases were the absorbance of the reference and the unknown compound are not completely matched at the excitation wavelength an additional correction is introduced in the previous equation,

$$\phi_F^{cp} = \frac{\int I(\lambda)^{cp} d\lambda}{\int I(\lambda)^{ref} d\lambda} \cdot \frac{OD_{ref}}{OD_{cp}} \cdot \frac{n_{cp}^2}{n_{ref}^2} \cdot \phi_F^{ref} \qquad (20)$$

with OD_x the optical density of the reference (ref) and compound (cp) at the excitation wavelength. References used: Leuco indigo (ϕ_F=0.35 in DMF[10]) for indigo derivatives in their leuco form, quinquethiophene (ϕ_F=0.36 in dioxane[11]) for dehydroindigo, rhodamin B (ϕ_F=0.65 in methanol[12]) for thioindigo and ciba brilliant pink, indigo (ϕ_F=0.0023 in DMF[10]) for polymeric indigo, rubrene (ϕ_F=0.27 in methanol [12]) for dracorhodin and brazilein, erithrosin (ϕ_F=0.09 in methanol[12]) for dracoflavilium and naphtalen (ϕ_F=0.2 in ciclohexane[12]) for brazilin.

12.5.2- SOLID-STATE FLUORESCENCE QUANTUM YIELDS

The solid-state fluorescence quantum yields in powder samples were obtained using the integrating sphere, using the method outlined by de Mello *et. al.*[13] and developed by Palsson and Monkman[14]. Since it was not possible to

deposit the compound in the sapphire, a quartz triangular cell was used. The following equation was used to determine the solid state fluorescence quantum yields (ϕ_F^{Solid}),

$$\phi_F^{Solid} = \frac{\int^{cp} I(\lambda)d\lambda}{\left(\int^{SA} I(\lambda)d\lambda - \int^{SS} I(\lambda)d\lambda\right)\cdot 10^{\Delta OD(\lambda_{exc})}} \qquad (21)$$

where $\int^{cp} I(\lambda)d\lambda$ is the integrated area under the emission of the sample compound in the cell (which excludes the integration of Rayleigh peak), $\int^{SA} I(\lambda)d\lambda$ is the integrated area under the Rayleigh peak of the integrating sphere alone and $\int^{SS} I(\lambda)d\lambda$ is the integrated area under the Rayleigh peak in the emission spectra of the compound under investigation. Since the emission from the samples is much weaker than the scattered excitation light (Rayleigh peak) the spectra is recorded with a filter that attenuates the emission intensity at the excitation wavelength. This is considered in Equation 21 with $10^{\Delta OD(\lambda_{exc})}$, the filter transmittance at the excitation wavelength.

12.6 – REACTION QUANTUM YIELD

For the reaction quantum yields (ϕ_R), irradiation was carried out in the Horiba-Jovin-Yvon Spex Fluorog 3-2.2. spectrophotometer in which 3mL of each solution were irradiated at 335nm, with 2mm slits (bandwidth of 4.2 nm) and continuous magnetic stirring.

12.6.1 - REACTION QUANTUM YIELD OF LEUCO FORM PHOTOISOMERISATION

Photoreaction yields for the leuco forms were performed with irradiation at 370nm for indigo, and 405 nm for 4,4'-dibutoxy-7,7'-dimethoxy-5,5'-dinitroindigo. In order to obtain the I_0 from the irradiation source (450 W Xe lamp), the actinometer potassium ferrioxalate was used [ϕ_R=1.14 (405nm) and ϕ_R=1.12 (416 nm) in aqueous 0.05M H_2SO_4], using the "micro-version" procedure,[12,15] and by collecting the change in the optical density at 510 nm, after several periods of time of irradiation (λ_{exc}=405 nm, 4 mm bandwidth for DBMNI and λ_{exc}=416 nm, 2 mm bandwidth for indigo) in the fluorimeter. At each irradiation wavelength (405 and 416 nm), a solution of 3mL (0.006M) of the actinometer was irradiated, keeping a constant stirring, for 10 minutes. At the end of this, the cell was immediately taken out of the fluorimeter and 0.5mL of buffered phenanthroline was added. The absorbance at 510 nm was measured immediately and after 10, 20 and 30 minutes. In the mean time the solution was kept in the dark. The same was done with a reference solution that had also been kept in the dark. The experiment was repeated, irradiating for 20 and 30 minutes. Assuming that the entire incident light is absorbed by the solution, the intensity of light is given by Equation (22)

$$I_0 = \frac{\Delta A V}{\varepsilon_{510}\, d\, \phi_R\, t} \qquad (22)$$

where ΔA is the absorbance of the irradiated solution at 510 nm, corrected by the absorbance of the reference solution, d the optical path of the absorption cell measured in centimeters, ε_{510} =1.11×10^4 M^{-1} cm^{-1}, ϕ_R the quantum yield of production of Fe^{2+} at the wavelength used in the photolysis, t the irradiation time

(minutes) and V the volume (dm^3) of the solution used in the determination of the absorbance.[15]

The quantum yield of reaction for leuco indigo (at λ_{exc}= 416 nm) and its derivative DBMNI (λ_{exc}= 405 nm) was calculated from Eq. (23)[16]:

$$\phi_R = \frac{\Delta A V}{\varepsilon 1000 I_0 \ \Delta t} \tag{23}$$

where I_0 is the light absorbed by the solution at the irradiation wavelength (calculated from Equation 22), V is the volume of irradiated solution (in mL), ΔA is the change in absorbance (at the monitoring wavelength) over the irradiation time period, Δt, and ε is the molar absorption coefficient of the compound at the monitoring wavelength.

Considering that in these experiments the changes observed were registered in terms of fluorescence emission, instead of absorbance, the factor $(\Delta A/\varepsilon)$ in Eq.23 was replaced by the change in normalized concentration C(t) along the irradiation time, according to Eq.24

$$C(t) = \frac{fluor.int.(t) \times final\ concentration}{final\ \ fluo.\ int.} \tag{24}$$

where 'fluo. int (t)' stands for the intensity of the fluorescence emission at time t, 'final concentration' for the concentration of the leuco form (when the total isomerisation has been achieved), and 'final fluo. int.' the intensity of fluorescence emission upon total isomerisation, i.e., at the end of the experiment. As a consequence of this, Eq. 23 now transforms into Eq. 25:

$$\phi_R = \frac{V_{sol}\,\Delta C}{1000\, I_0\ \Delta t} \qquad (25)$$

where the ratio $\Delta C/\Delta t$ is obtained from the slope of the plot of C(t) *vs* time.

12.6.2 - REACTION QUANTUM YIELD FOR INDIGO AND POLYMERIC INDIGO

The intensity of the incident light (I_0) at 335nm was measured using potassium hexacyanocobaltate (III) ($K_3[Co(CN_6)]$)[17] as actinometer. The I_0 value was calculated, with correction to the absorbed light, according to Equation 26:

$$I_0 = V_{sol}\,(\Delta A/\Delta\varepsilon)\ /\ 1000\ \phi_R\,\Delta t \qquad (26)$$

where V_{sol} is the volume of irradiated solution in mL; ΔA is the change in absorbance at the monitoring wavelength over the irradiation time period, Δt; $\Delta\varepsilon$ is the difference between the molar absorption coefficients of reagent and product at the monitoring wavelength; and ϕ_R is the quantum yield of reaction.[3]

The quantum yield of reaction for indigo was calculated with Eq. 26 rearranged as:

$$\phi_R = V_{sol}\,(\Delta A/\Delta\varepsilon)\ /\ 1000\ \ I_{Abs}\ \Delta t \qquad (27)$$

where, I_{Abs} is the light absorbed by the solution at the irradiation wavelength; I_{Abs} was made equal to $I_0\times(1\text{-}10^{-Airrad})$ when $A < 2$ and to I_0 when $A > 2$.[3]

For the polymeric indigo the actinometry was made comparing directly the variance of absorption of both compounds polymer and indigo, and corrected

with the optical density values (absorbance) at the irradiation wavelength, using Equation 28

$$\phi_R = \frac{\Delta OD_{polymer}}{\Delta OD_{indigo}} \cdot \frac{Abs_{indigo}}{Abs_{polymer}} \cdot \phi_R^{indigo} \quad (28)$$

where $\Delta OD_{polymer}$ is the change in the optical density (ΔOD) of the polymer solution with the irradiation time, ΔOD_{indigo} is the change in optical density of the solution with indigo with the time of irradiation, Abs_{indigo} is the optical density value (absorption) of indigo at the wavelength of irradiation (335nm), $Abs_{polymer}$ is the optical density value of the polymer at the wavelength of irradiation (335nm) and ϕ_R^{indigo} is the reaction quantum yield of indigo.

12.7- TIME-RESOLVED FLUORESCENCE

12.7.1- FLUORESCENCE DECAYS WITH NANOSECOND TIME-RESOLUTION

Fluorescence decays were measured using a home-built time correlated single photon counting (TCSPC) apparatus with an IBH NanoLED (460 nm) as the excitation source, Jobin-Yvon excitation and emission monochromators, a Philips XP2020Q photomultiplier and Canberra instruments time-to-amplitude converter and multi channel analyzer. Alternate measurements (1000 counts per cycle) of the pulse profile were performed until $5x10^4$ counts at the maximum were reached.

The fluorescence decays were analyzed using the modulating functions method of Striker with automatic correction for the photomultiplier "wavelenght shift".[18]

12.7.2- FLUORESCENCE DECAYS WITH PICOSECOND TIME-RESOLUTION

In this case the fluorescence decays were measured using a home-built picosecond TCSPC apparatus. The excitation source consists of a picosecond Spectra Physics mode-lock Tsunami® Laser (Ti:Sapphire) Model 3950 (repetition rate of about 82 MHz, tuning range 700-1000 nm), pumped by a Millennia® Pro-10s, frequency-doubled continuos wave (CW), diode-pumped, solid-state laser (λ_{em}= 532 nm). A harmonic generator model GWU-23PS (Spectra Physics) is used to produce the second and third harmonic from the Ti:Sapphire laser exciting beam frequency output. The samples where measured with excitation at 395 nm and the horizontally polarized output beam from the GWU (second harmonic) was first passed through a ThorLabs depolarizer (WDPOL-A) and after by a Glan-Thompson polarizer (Newport 10GT04) with vertical polarization. Emission at 90º geometry collected at magic angle polarization was detected through a Oriel Cornerstone™ 260 monochromator by a Hamamatsu microchannel plate photomultiplier (R3809U-50). Signal acquisition and data processing was performed employing a Becker & Hickl SPC-630 TCSPC module. The full width at half maximum (FWHW) of the IRF was about 22 ps and was highly reproducible with identical system parameters. Deconvolution of the fluorescence decays curves was performed using the Globals WE software package[19] and the method of modulating functions of Striker[18].

In the case of the solid samples, the fluorescence decays of the compounds were obtained using a PicoQuant Picoled (model LDH-P-C-450b, λ_{exc}= 450nm) as excitation source. To eliminate the light quantity of dispersed light a RG475 filter was used in the after the sample holder and before the emission monochromator.

12.8- PHOSPHORESCENCE

Phosphorescence measurements were made in glasses at 77 K and used the Horiba-Jobin-Yvon Fluorolog 3-2.2 spectrometer equipped with a 1934 D phosphorimeter unit and a 150 W pulsed xenon lamp. The phosphorescence spectra were corrected for the wavelenght response of the system.

12.9- ROOM TEMPERATURE SINGLET-OXYGEN PHOSPHORESCENCE

Room-temperature singlet oxygen phosphorescence was detected at 1270 nm with a Hamamatsu R5509-42 photomultiplier cooled to 193 K in a liquid nitrogen chamber (Products for Research model PC176TSCE-005) following laser excitation of aerated solutions at 355 nm or 532 nm in an adapted Applied Photophysics flash kinetic spectrometer. The modification of the spectrometer involved the interposition of a 600-line diffraction grating instead of the standard spectrometer, to extend spectral response to the infrared.

Measurements were performed in a Horiba-Jobin-Ivon SPEX Fluorog 3-2.2 using the Hamamatsu R5509-42 photomultiplier previously reported. In both cases the use of a Schott RG1000 filter was essential to eliminate from the infrared signal all of the first harmonic contribution of the sensitizer emission in the region below 850 nm.

12.9.1- SINGLET-OXYGEN FORMATION QUANTUM YIELDS

When using the Applied Photophysics apparatus the singlet oxygen formation quantum yields (ϕ_Δ) were obtained by direct measurement of the phosphorescence at 1270 nm following irradiation of aerated solutions of the compounds. The ϕ_Δ values were determined by plotting the initial emission intensity for optically matched solutions as a function of the laser energy and comparing the slope with that obtained upon sensitization with the reference compound. 1*H*-phenalen-1-one in toluene (λ_{exc}= 355 nm, ϕ_Δ= 0.93)[20], rose bengal in methanol (λ_{exc}= 532 nm, ϕ_Δ = 0.76)[20] and tetraphenyl porphyrin, TPP, in benzene (λ_{exc}= 532 nm, ϕ_Δ = 0.66)[21] were used as the standard.

In the Fluorolog 3-2.2 the sensitized phosphorescence emission spectra of singlet oxygen from optically matched solutions of the samples and that of the reference compound were obtained in identical experimental conditions. The singlet oxygen formation quantum yield was then determined by comparing the integrated area under the emission spectra of the samples solutions ($\int I(\lambda)^{cp} d\lambda$) and that of the reference solution ($\int I(\lambda)^{ref} d\lambda$) and applying Equation 29,

$$\phi_\Delta^{cp} = \frac{\int I(\lambda)^{cp} d\lambda}{\int I(\lambda)^{ref} d\lambda} \cdot \phi_\Delta^{ref} \qquad (29)$$

with ϕ_Δ^{ref} the singlet oxygen formation quantum yield of the reference compound.

12.10 - TRIPLET-TRIPLET TRANSIENT ABSORPTION SPECTRA

The experimental setup used to obtain triplet spectra and triplet lifetimes consists of an Applied Photophysics laser flash photolysis apparatus pumped by the fourth harmonic (266 nm), third harmonic (355 nm) or second harmonic (532 nm) of a Nd:YAG laser (Spectra Physics). The detection system (Hamamatsu IP28 or R928 photomultipliers) is at right angle to the excitation beam, and a pulsed 150 W Xe lamp is used to analyze the transient absorption. The signal obtained is fed into a Tektronix TDS 3052B digital analyzer and transferred to an IBM RISC computer where the optical density (OD) at different wavelengths and different delays after flash are collected using the appropriate software (Applied photophysics). Transient spectra were collected by monitoring the optical density change at intervals of 5-10 nm over the range 250-850 nm and averaging at least 10 decays at each wavelength. First order kinetics were observed for the decays of the lowest triplet state. Special care was taken in order to have low laser energy (≤2 mJ) to avoid multiphoton and triplet-triplet annihilation effects. Before experiments were taken, all solutions were degassed with argon for ≈20 min and sealed.

12.10.1- TRIPLET MOLAR ABSORPTION COEFFICIENTS MEASUREMENT

12.10.1.1- SINGLET DEPLETION METHOD

This technique uses flash photolysis excitation and involves comparing the loss of ground state absorption with the gain in triplet absorption obtained. The

triplet molar absorption coefficients (ϕ_T) were determined according to the well-known relationship, [22,23]

$$\varepsilon_T = \frac{\varepsilon_S \cdot \Delta OD_T}{\Delta OD_S} \qquad (30)$$

where ΔOD_S and ΔOD_T are the change in optical density due to singlet depletion and to triplet absorption respectively in the triplet-singlet difference transient absorption spectra and ε_S is singlet molar extinction coefficient.

12.10.1.2- ENERGY TRANSFER METHOD

This is the most generally applicable method and involves comparing the unknown triplet molar absorption coefficient with that of another triplet, of known molar absorption coefficient. The samples under study were dissolved in solutions of relatively high concentrations of the donor compounds (10^{-2}-10^{-4} M solutions). The concentration for the samples with unknown ε_T was 10^{-5} M. The molar triplet-triplet absorption coefficients were then determined from Equation 31:[22]

$$\frac{\varepsilon_T^D}{\varepsilon_S^A} = \frac{\Delta OD^D}{\Delta OD^A} \qquad (31)$$

where ε_T^D and ε_T^A stand for the triplet molar absorption coefficients of donor and acceptor respectively; ΔOD^D is the maximum absorbance from the transient triplet-triplet absorption spectra of the donor in the absence of acceptor: ΔOD^A is

the maximum absorbance of the acceptor triplet when both the donor and acceptor are present. For determination of ΔOD^A, additional corrections were taken into account, in particular when the acceptor decay rate constant (k_3) is not negligible. For this situation Equation 32 was applied[22]

$$\Delta OD^A_{obs} = \Delta OD^A \exp\left[-\frac{\ln k_2/k_3}{k_2/k_3 - 1} \right] \qquad (32)$$

where k_2 is the donor decay rate constant in the presence of acceptor and ΔOD^A_{obs} is taken from the maximum observed in the triplet-triplet difference spectra of the acceptor in the presence of donor.

12.10.1.3-PARTIAL SATURATION METHOD

This method makes use of the large photon fluxes available with lasers. The basic equation of the method is derived from a two-state model of the excitation process, where the two states considered are the ground state and the triplet state.[23]

Using Eq 33 to fit the plot of the ΔO.D. of the compound (@triplet max) vs laser intensity (I_p),

$$\Delta O.D. = a(1 - \exp(-b\, I_p)) \qquad (33)$$

considering the values of a and b taken from the fit, where ε_T is the triplet molar absorption coefficient, ε_S is the singlet molar absorption coefficient, $[^1M_0]$ is the initial concentration of the compound in the singlet state, *l* is the optical path (cm), and *t* is the time after flash at wich the ΔO.D. value is registered.

$$a = (\varepsilon_T - \varepsilon_S)\left[\,^1M_0\right]l \qquad (34)$$

$$b = 2303\ \varepsilon_S\ t\ \phi_T \qquad (35)$$

12.10.2- INTERSYSTEM CROSSING QUANTUM YIELDS DETERMINATIONS

The singlet-triplet intersystem crossing quantum yields (ϕ_T) for the compounds with unknown ϕ_T^{cp}, but known triplet molar absorption coefficient, ε_T^{cp}, was obtained by comparing the ΔOD_T^{cp} in the triplet-triplet absorption maximum of the compounds with the ΔOD_T^{ref} in the triplet wavelength absorption maximum of a reference compound with known ϕ_T^{ref} and ε_T^{ref}, using Equation 36;[24]

$$\phi_T^{cp} = \frac{\varepsilon_T^{ref}}{\varepsilon_T^{cp}} \cdot \frac{\Delta OD_T^{cp}}{\Delta OD_T^{ref}} \cdot \phi_T^{ref} \qquad (36)$$

Care was taken in order to have diluted solutions of the compounds and the reference optically matched at the laser excitation wavelength.

The ϕ_T values were determined using as standards benzophenone in benzene (ϕ_T= 7220 M^{-1} cm^{-1}@530 nm, ϕ_T= 1) with λ_{exc} = 355 nm and

tetraphenyl-porphyrin in toluene (ϕ_T= 6000 M^{-1} cm^{-1}@790 nm, ϕ_T= 0.82) for λ_{exc} = 532 nm.[9,23]

12.11 – TIME-RESOLVED PHOTOACOUSTIC CALORIMETRY

Time-resolved PAC measurements were performed in a homemade apparatus following the front-face irradiation design described elsewhere.[25] The solutions were pumped through a 0.11 mm thick cell at a 1 ml min-1 flow with Kloehn V6 Syringe pump, irradiated with a EKSPLA PL2143A Nd:YAG laser (FWHM = 30 ps) and collected with a Tektronix DPO 7254 oscilloscope. The acoustic waves were detected with a 2.25MHz Panametrics transducer (model A106S) and preamplified with a Panametrics ultrasonic amplifier (model 5676). Sample and reference solutions were matched to better than 1% absorbances at wavelength of 532nm. Data was analyzed using a software developed by Schaberle et al.[26]

12.12

References

(1) Voss, G.; Gradzielski, M.; Heinze, J.; Reinke, H.; Unverzagt, C. *Helv. Chim. Acta* **2003**, *86*, 1982.

(2) Rondao, R.; Seixas de Melo, J. S.; Bonifacio, V. D. B.; Melo, M. J. *J. Phys. Chem. A.* **2010**, *114*, 1699.

(3) Sousa, M. M.; Melo, M. J.; Parola, A. J.; de Melo, J. S. S.; Catarino, F.; Pina, F.; Cook, F. E. M.; Simmonds, M. S. J.; Lopes, J. A. *J. Chromatogr. A* **2008**, *1209*, 153.

(4) Berger, S.; Sicker, D. *Classics in Spectroscopy: Isolation and Structure Elucidation of Natural Products*; Wiley-VCH, 2009.

(5) Voss, G.; Drechsler, M.; Eller, S.; Gradzielski, M.; Gunzelmann, D.; Mondal, S.; van Smaalen, S.; Voertler, C. S. *Helv. Chim. Acta* **2009**, *92*, 2675.

(6) Perrin, D. D.; Aunarego, W. L. F.; Perrin, D. R. *Purification of Laboratory Chemicals*; Pergamon Press, 1980.

(7) Seixas de Melo, J. *Chem. Educator* **2005**, *10*, 29.

(8) Van Olphen .H. *Science* **1966**, *154*, 645.

(9) Murov, S.; Charmichael, I.; Hug, G. L. *Handbook of Photochemistry*; M. Dekker Inc.: New York, 1993.

(10) de Melo, J. S.; Moura, A. P.; Melo, M. J. *J. Phys. Chem. A.* **2004**, *108*, 6975.

(11) Becker, R. S. *Theory and Interpretation of Fluorescence and Phosphorescence*; Wiley-Interscience: New York, 1969.

(12) Montalti, M.; Credi, A.; Prodi, L.; Gandolfi, M. T. *Handbook of Photochemistry*, 3rd ed.; CRC Press: Boca Raton, FL, 2006.

(13) deMello, J. C.; Wittmann, H. F.; Friend, R. H. *Adv. Mater.* **1997**, *9*, 230.

(14) Palsson, L. O.; Monkman, A. P. *Adv. Mater.* **2002**, *14*, 757.

(15) Arnaut, L.; Formosinho, S.; Burrows, H. *Chemical Kinetics, From Molecular Structure to Chemical Reactivity*; Elsevier: Oxford, 2007.

(16) Sousa, M. M.; Miguel, C.; Rodrigues, I.; Parola, A. J.; Pina, F.; de Melo, J. S. S.; Melo, M. J. *Photochem. Photobiol. Sci.* **2008**, *7*, 1353.

(17) Pina, F.; Moggi, L.; Manfrin, M. F.; Balzani, V.; Hosseini, M. W.; Lehn, J. M. *Gazz. Chim. Ital* **1989**, *119*, 65.

(18) Striker, G.; Subramaniam, V.; Seidel, C. A. M.; Volkmer, A. *J. Phys. Chem. B* **1999**, *103*, 8612.

(19) Beechem, J. M.; Gratton, E. *Biophys. J.* **1988**, *53*, A403.

(20) Martinez, C. G.; Neumer, A.; Marti, C.; Nonell, S.; Braun, A. M.; Oliveros, E. *Helv. Chim. Acta* **2003**, *86*, 384.

(21) Pineiro, M.; Carvalho, A. L.; Pereira, M. M.; Gonsalves, A.; Arnaut, L. G.; Formosinho, S. J. *Chem-Eur J.* **1998**, *4*, 2299.

(22) Bensasson, R. V.; Land, E. J.; Truscott, T. G. *Excited States and Free Radicals in Biology and Medicine. Contributions from Flash Photolysis and Pulse Radiolysis*; Oxford University Press: Oxford, 1993.

(23) Carmichael, I.; Hug, G. L. *J. Chem. Phys.* **1986**, *15*, 1.

(24) Kumar, C. V.; Qin, L.; Das, P. K. *J. Chem. Soc. Faraday Trans 2* **1984**, *80*, 783.

(25) Arnaut, L. G.; Caldwell, R. A.; Elbert, J. E.; Melton, L. A. *Rev. Sci. Instrum.* **1992**, *63*, 5381.

(26) Schaberle, F. A.; Nunes, R. M. D.; Barroso, M.; Serpa, C.; Arnaut, L. G. *Photochem. Photobiol. Sci.* **2010**, *9*, 812.